UNIVERSITÉ DE LORRAINE | BIBLIOTHÈQUES UNIVERSITAIRES

AVERTISSEMENT
DROIT D'AUTEUR

Ce document est le fruit d'un long travail approuvé par le jury de soutenance et mis à disposition de l'ensemble de la communauté universitaire élargie.

Il est soumis à la propriété intellectuelle de l'auteur. Ceci implique une obligation de citation et de référencement lors de l'utilisation de ce document. Toute contrefaçon, plagiat ou reproduction illicite encourt une poursuite pénale.

Contact bibliothèque : ddoc-theses-contact@univ-lorraine.fr
(Cette adresse ne permet pas de contacter les auteurs)

Code de la Propriété Intellectuelle. articles L 122. 4
Code de la Propriété Intellectuelle. articles L 335.2- L 335.10

UNIVERSITÉ DE LORRAINE
34 COURS LÉOPOLD — CS 25233
54052 NANCY CEDEX
TÉL : 03 54 50 54 00
CONTACT@UNIV-LORRAINE.FR
WWW.UNIV-LORRAINE.FR

UNIVERSITÉ DE LORRAINE

UNIVERSITÉ INTERNATIONALE DE RABAT

THÈSE

Présentée à L'UNIVERSITÉ INTERNATIONALE DE RABAT en vue de l'obtention du titre :
DOCTEURE DE L'UNIVERSITÉ DE LORRAINE
Spécialité : Énergie et mécanique
ET
DOCTEURE DE L'UNIVERSITÉ INTERNATIONALE DE RABAT
Spécialité : Énergies
Par **Houda EL OUADOUD**

Sous la direction de **Serge PIERFEDERICI** et **Mohamed BAKHOUYA**

A Contribution Towards a Holistic Control Approach for Energy Management in Distributed DC Microgrid Systems

---

Soutenue publiquement le 19/12/2025 devant un jury composé de :

Pr. Nadia Yousfi	**Présidente**	Université Internationale de Rabat
Pr. Mohamed Machmoum	**Rapporteur**	Institut de Recherche en Energie Electrique de Nantes Atlantique
Pr. Jean-Paul Gaubert	**Rapporteur**	LIAS, université de Poitiers
Pr. Nadia Yousfi	**Rapporteure**	Université Internationale de Rabat
Pr. Xuefang Shi	**Examinatrice**	Institut National des Sciences Appliquées de Lyon
Pr. Serge Pierfederici	**Directeur de thèse**	Université de Lorraine
Pr. Mohamed Bakhouya	**Directeur de thèse**	Université Internationale de Rabat
Pr. Radouane Ouladsine	**Co-Directeur de thèse**	Université Internationale de Rabat
Dr. Matthieu Urbain	**Co-Directeur de thèse**	Université de Lorraine

1. Declaration of Authorship

I, Houda El ouadoud, hereby declare that the work presented in this thesis manuscript entitled: **A Contribution Towards a Holistic Control Approach for Energy Management in Distributed DC Microgrid Systems** is the original result of my own research, carried out as part of my doctorate at International University of Rabat and University of Lorraine.

And confirm that:

- Data, results, figures and analyses come from my personal work or from duly mentioned collaborations.
- Extracts, figures or publications from other sources are properly cited and referenced, in accordance with current citation rules.
- No substantial part of this thesis has been previously submitted for any other university degree or certificate, either at this or any other university.
-
- I also acknowledge that I have respected the principles of scientific integrity and the ethical rules applicable to the conduct of research, scientific writing and the publication of results.

Signed: 

Date: 19/12/2025

2. Thesis's Framework

The present research work is supported by MG-FARM project (LEAP-RE, 2022-2026), which is funded by "Ministère de l'Enseignement Supérieur, de la Recherche Scientifique et de l'Innovation, MESRSI" under the LEAP-RE program. It was also supported by HOLSYS project (A Holistic IoT and Big Data Platform for Smart Building Energy Management Systems), funded by the Institut de Recherche en Énergie Solaire et Énergies Nouvelles (IRESEN) as part of the Green INNO-PROJECT 2018 call for projects (2020-2024). This project also builds on the achievements of the MIGRID 2 project (Towards Smart Grids: Renewable Energy Integration into Smart Buildings), funded by the National Academy of Sciences (NAS) as part of the USAID PEER (Partnership for Enhanced Engagement in Research) programme, cycle 5-398 (2017-2021).

3. Acknowledgment

This thesis would never have been possible without the support, guidance, and kind presence of many people whom I would like to thank from the bottom of my heart.

First, I would like to thank my thesis advisors, Professor Serge Pierfederici and Professor Mohamed Bakhouya, for their constant support, their trust, and their rigorous scientific insight. Their guidance enabled me to conduct this research in a structured, rigorous, and enriching environment. Their availability and commitment throughout this work were invaluable.

I would also like to express my deep gratitude to Doctor Matthieu Urbain for his great rigor, his unfailing availability, and for following my work step by step with a sense of detail and precision that greatly contributed to the quality of this thesis.

My thanks also go to Doctor Radouane Ouladsine for his invaluable support throughout this journey. Through his generosity, advice, and kind guidance, he has been a fundamental pillar of this scientific and human adventure. I owe a significant part of the progress of this work to him.

I would also like to thank the International University of Rabat (UIR) and the University of Lorraine (UL) for offering me this unique opportunity to benefit from a rich research environment, excellent laboratories, and the valuable expertise of my supervisors. This international collaboration has been a real source of intellectual and human enrichment.

My special thanks to the administrative team at the SIMPPE doctoral school at the University of Lorraine and at UIR for their effective support, responsiveness, and professionalism throughout these years.

Finally, I would like to express my heartfelt thanks to my family, especially my parents and siblings for their unwavering love, constant moral support, and reassuring presence at every stage of this journey. Thanks to them, the difficult moments were made easier, and the success took on a special meaning.

To all these people, thank you.

4. Abstract

This thesis project is part of developing practical solutions for energy autonomy in isolated rural areas, based on DC microgrids operated via renewable energy sources and energy storage devices and driven by advanced control strategies. The challenge is to guarantee a reliable, economical and resilient local supply, while reducing reliance on conventional electric grids.

The first part of this research work explores energy issues in rural areas of Morocco and Africa, while considering territorial, agricultural and social backgrounds. It highlights the relevance of decentralized microgrids as a sustainable solution, by analyzing their architectures, essential components and the most appropriate control approaches.

In technical terms, a centralized hierarchical strategy is designed to coordinate multiple energy storage devices - such as supercapacitors, batteries and fuel cells - installed in close proximity. This approach ensures precise regulation of the DC bus voltage, efficient power distribution according to the specific dynamics of each technology, and effective control of the state of charge. The proposed strategy is validated both by simulation and experimentally using a test bench.

The study then turns to a distributed architecture in which the generators are remote and require local coordination. A cooperative and distributed control approach, based on limited exchange of information between neighboring units, is introduced, this approach ensures proportional sharing of currents, robust regulation of the average voltage, and resilience in the face of disturbances, interruptions or communication delays.

Finally, an energy management layer is developed to coordinate exchanges between several interconnected microgrids. A predictive method based on Predictive Functional Control (PFC) is used to anticipate load and production profiles. A cooperative exchange algorithm is implemented to distribute energy surpluses and deficits according to criteria, such as local consumption and battery state of charge using PV solar panels. Simulation results confirm the system's ability to optimize energy flows while maintaining the autonomy of local units.

Therefore, this thesis leads to a comprehensive contribution to the design of distributed DC microgrids, combining centralized and cooperative control approaches, with potential application in isolated areas (e.g., isolated farms) seeking sustainable energy independence.

5. Résumé

La transition énergétique mondiale représente l'une des transformations les plus profondes et structurelles des systèmes énergétiques modernes. Elle est motivée par l'épuisement progressif des ressources en combustibles fossiles, l'intensification des effets du changement climatique, la pression croissante pour réduire les émissions de gaz à effet de serre et le besoin croissant de sécurité et de résilience énergétiques. Les systèmes électriques, qui reposaient historiquement sur des infrastructures de production centralisées et de transport à longue distance, évoluent désormais vers des architectures décentralisées et distribuées capables d'intégrer à grande échelle les sources d'énergie renouvelables. Cette évolution n'est pas seulement technologique, mais aussi économique, réglementaire et sociétale, car elle nécessite de nouvelles méthodes de planification, de nouveaux paradigmes opérationnels et de nouvelles stratégies de contrôle adaptés à des systèmes énergétiques hautement distribués.

Dans les régions isolées et rurales, les défis liés à cette transition sont particulièrement importants. L'extension du réseau dans ces zones implique souvent des coûts d'investissement élevés, un terrain difficile et une faible densité de population, ce qui réduit considérablement la viabilité économique. Même lorsque le raccordement au réseau est possible, la qualité et la fiabilité de l'approvisionnement en électricité peuvent rester insuffisantes pour des utilisations productives. En conséquence, les communautés rurales et les activités agricoles sont souvent confrontées à une insécurité énergétique qui freine directement le développement économique, la sécurité alimentaire et le bien-être social. Dans ce contexte, les solutions énergétiques décentralisées capables de fonctionner de manière autonome sont devenues une priorité stratégique.

Les micro-réseaux se sont progressivement imposés comme une réponse technologique clé à ces défis. En intégrant des unités de production décentralisées, des systèmes de stockage d'énergie et des charges locales dans un périmètre géographique limité, les micro-réseaux permettent un fonctionnement autonome ou semi-autonome tout en maintenant des niveaux acceptables de qualité de l'énergie et de continuité du service. Initialement développés pour des applications industrielles et militaires exigeant une grande fiabilité, les micro-réseaux se sont étendus à des contextes civils, notamment l'électrification rurale, les systèmes agricoles, les communautés insulaires et les infrastructures critiques telles que les hôpitaux et les centres de

données.

La capacité des micro-réseaux à fonctionner en mode isolé lors de perturbations en amont du réseau améliore considérablement la résilience locale et l'indépendance énergétique. Cette caractéristique est particulièrement précieuse dans les régions où la fiabilité du réseau ne peut être garantie ou où des événements météorologiques extrêmes perturbent de plus en plus les infrastructures centralisées. De plus, les micro-réseaux facilitent la consommation locale d'énergie renouvelable, réduisant les pertes de transmission et atténuant la congestion des réseaux de distribution.

Parmi les différentes architectures de micro-réseaux, les micro-réseaux à courant continu ont suscité un intérêt croissant en raison de leur compatibilité intrinsèque avec les sources d'énergie renouvelables et les interfaces électroniques de puissance. Les générateurs photovoltaïques, les batteries, les supercondensateurs, les piles à combustible et de nombreuses charges électroniques modernes fonctionnent intrinsèquement en courant continu. Par conséquent, la distribution en courant continu évite les multiples étapes de conversion CA/CC, ce qui réduit les pertes d'énergie, simplifie l'architecture du système et améliore l'efficacité globale. En outre, les micro-réseaux à courant continu éliminent les contraintes liées à la fréquence, déplaçant l'accent mis sur la stabilité du système vers la régulation de la tension et l'équilibre de puissance. Malgré ces avantages, les micro-réseaux à courant continu présentent des défis techniques spécifiques. La régulation de la tension doit être assurée dans des conditions de charge et de production variant rapidement, l'énergie doit être répartie équitablement entre les unités distribuées et les systèmes de stockage d'énergie doivent être coordonnés efficacement pour s'adapter à l'intermittence des énergies renouvelables. Ces défis sont encore amplifiés dans les environnements ruraux et agricoles, où les profils de demande sont très variables et fortement liés aux cycles saisonniers et opérationnels tels que l'irrigation, la réfrigération et la transformation des récoltes.

Dans de nombreuses régions rurales, malgré les progrès significatifs réalisés grâce aux programmes nationaux d'électrification, l'accès à l'électricité à des fins productives reste limité. L'approvisionnement énergétique se caractérise souvent par une capacité insuffisante, une mauvaise qualité et des coûts élevés. Les générateurs diesel sont souvent utilisés comme solutions de secours, ce qui entraîne des frais d'exploitation élevés, des contraintes logistiques et des impacts environnementaux importants. Les micro-réseaux à courant continu basés sur les énergies renouvelables représentent donc une alternative durable, à condition que leur fonctionnement soit soutenu par des stratégies avancées de contrôle et de gestion de l'énergie.

Le contexte énergétique marocain offre un exemple représentatif de ces défis. Si les taux d'électrification rurale ont atteint des niveaux très élevés, les zones agricoles souffrent toujours d'un accès insuffisant à une électricité de haute qualité pour les activités productives. Des situations similaires sont observées sur tout le continent africain, en particulier dans les régions subsahariennes, où une grande partie de la population n'a toujours pas accès à l'électricité. Ces observations justifient le développement de solutions énergétiques décentralisées adaptées aux contraintes locales et capables de soutenir le développement agricole et socio-économique.
D'un point de vue technique, la conception et le fonctionnement des micro-réseaux à courant continu reposent sur des choix appropriés en matière d'architectures, de composants et de stratégies de contrôle hiérarchiques. Diverses configurations topologiques, notamment les architectures radiales, en anneau et maillées, présentent différents compromis en termes de simplicité, de fiabilité, d'évolutivité et de coût. Quelle que soit la topologie choisie, les systèmes de stockage d'énergie jouent un rôle central pour garantir la stabilité du système et la continuité de l'approvisionnement.

Les systèmes hybrides de stockage d'énergie, combinant batteries, supercondensateurs et piles à combustible, sont particulièrement intéressants en raison de leurs caractéristiques complémentaires. Les batteries assurent un stockage d'énergie à moyen terme, les supercondensateurs permettent une réponse rapide aux transitoires de puissance rapides et les piles à combustible fournissent une énergie de longue durée avec une densité énergétique élevée. Le contrôle coordonné de ces dispositifs est essentiel pour exploiter pleinement leur potentiel tout en respectant les limites opérationnelles individuelles.
Des structures de contrôle hiérarchiques sont couramment adoptées pour gérer les micro-réseaux à courant continu sur plusieurs échelles de temps. Le contrôle primaire assure une stabilité locale rapide et un partage de puissance de base entre les unités distribuées. Le contrôle secondaire compense les écarts en régime permanent introduits par les mécanismes primaires, tels que les chutes de tension résultant du contrôle de la dérive. Le contrôle tertiaire traite de la gestion et de l'optimisation de l'énergie sur des horizons temporels plus longs et des échelles spatiales plus grandes.

Les stratégies classiques de contrôle primaire basées sur le statisme offrent simplicité et fonctionnement décentralisé, mais introduisent intrinsèquement des écarts de tension et peuvent entraîner un partage inégal de la puissance lorsque les paramètres du système diffèrent. Le contrôle secondaire centralisé peut rétablir les conditions de fonctionnement nominales, mais souffre de limitations en termes d'évolutivité et de vulnérabilité aux points de défaillance

uniques. Ces limitations motivent le développement d'approches de contrôle avancées capables d'améliorer la précision, la robustesse et l'évolutivité.

Une contribution majeure de cette recherche réside dans le développement d'une stratégie de contrôle centralisé générique et hiérarchique pour les micro-réseaux CC intégrant des systèmes de stockage d'énergie hybrides situés à proximité immédiate. L'approche proposée est basée sur des boucles de contrôle en cascade. Les boucles de contrôle internes régulent les courants des convertisseurs à l'aide de techniques de linéarisation des entrées-sorties, garantissant une réponse dynamique rapide et robuste. Les boucles de contrôle externes gèrent des objectifs de plus haut niveau tels que l'énergie du bus CC et l'état de charge des dispositifs de stockage individuels.

Une des principales originalités de cette stratégie réside dans sa formulation générique, qui établit une relation bijective entre les objectifs contrôlés et la puissance fournie. Cela permet d'étendre l'approche à un nombre arbitraire de technologies de stockage sans modification fondamentale de la structure de contrôle. En conséquence, la stratégie est adaptable à diverses configurations de systèmes et à des environnements technologiques en constante évolution.

Dans ce cadre hiérarchique, la répartition de la puissance suit naturellement les caractéristiques dynamiques intrinsèques de chaque dispositif de stockage. Les supercondensateurs absorbent les fluctuations rapides de puissance et atténuent les perturbations transitoires, les batteries gèrent les variations d'énergie à moyen terme et les piles à combustible fournissent l'énergie nécessaire à long terme dans les limites de leur dynamique. Ce fonctionnement coordonné améliore la régulation de la tension, réduit la contrainte sur les composants individuels et contribue à prolonger la durée de vie globale du système.

La stratégie de contrôle centralisé proposée est validée par des études de simulation approfondies et des tests expérimentaux menés sur un banc d'essai de micro-réseau CC à l'échelle du laboratoire. Les résultats démontrent une régulation précise de la tension du bus CC, un partage harmonieux de la puissance entre les dispositifs de stockage et un contrôle efficace des trajectoires d'état de charge dans divers scénarios de fonctionnement, y compris les variations de charge et l'intermittence des énergies renouvelables.

Reconnaissant les limites du contrôle centralisé en termes d'évolutivité, de dépendance à la communication et de vulnérabilité aux points de défaillance uniques, cette recherche propose en outre une stratégie de contrôle coopératif distribué pour les micro-réseaux CC avec des unités de production dispersées géographiquement. L'approche proposée repose sur la théorie des graphes et les algorithmes de consensus distribués, permettant aux contrôleurs locaux

d'échanger des informations limitées avec les unités voisines.
L'objectif de la stratégie coopérative distribuée est de parvenir à un partage proportionnel du courant et à une régulation moyenne de la tension sans s'appuyer sur une référence globale ou un superviseur centralisé. En combinant un comportement de type droop avec des termes de correction basés sur le consensus, le contrôleur distribué assure un fonctionnement coordonné tout en préservant l'autonomie locale et en réduisant les besoins en communication.
L'analyse de stabilité et les résultats de simulations approfondies et validées sur la plateforme HIL démontrent la robustesse de la stratégie coopérative distribuée en cas de variations de charge, de retards de communication et de défaillances de liaison. Par rapport au contrôle conventionnel de type statisme, l'approche proposée améliore considérablement la précision de la régulation de tension et les performances de partage de courant tout en renforçant la résilience du système. Cette stratégie distribuée offre une solution évolutive et tolérante aux pannes, bien adaptée aux micro-réseaux CC isolés fonctionnant avec une infrastructure de communication limitée.

Au niveau tertiaire, la recherche porte sur la gestion de l'énergie dans les micro-réseaux CC interconnectés, également appelés systèmes multi-micro-réseaux. Dans de telles configurations, la coordination entre plusieurs micro-réseaux autonomes permet le partage des ressources et améliore les performances globales du système. Un cadre de gestion coopérative de l'énergie est proposé, combinant un contrôle fonctionnel prédictif avec des mécanismes d'échange d'énergie distribués.
La prévision de la demande de charge et de la production d'énergie renouvelable permet d'anticiper les déséquilibres énergétiques, tandis que les techniques de contrôle prédictif garantissent une régulation précise de l'état de charge des batteries. L'algorithme d'échange d'énergie proposé permet aux micro-réseaux de partager l'énergie excédentaire en fonction des conditions locales, des niveaux de consommation et des états de stockage, tout en préservant leur autonomie opérationnelle.
Les résultats de la simulation confirment que la gestion coopérative de l'énergie améliore l'efficacité globale, réduit les restrictions énergétiques et renforce la résilience face aux perturbations locales. Cette approche illustre le potentiel des communautés énergétiques décentralisées dans lesquelles les micro-réseaux collaborent pour obtenir des avantages collectifs sans sacrifier la stabilité individuelle.
En conclusion, cette thèse apporte une contribution cohérente, complète et scientifiquement fondée au contrôle et à la gestion énergétique des systèmes de micro-réseaux CC distribués. En

intégrant un contrôle hiérarchique centralisé, des stratégies coopératives distribuées et une gestion énergétique prédictive de niveau tertiaire, le cadre proposé répond aux principaux défis liés à l'intégration des énergies renouvelables, à la coordination du stockage et à l'évolutivité du système. Les résultats sont particulièrement pertinents pour les applications rurales et agricoles, offrant des solutions pratiques pour parvenir à une autonomie énergétique durable dans des environnements isolés.

Table of Contents

1. Declaration of Authorship 1
2. Thesis's Framework 2
3. Acknowledgment 3
4. Abstract 4
5. Résumé 5
Table of Contents 11
6. List of Abbreviations 14
7. List of Figures 16
8. List of tables 18
Introduction 19
1. General background 19
2. Objectives and Contribution of the Thesis 21
3. Thesis Outline 22
CHAPTER 1. State of the Art Review 24
1.1 Introduction 24
1.1.1 Evolution of electrification rate in rural areas 24
1.1.2 Accomplishments of the PERG 25
1.1.3 Use of electricity in rural areas 26
1.1.4 PERG action plan for 2023-2025 26
1.1.5 Origin and structure of Moroccan energy mix 26
1.2 Analysis of the Moroccan energy context on farms 27
1.2.1 Energy needs and sources 28
1.2.2 Public policies and pilot projects 28
1.2.3 Potential solutions 29
1.3 The challenge of energy in Africa 29
1.4 Microgrids' Structures and Components 30
1.4.1 Different microgrids' architectures 30
1.4.2 Components of microgrids 33
1.5 Review on microgrids control strategies 36
1.6 Additional microgrids issues 43
1.7 Conclusion 43
CHAPTER 2. A Generic and Hierarchical Approach for Energy Management in HESS based DC Microgrid 44
2.1 Introduction 44
2.2 Proposed strategy 47
2.2.1 Scope and objectives of the strategy 47
2.2.2 Design of the inner loop 49

2.2.3 Design of the outer loop and objective definition 51
2.3 Controls parameter sizing 57
2.3.1 Trajectory filter parameters ξf and $\omega f, k$ 57
2.3.2 input/output linearization control parameters $\boldsymbol{\xi}$ and $\boldsymbol{\omega k}$ 59
2.4 Implementation and test bench 59
2.4.1 Experimental set up and test bench 59
2.4.2 Normal mode 63
2.4.3 Overcharge mode 64
2.4.4 Regenerative mode 65
2.5 Conclusion 67
CHAPTER 3. A Control Strategy for DC Microgrids with Integrated Distributed Generators 68
3.1 Introduction 68
3.2 Theoretical Foundations of Distributed Control 72
3.2.1 Graph Theory 72
3.2.2 Distributed Consensus Protocol 73
3.3 DC microgrid configuration 73
3.4 Proposed Distributed Cooperative Control strategy 74
3.4.1 Control objectives 74
3.4.2 The proposed controller 75
3.4.3 Steady state analysis 77
3.4.4 Voltage and current loops control 78
3.4.5 Stability analysis 80
3.5 Simulation results 82
3.5.1 Comparison between Classic Droop Control and the proposed controller 83
3.5.2 Effect of common load changes on the common DC bus 84
3.5.3 Effect of local load changes on the local buses 86
3.5.4 Communication failure assessment 87
3.5.5 Performance evaluation under communication delays 88
3.6 Conclusion 90
CHAPTER 4. Cooperative Tertiary Control for Energy Management in Multi DC Microgrids 92
4.1 Introduction 92
4.2 Energy Management Strategy 95
4.3 Simulation results 99
4.4 Conclusion 104
General Conclusions and Perspectives 106
Appendix A 108
1. convergence of the sum of ykt 108

2. Convergence to $v*$ demonstration 108
Appendix B: 115
Author's publications 116
References 117

6. List of Abbreviations

PERG	Programme d'Electrification Rural Global
ONEE	Office National d'Eau et d'Electricité
MASEN	Moroccan Agency for Sustainable Energy
IEA	International Energy Agency
RES	Renewable Energy Source
DGU	Distributed Generator Unit
MG	Microgrid
DC	Direct Current
AC	Alternative Current
ESS	Energy Storage System
HESS	Hybrid Energy Storage System
PV	Photovoltaic
WT	Wind Turbine
FC	Fuel Cell
SC	Supercapacitor
LED	Light-Emitting Diode
CPL	Constant Power Load
PCC	Point of Common Coupling
MPPT	Maximum Power Point Tracking
MPC	Model Predictive Control
PFC	Predictive Functional Control
PI	Proportional Integral

SPoF	Single Point of Failure
IC	Incremental Cost
PnP	Plug-and-Play
LV	low voltage
MV	medium voltage
OCV	open circuit voltage
BMS	Battery Management System
SoH	State of Health
PWM	Pulse Width Modulation
TRL	Technology Readiness Level
DGs	Distributed Generators
MAS	Multi Agent System
GPC	Generalized Predictive Control
PCM	Parallel Connected Microgrids
GSIM	Grid Series Interconnected Microgrids
MPSC	Mixed Parallel-Series Connection
RMSE	Root-Mean-Square Error
IEA	International Energy Agency
RES	Renewable Energy Source
DGU	Distributed Generator Unit

7. List of Figures

Figure 0-1 : Evolution of the global energy mix between 2017 and 2050 in the energy transition scenario [1] 19
Figure 0-2: Historical development of microgrids [2] 20
Figure 1-1: Cumulative rural electrification rate in Morocco (2011-2022) [9] 25
Figure 1-2: Distribution of national electricity production by energy source (2022) [12] 27
Figure 1-3: Electricity generated in TWh by energy source in 2018 [18] 30
Figure 1-4: Radial architecture of a DC microgrid 31
Figure 1-5: Ring architecture of a DC microgrid 32
Figure 1-6 : Mesh architecture of a DC microgrid 32
Figure 1-7 : Effect of irradiance and temperature on the I-V and P-V curves of a PV module [25] 33
Figure 1-8: Topologies of HESS: (a) passive, (b-c) semi-active, (d) active 36
Figure 1-9 : Microgrid energy management levels [34] 37
Figure 1-10 : Control structures of the primary (with two tiers controllers) and secondary levels. 38
Figure 1-11 : Centralized control topology [48] 40
Figure 1-12 : Decentralized control topology [48] 40
Figure 1-13 : Distributed control topology [48]. 41
Figure 1-14 : Control structure of the tertiary level. 42
Figure 2-1 : Power allocation using filtering approach 45
Figure 2-2: Adaptive power allocation using artificial potential field [63] 46
Figure 2-3 : A proposed energy management strategy using wavelet fuzzy logic control [65] 46
Figure 2-4: Structural architecture of a DC microgrid integrating several storage systems and sources 48
Figure 2-5: Diagram of Ragone [68] 48
Figure 2-6: Bidirectional converter diagram 49
Figure 2-7 : Control block related to the first objective 53
Figure 2-8 : Electrical diagram of the supercapacitor 54
Figure 2-9 : Control block related to the second objective 55
Figure 2-10: Control block related to the third objective 57
Figure 2-11: Evolution of fuel cell power and current derivative 59
Figure 2-12 : FC static characteristic $vfc = f(ifc)$ 60
Figure 2-13 : Architecture of the studied microgrid 61
Figure 2-14 : Experimental testbench 61
Figure 2-15: Real-time control setup 62
Figure 2-16 : Normal mode – power allocation 63
Figure 2-17 : Normal mode – objectives regulation 64
Figure 2-18 : Overcharge mode – power allocation 65
Figure 2-19 : . Overcharge mode – objectives regulation 65
Figure 2-20 : Overcharge mode – power allocation 66
Figure 2-21 : Overcharge mode – objectives regulation 67
Figure 3-1 : Conventional droop controller 69
Figure 3-2 : Principle of distributed hierarchical control strategy used in [79] 71
Figure 3-3 : The proposed unified distributed cooperative strategy in [81]. 72
Figure 3-4 : The considered DC microgrid architecture 74

Figure 3-5 : Communication layer related to the considered electrical grid 74
Figure 3-6 : Multi-layer diagram of the proposed strategy 77
Figure 3-7 : Boost converter..... 79
Figure 3-8 : Eigenvalues evolution of the system under local load variation 82
Figure 3-9 : Movement of the poles of the system during an increase of α from 40 to 400 82
Figure 3-10 : Comparison of the proposed cooperative control with the conventional droop control..... 84
Figure 3-11 : Response of the DC microgrid under common load variation 85
Figure 3-12 : Evolution of droop gains and state variables during common load variation 86
Figure 3-13 : Response of the DC microgrid under local loads' variation..... 87
Figure 3-14 : Evolution of voltages and currents under link 2-3 communication failure 88
Figure 3-15 : Evolution of voltages and currents under communication delay of 15 ms 89
Figure 3-16 : Evolution of voltages and currents under communication delay of 30 ms 90
Figure 4-1 : a) the PCM, b) GSIM, and c) MPSC 94
Figure 4-2 : ARIMA-based data prediction framework 96
Figure 4-3 : Microgrid configuration and control strategy..... 96
Figure 4-4 : Battery current regulation via PFC and predictive estimation 97
Figure 4-5 : An energy management algorithm for the studied MMGs 99
Figure 4-6 : PV production and consumption profiles for the considered MGs 100
Figure 4-7 : Simulation results for each MGs using the PFC and PI controllers 101
Figure 4-8 : Zoomed-in comparison of battery current tracking performance between PFC and PI controllers over the time interval between 10 h and 11 h..... 102
Figure 4-9 : SoC values with and without energy exchange 103
Figure 4-10 : Power exchanged between MGs..... 104

8. List of tables

Tableau 1-1 : Daily electricity consumption by agricultural use..... 28
Tableau 2-1 : System and control parameters..... 62
Tableau 3-1 : System and Controller parameters 83

Introduction

1. General background

The global energy transition is a major strategic challenge for the coming decades. Faced with the gradual depletion of fossil fuel resources and the urgency of climate change, electricity systems must evolve towards more advanced, flexible and resilient architectures, integrating Renewable Energy Sources (RES) on a massive scale. This development is part of an overall scenario aimed at transforming the energy mix by 2050, with a growing share of electricity coming from renewable sources, as illustrated in Figure 0-1, where the share of RES in electricity rises from 25% in 2017 to 86% in the target scenario [1].

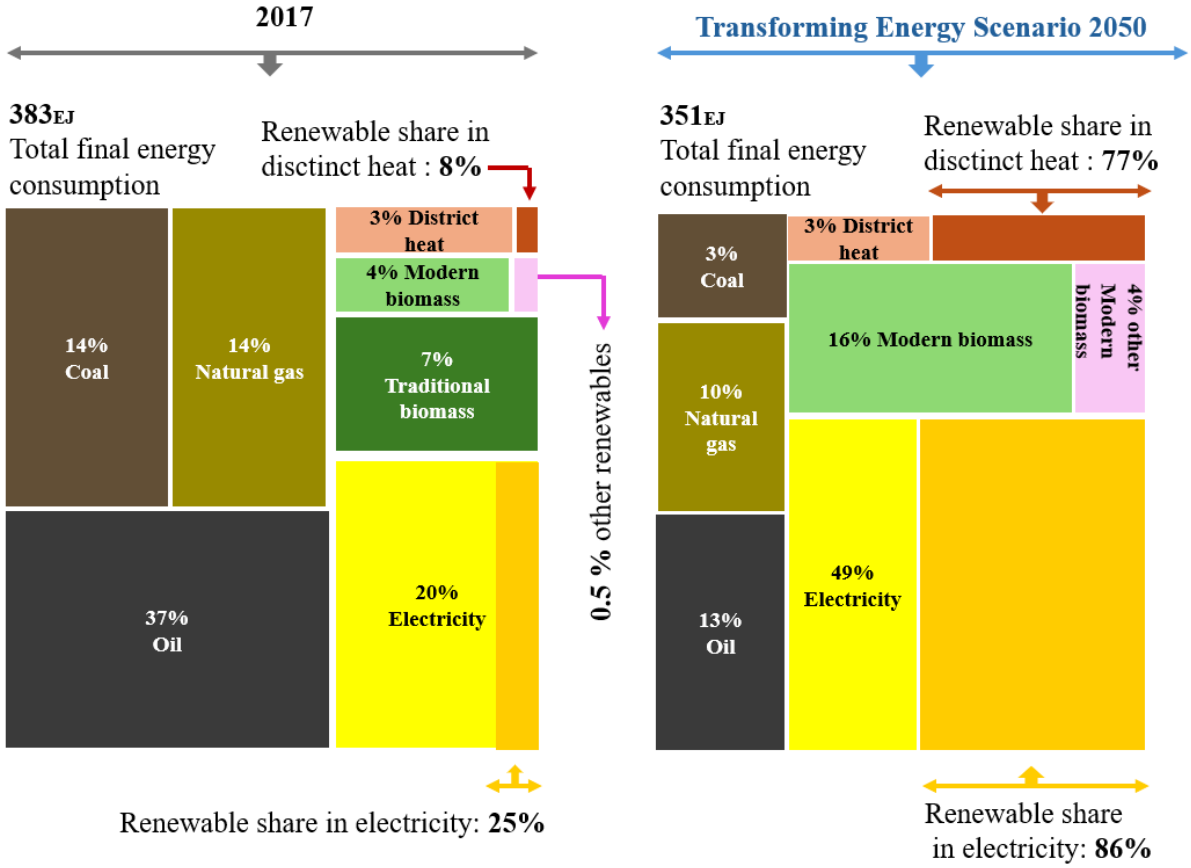

Figure 0-1 : Evolution of the global energy mix between 2017 and 2050 in the energy transition scenario [1]

Against this backdrop, the microgrid concept has gradually emerged as a key component of smart grids. As Figure 0-2 shows, the evolution of microgrids has been structured around major phases: cogeneration in the 1980s, isolated systems in the 1990s, island expansion in the 2000s, and then approaches focusing on energy resilience from the 2010s onwards [2].



Figure 0-2: Historical development of microgrids [2]

Initially, microgrids were deployed in industrial or military contexts requiring a reliable and continuous local power supply (such as naval bases or hospitals). The increased penetration of distributed renewable energies (particularly photovoltaics) from the 2000s onwards has encouraged their adoption in civilian contexts, particularly in isolated areas, university campuses, critical sites or island territories [2]. Their ability to operate in grid-tied or island mode represents a major advance in terms of resilience and energy independence.

Designed to operate autonomously or in interaction with the main grid, microgrids enable the coordinated integration of Distributed Generation Units (DGUs), local storage devices and specific loads within a geographically restricted perimeter. This ability to maintain the production-consumption balance, while guaranteeing stability and continuity of service, makes them a preferred solution for isolated areas, critical installations or environments with a high penetration of intermittent RES [3].

Among the most notable developments, direct current microgrids (DC MGs) have attracted growing interest due to their structural and functional advantages. Unlike traditional AC MG architectures, DC MGs eliminate unnecessary AC/DC conversions, facilitate the direct integration of photovoltaic (PV) sources, batteries or supercapacitors, and simplify grid control by eliminating frequency or reactive power management. These characteristics make them particularly suitable for installations with exclusively DC consumption, as well as in contexts where conversion losses need to be reduced to a minimum [4].

The role of Energy Storage Systems (ESSs) is fundamental. Not only do they ensure continuity of supply by compensating for the intermittency of RES, it also dynamically stabilizes the microgrid in the face of load variations. The most advanced architectures adopt Hybrid Energy Storage Systems (HESS) - combining batteries and supercapacitors, Fuel Cells for example - to respond effectively to energy dynamics on different timescales [5].

Microgrids are particularly promising in rural areas, where traditional grid infrastructure is either non-existent or unreliable. By using locally available renewable and storage resources,

microgrids offer a route to energy autonomy and self-sufficiency. Rural areas often face challenges, such as the high cost of electricity, limited grid accessibility and unreliable energy supplies, all of which can hinder economic and social development. Microgrids can address these challenges by enabling communities to produce and manage their own energy, reducing dependence on centralized grids and building resilience.

Aggregating several microgrids into distributed microgrid systems further enhances their flexibility and scalability, enabling the integration of additional energy producers and consumers in a "plug-and-play" approach. This distributed architecture has the potential to revolutionize modern energy systems, paving the way for decentralized power grids [6].

Therefore, in a context where DC microgrids are becoming fundamental building blocks of decentralized energy systems, it is essential to equip these architectures with advanced control strategies capable of responding to both local constraints (sources and loads demand variability, ESSs dynamics) and global requirements (stability, resilience, inter-MG coordination). The development of such strategies, combining power allocation, cooperative approaches, and operational autonomy, is today an essential lever for guaranteeing reliable, optimized and sustainable energy management, particularly in isolated areas or areas with poor connections to centralized grids. It is precisely in this context that this research is being carried out.

2. Objectives and Contribution of the Thesis

The overall objective of this thesis is to design, model and validate advanced control strategies for direct current (DC) microgrids, in response to the specific needs of isolated rural areas with low energy density. In such a context, the challenge is to guarantee autonomous, efficient and reliable operation of an energy system based essentially on local renewable sources and distributed storage devices, without permanent access to a main electricity grid.

The problem lies at the intersection of several major scientific and technological barriers:

- Local energy autonomy, conditioned by efficient coordination between sources, loads and storage devices, despite the intermittent nature of the resources.
- The stability of the DC microgrid, particularly the regulation of the common bus voltage, subject to load variations and the heterogeneity of equipment.
- The absence of a central supervisor or global communication channel necessitates distributed control, while ensuring cooperative behavior among DGUs.

- Optimization of energy flows on the scale of several microgrids, particularly with a view to aggregation (multi-microgrids), to maximize collective autonomy and share resources.

3. Thesis Outline

To meet these challenges, this thesis adopts a progressive approach based on the following chapters:

Chapter 1 begins with an in-depth analysis of the energy context in rural areas, with a particular focus on Morocco and, more broadly, sub-Saharan Africa, where electrification remains a fundamental lever for development. Then, it provides an in-depth review of the state of the art in microgrids, focusing on DC architecture, energy storage devices and the various control layers (primary, secondary and tertiary). This framework clearly positions the objectives of the thesis.

Chapter 2 introduces a centralized hierarchical control strategy for DC microgrids, integrating several storage technologies (batteries, supercapacitors, fuel cells, etc.). The aim is to stabilize the DC bus voltage while dynamically distributing the loads according to the capacity and dynamics of each source. The chapter formalizes the associated control laws and validates the strategy by simulation and experimentation.

Chapter 3 proposes a robust distributed control approach, based on a local exchange of information between decentralized generation units. This strategy enables proportional current sharing and average voltage regulation, without the need for a global reference or ubiquitous communication. Simulations are carried out to assess the resilience of the system to disturbances such as load variations or communication failures.

Chapter 4 presents a holistic control approach dedicated to energy management in multi-DC MGs. The strategy developed is based on a predictive controller to regulate the state of charge (SoC) of batteries. At the inter-microgrid scale, a distributed power exchange algorithm is introduced to coordinate energy flows in a cooperative manner. Simulations show the performance of the proposed strategy in terms of optimizing resources and reducing energy losses.

Finally, a general conclusion concludes this work by summarizing the main scientific contributions of the thesis. It puts the results obtained into perspective and suggests several avenues for future research.

CHAPTER 1. State of the Art Review

The aim of this chapter is to provide an in-depth literature review on DC microgrids from a technical point of view. It begins with an analysis of the specific context of this thesis project, emphasizing rural electrification and its implications within the Moroccan context, while also extending the discussion to the broader African level. The aim is to place energy issues in their territorial, social and agricultural dimensions. The chapter then explores decentralized solutions, in particular microgrids, using concrete examples from projects carried out in Morocco, as well as comparisons with other African countries. Finally, a review of the technical literature on DC microgrids is presented, covering their various topological configurations, main components and control strategies. The existing architectures and components of a DC microgrid are first described, highlighting the specific features for each one of them.

1.1 Introduction

1.1.1 Evolution of electrification rate in rural areas

Morocco has seen enormous progress in rural electrification since the launch of the Programme d'Électrification Rurale Globale (PERG) in 1996. This program is based on a participatory financing model involving ONE (Office National d'Electricité), local authorities and beneficiary households. For grid electrification projects, local authorities contribute up to 2 085 DH per household, either in a single payment or in annual payments of 500 DH for 5 years. Households contribute 2 500 DH, paid either at the time of subscription or in monthly sections of 40 DH over 7 years. The ONEE provides additional funding, covering 55% of the total investment.

Under this program, 41,649 villages have been connected, representing more than 2.15 million households and around 13 million people [7]. The rural electrification rate rose from 18% in 1995 to 99.89% in 2024, according to official ONEE statistics [8]. Figure. 1-1 shows the evolution, between 2011 and 2022, of the rural electrification rate in Morocco. This rate has risen steadily, from 96.8% in 2011 to 99.86% in 2022.

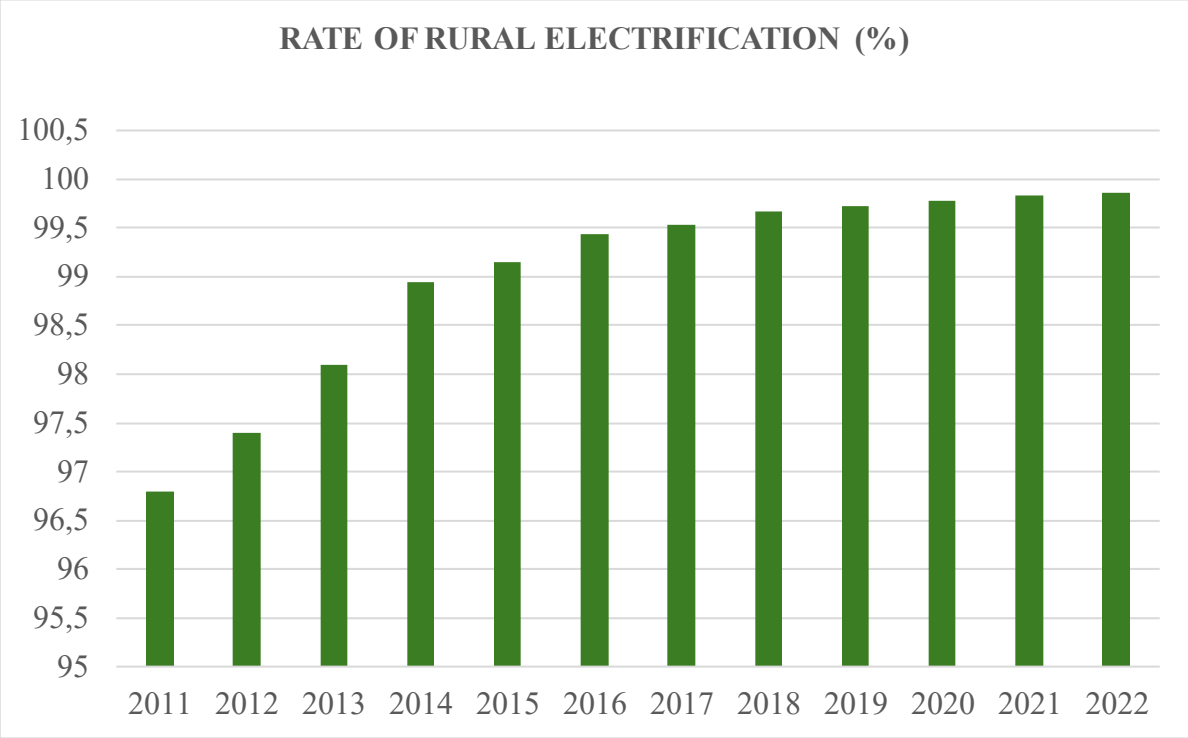

Figure 1-1: Cumulative rural electrification rate in Morocco (2011-2022) [9]

1.1.2 Accomplishments of the PERG

Alongside conventional connections, decentralized solutions have been implemented, in particular the installation of individual PV kits. These provide electricity to:

- 51 559 households in 3 663 villages between 1998 and 2009. However, due to strong local demand and the extension of the grid, 3 505 of these villages (i.e. 50 086 households) were subsequently rescheduled for conventional connection [9].
- 19 438 households in 900 villages, as part of a solar project supported by the National Initiative for Human Development (INDH) between 2015 and 2018 [9].

In total, an estimated 12.8 million people will benefit from the PERG.
In terms of infrastructure, the program has enabled the construction of:

- 50 356 km of medium-voltage (MV) lines,
- 134 744 km of low-voltage (LV) lines,
- 25 503 transformer stations, with a total capacity of 1 957 MVA [9].

1.1.3 Use of electricity in rural areas

In rural areas of Morocco, electricity is mainly used for essential domestic needs, such as lighting, televisions and recharging mobile phones, as well as for refrigeration in some cases (particularly with 200 Wp kits). Electricity can also be used to equip community infrastructures, such as schools, health centers and mosques. Although decentralized electrification solutions have been designed to supply certain agricultural uses (pumping, small equipment), these applications remain relatively limited within the specific framework of the PERG. However, complementary programs, such as the national initiatives to promote solar pumping, have made it possible to gradually extend these uses to the agricultural sector".

1.1.4 PERG action plan for 2023-2025

The PERG action plan for the period 2023-2025 provides for the electrification of 570 villages, representing around 13 300 households, as well as the electrification of 1 950 schools and 800 mosques, for an overall budget estimated at 598 million dirhams MDH, approximately 59 million $ [10].

1.1.5 Origin and structure of Moroccan energy mix

In December 2015, Morocco strengthened its energy strategy by setting itself more ambitious targets, aiming to increase the share of renewable energies to 52% of the national electricity mix by 2030 [11]. The goal set for 2020 has not yet been fully achieved, according to data for 2022 available in [12], which shows that the installed capacity of 831 MW, being 7.5% of total national electricity capacity and 20% of renewable energy capacity. In terms of production, solar energy accounted for 3.5% of national electricity production, with Moroccan Agency for Sustainable Energy (MASEN) (85%) and ONEE (15%) making the bulk of the contribution. As for wind power, the installed capacity in 2022 reached 1 590 MW, making a significant advance on the initial target of 2 000 MW.

These commitments are in line with the country's climate policy, which aims to reduce greenhouse gas emissions by 42% by 2030 [11].

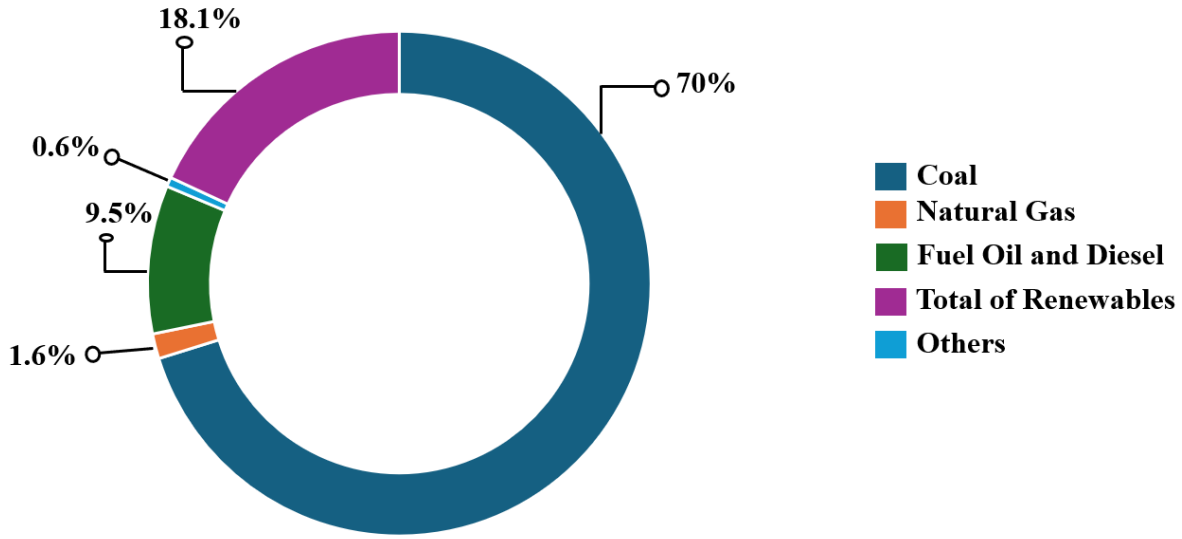

Figure 1-2: Distribution of national electricity production by energy source (2022) [12]

Figure 1-2 shows the allocation of national electricity generation by energy source in 2022 and highlights the efforts underway to diversify the energy mix and integrate a growing share of renewable energies (hydro, solar and wind).

Although Morocco has a rural electrification rate of 99.86%, agricultural areas still suffer from inadequate energy access, especially for productive uses. Many farms are either not connected to the grid or are partially powered by diesel generators, resulting in high costs and significant pollution [13].

1.2 Analysis of the Moroccan energy context on farms

The sector of agriculture in Morocco accounts for around 14% of National Gross Domestic Product (GDP), employs more than 40% of the working population and affects more than 80% of the population in rural areas. It plays a key role in the country's food security, regional development and socio-economic stability.

The agricultural sector is also directly affected by the energy transition, particularly through the increasing use of renewable energies. Programs, such as solar pumping, have enabled more than 30 000 farms to be equipped with photovoltaic irrigation systems in 2029 [14].

These factors fully justify the opportunity to integrate renewable energies into the agricultural sector, through local solutions, such as intelligent microgrids, in line with pilot projects such as MG-FARM[1].

[1] https://www.leap-re.eu/mg-farm/

1.2.1 Energy needs and sources

The energy needs of Moroccan farms are closely linked to essential production activities, such as irrigation, conservation and crop management.

A case study of a 37-hectare farm at Ribat El Kheir in the province of Sefrou shows typical consumption as follows [15] in Table 1-1:

Table 1-1 : Daily electricity consumption by agricultural use

Farming use	**Average daily consumption**
Water pumping (irrigation)	113 kWh/day
Cooling rooms	379 kWh/day
Administration (offices)	

This farm is supplied by a hybrid solution comprising 15 kW of PV panels, a 100-kW wind turbine and 40 kW power converters, all connected to the conventional grid. In this system, 81% of the electricity comes from local renewable sources (including 73% from wind and 8% from solar), and 19% is supplied by the grid. No diesel generator is used in the optimal solution. As far as storage is concerned, batteries (2 V, 1000 A.h) are used as back-up to store excess energy when production exceeds demand. However, the study shows that in a system connected to the grid, the economic interest of storage is limited, particularly in the absence of a policy of injecting energy into the grid.

The analysis of the agricultural farm at Ribat El Kheir highlights the scale of energy needs associated with productive uses, such as pumping and refrigeration, as well as the limitations of conventional supplies in rural areas, even those partially connected to the grid. This study underlines the need for more flexible and sustainable energy solutions, capable of meeting the specific needs of agricultural activities. This is the background to the MG-FARM project, which proposes an integrated approach combining renewable energies, energy storage and advanced energy management strategies including energy sharing aspects [16].

1.2.2 Public policies and pilot projects

Among the projects that have been developed as part of the policy of sustainable electrification of agricultural areas, the MG-FARM project is a benchmark pilot experiment. Organized by a Euro-Moroccan consortium as part of the LEAP-RE program (Horizon 2020), this project aims to demonstrate the feasibility of intelligent microgrids tailored to the specific needs of the

agricultural sector in rural areas. Two Moroccan farms[2] have been selected as demonstration sites: BLFARM (located in Saniat Berguig, Sidi Bennour), connected to the electricity grid, and RIMSAR (in Oulad Sbih, El Kelaâ des Sraghna), in an off-grid configuration. These farms have been equipped with RES (PV) and storage systems (batteries), and intelligent management platforms, powered by IoT sensors and cloud algorithms [13].

The project arose in response to several structural limitations faced by agricultural farms: dependence on diesel, the lack of a reliable connection to the conventional grid, the intermittency of renewable energies, and the impossibility of injecting or reselling surplus electricity produced locally. In addition, the high costs of storage systems, particularly those based on hydrogen, make it difficult to recover on a single farm scale. To address these challenges, MG-FARM is proposing a sustainable technical and economic alternative dedicated to agricultural needs [17].

1.2.3 Potential solutions

Faced with the limitations encountered on rural farms - particularly the diversity of energy requirements and needs, the absence of an energy resale policy, and the difficulties of accessing the grid - the MG-FARM project recommends several concrete avenues. The first is to pool energy infrastructures through community microgrids grouping together several farms (between 5 and 35 depending on the study), which would make it possible to amortize heavy equipment (electrolysis, hydrogen storage) while strengthening the resilience of the system [13]. Secondly, the integration of intelligent energy management systems is crucial. The data collected in real time (irradiation, temperature, humidity, consumption) should drive energy production and distribution according to agricultural cycles (irrigation, refrigeration, product processing). This approach made possible by a cloud platform and IoT sensors, optimizes the overall performance of the microgrid while reducing losses.

1.3 The challenge of energy in Africa

Africa, particularly the sub-Saharan region, is facing a growing demand for electricity, fueled by rapid urbanization, population growth and the need for industrialization. In 2018, nearly 600 million Africans had no access to electricity, more than two-thirds of them in sub-Saharan Africa. At this rate, 90% of the people without electricity in 2030 will be Africans [11]. The African energy mix is still dominated by:

[2] https://eeb.uir.ac.ma/index.php/2023/08/10/mgfarm/

- Gas in North Africa (over 75%),
- Coal in South Africa (around 70%),
- Hydroelectricity in Central and East Africa (over 50%),

as shown in figure 1-3, which compares electricity generation by source in different regions of the continent.

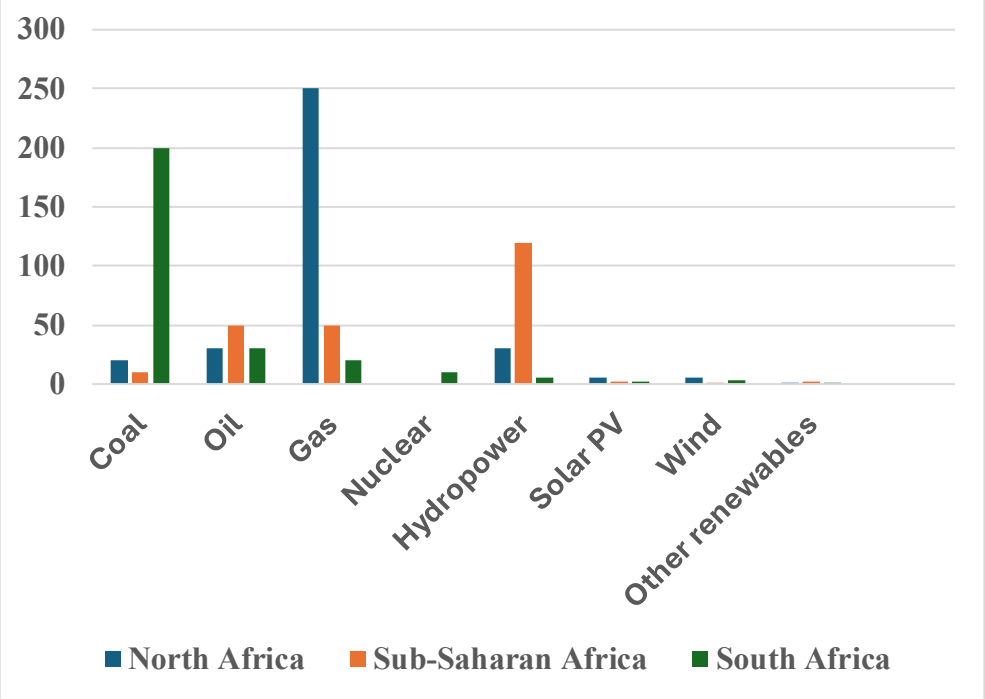

Figure 1-3: Electricity generated in TWh by energy source in 2018 [18]

Having carried out an in-depth analysis of the rural and agricultural energy context, both on a Moroccan and in Africa scale, it is now essential to explore the technical solutions capable of meeting the challenges identified. Among these, energy microgrids are particularly appropriate to isolated or variable-load environments. The following section provides an overview of the state of the art in microgrid structures, their main components and the control strategies deployed to ensure their stability, efficiency and autonomy.

1.4 Microgrids' Structures and Components

1.4.1 Different microgrids' architectures

DC microgrids can be defined as low-voltage power distribution systems that use direct current (DC) as their primary form of electricity. They typically consist of distributed energy sources (DERs) such as (PV) solar panels, fuel cells (FC) and energy storage systems (ESSs), such as batteries and supercapacitors, as well as DC loads. DC microgrids offer several advantages over

alternating current (AC) microgrids, including increased efficiency, reduced control complexity and better integration of RES and storage devices. They can be classified into different structures, depending on how DERs, ESSs and loads are connected. The most common structures are as follows:

• In radial DC microgrid, as depicted in figure 1-4, DERs, ESSs and loads are connected to a central DC bus via DC-DC and eventually AC/DC converters. The energy flows from this central bus and is distributed along lines or branches to supply the loads. It is considered as the simplest and most common DC microgrid structure, because of its easy design and control, but can be vulnerable to failures and voltage problems if a single DC bus fails [19].

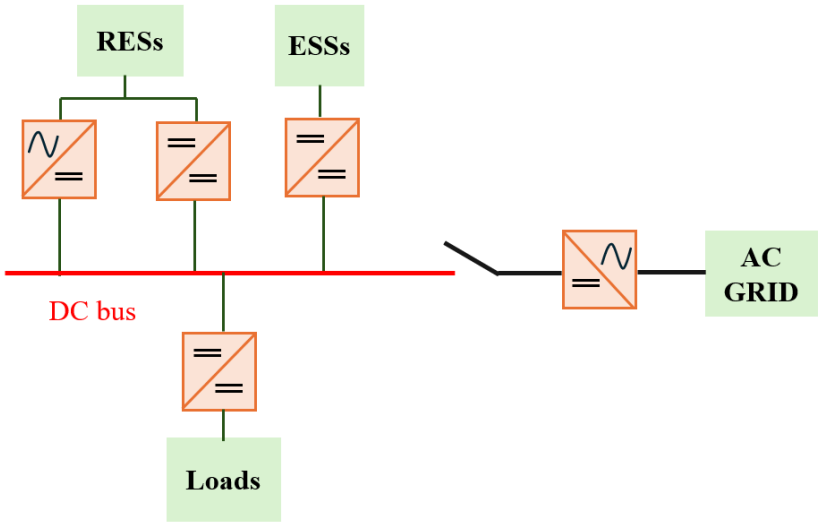

Figure 1-4: Radial architecture of a DC microgrid

•The ring DC microgrid is the configuration where the components of the microgrid are interconnected in a circular manner, as shown in figure 1-5, offering several paths for energy flow. Thus, it offers greater reliability than the radial structure by providing redundant power supply paths, which, in turn, introduces a greater control complexity [20].

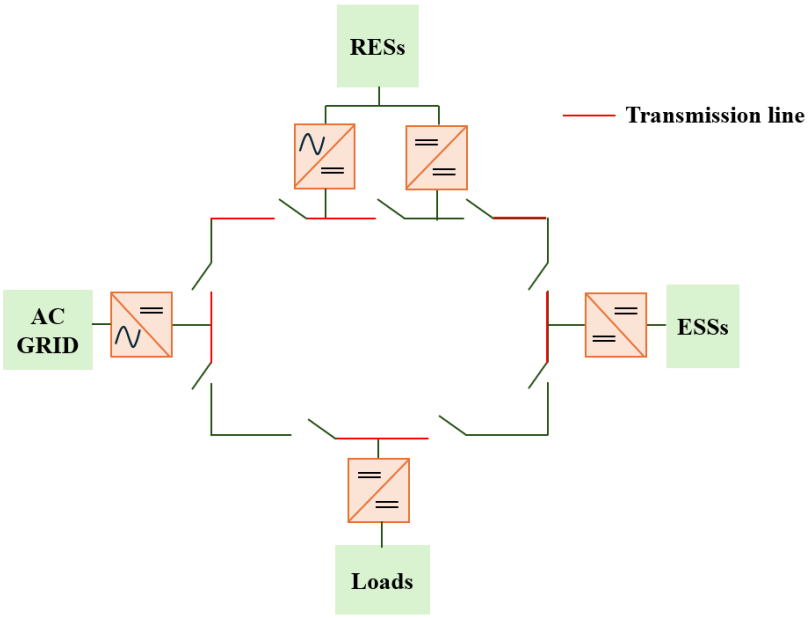

Figure 1-5: Ring architecture of a DC microgrid

Mesh DC microgridis the structure where the microgrid units are interconnected in multiple ways, via dedicated DC lines, forming a kind of "grid" or mesh network, as represented in figure 1-6. This configuration offers high redundancy, good flexibility and resilience, as new devices can be easily added or removed accordingly. However, this complexity leads to higher implementation and maintenance costs [21].

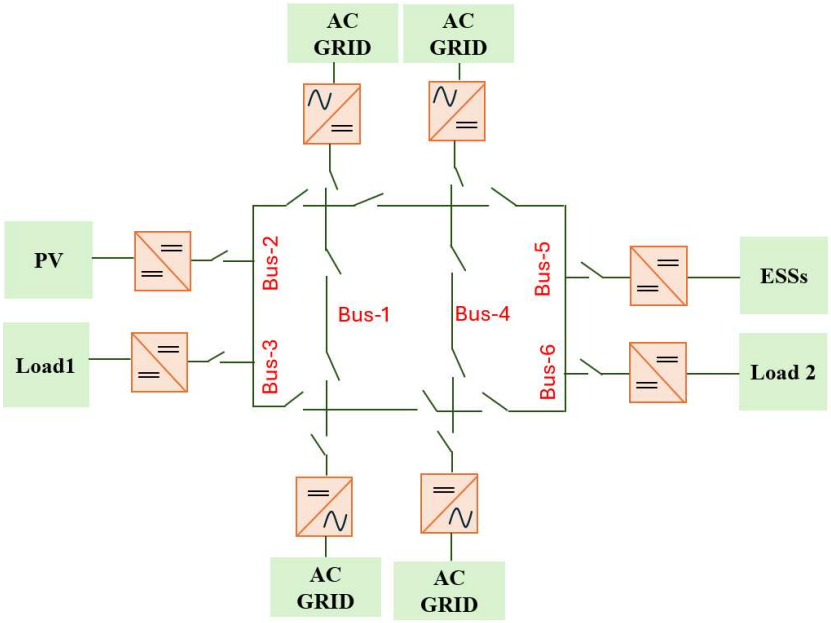

Figure 1-6 : Mesh architecture of a DC microgrid

1.4.2 Components of microgrids

A DC microgrid comprises several key components that work together to generate, store, distribute and manage DC energy. These components include PV solar panels and fuel cells (FCs) as sources and energy storage systems (ESS), such as batteries and supercapacitors, DC loads, power electronics converters and control systems. In what follows, we will go through the definition of each one of the above-mentioned units.

A (PV) solar panel is an energy source that converts solar energy directly into DC electricity using the PV effect. They consist of several PV modules connected in series and/or in parallel to achieve the desired voltage and current levels. The performance of the energy produced depends on sunlight and temperature conditions, which modify their maximum power point as illustrated in figure 1-7 which, indeed, demonstrates that the maximum power point moves upwards as irradiation increases and to the right as temperature rises, affecting then the performance of the PV module.

MPPT (Maximum Power Point Tracking) is a technique used to adjust the PV output voltage in real-time to extract the maximum available power under varying solar irradiance and temperature conditions. Common MPPT techniques include Perturber and Observer (P&O) [22], incremental conductance (InCond) [23], and Fuzzy Logic Control [24].

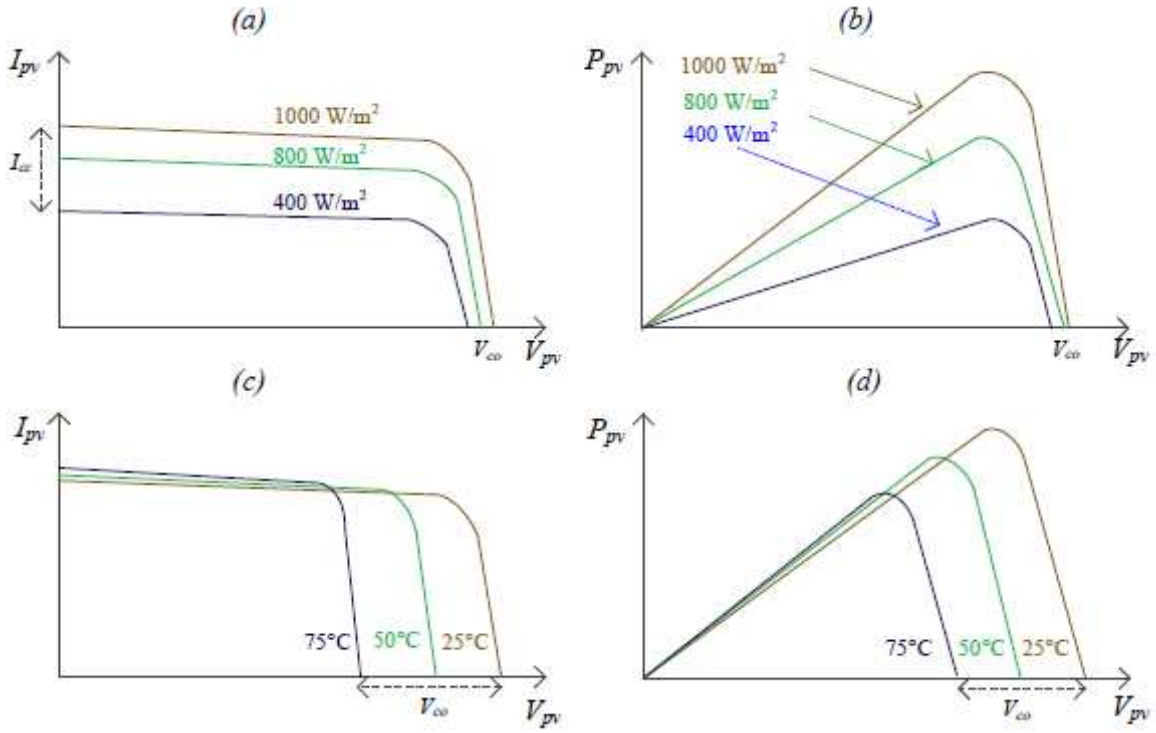

Figure 1-7 : Effect of irradiance and temperature on the I-V and P-V curves of a PV module [25]

A fuel cell is an electrochemical device that directly converts the chemical energy of a fuel (usually hydrogen) and an oxidizer (often oxygen from the air) into electricity using, mainly, water and heat as byproducts. It is an efficient, scalable power source for DC microgrids, as it generates DC current directly [26]. Another advantageous feature is its ability to store a large amount of energy in a small volume compared to other energy storage technologies. However, the FC suffers from a significant drop due to gas exhaustion when handling abrupt load dynamic, making it inappropriate for most applications [27].

Unlike FC, a battery is a device that stores energy in the form of chemical energy and releases it in the form of electricity. It is characterized by its reversible charge/discharge cycles. Compared to FC, batteries offer a medium power density and their response to peak fluctuations is also moderate [28]. In a DC microgrid, this means they can provide sufficient dynamic response to stabilize the DC bus under common load variations. Lithium-ion batteries are widely used in DC microgrids due to their high energy density, long life and low self-discharge rate [29], in comparison to lead-acid batteries, namely the most economical ones.
A supercapacitor is an energy storage device that stores energy electrically in the form of charges separated between two conductive electrodes and an electrolyte. Unlike batteries, supercapacitors are not based on chemical reactions, but on the electrostatic storage of charges, enabling them to charge and discharge much more rapidly. Supercapacitors have several advantageous features, including very high-power density, long lifespan in charge/discharge cycles, and high energy efficiency when absorbing or restituting energy. Supercapacitors play a crucial role in the rapid regulation of the DC bus in microgrids. Indeed, thanks to their ability to deliver high power over very short periods, they can rapidly absorb or supply energy to compensate for voltage fluctuations and maintain DC bus stability as well [30].

A (HESS) is a combination of several energy storage technologies (e.g. batteries, supercapacitors, fuel cells, etc.) combined in a single infrastructure. The main aim is to take advantage of each technology features: one may offer a high energy density to provide sustained power over a long period, while another may have a high-power density to respond rapidly to variations in load or peaks in demand. For example, in a DC microgrid, the three above-mentioned storage units can be combined. The fuel cell provides sustainable energy thanks to its high energy density, the battery ensures moderate storage and voltage stability, while the supercapacitor reacts quickly to handle either peak demand or high regenerative sequence.

DC loads are devices that consume DC power (e.g., LEDs, DC motors, home appliances, inverter). They can be classified as constant power loads (CPL), constant current loads or constant resistance loads. Power electronics converters are interface electronic devices that transform electrical energy from one form to another, adapting voltage, current or frequency to the needs of the connected systems. They are essential for interfacing different components in a DC microgrid, enabling voltage conversion, power flow control and system protection. Common converter topologies include DC-DC converters (buck, boost, buck-boost), DC-AC inverters and AC-DC rectifiers.

In the context of HESS interconnection methods, three types of topologies have been used, namely the passive connection [31], the semi-active connection [32] and the active connection [33]. Each one of these topologies has advantages and limitations in terms of efficiency, dynamic performance, flexibility, cost, etc. In the passive connection, the one shown in figure 1-8(a), energy storage systems are connected directly to the DC bus, suffering from a lack of flexibility and controllability, despite being less costly. In the case of semi-active connection, as depicted in figure 1-8(b,c), only one single storage device is connected to the DC bus via a DC/DC converter, while the other is directly linked to the DC bus. Thus, controllability and flexibility are not fully reached and still need to be enhanced. Finally, with the active connection illustrated in figure 1-8(d) all storage systems are connected to the DC bus via DC/DC converters, resulting in a large controllability and flexibility. Also, by minimizing energy losses during transfers, this topology increases the overall system efficiency while reducing its environmental impact with guaranteeing stable, sustainable operation even in fluctuating conditions due to RESs intermittency.

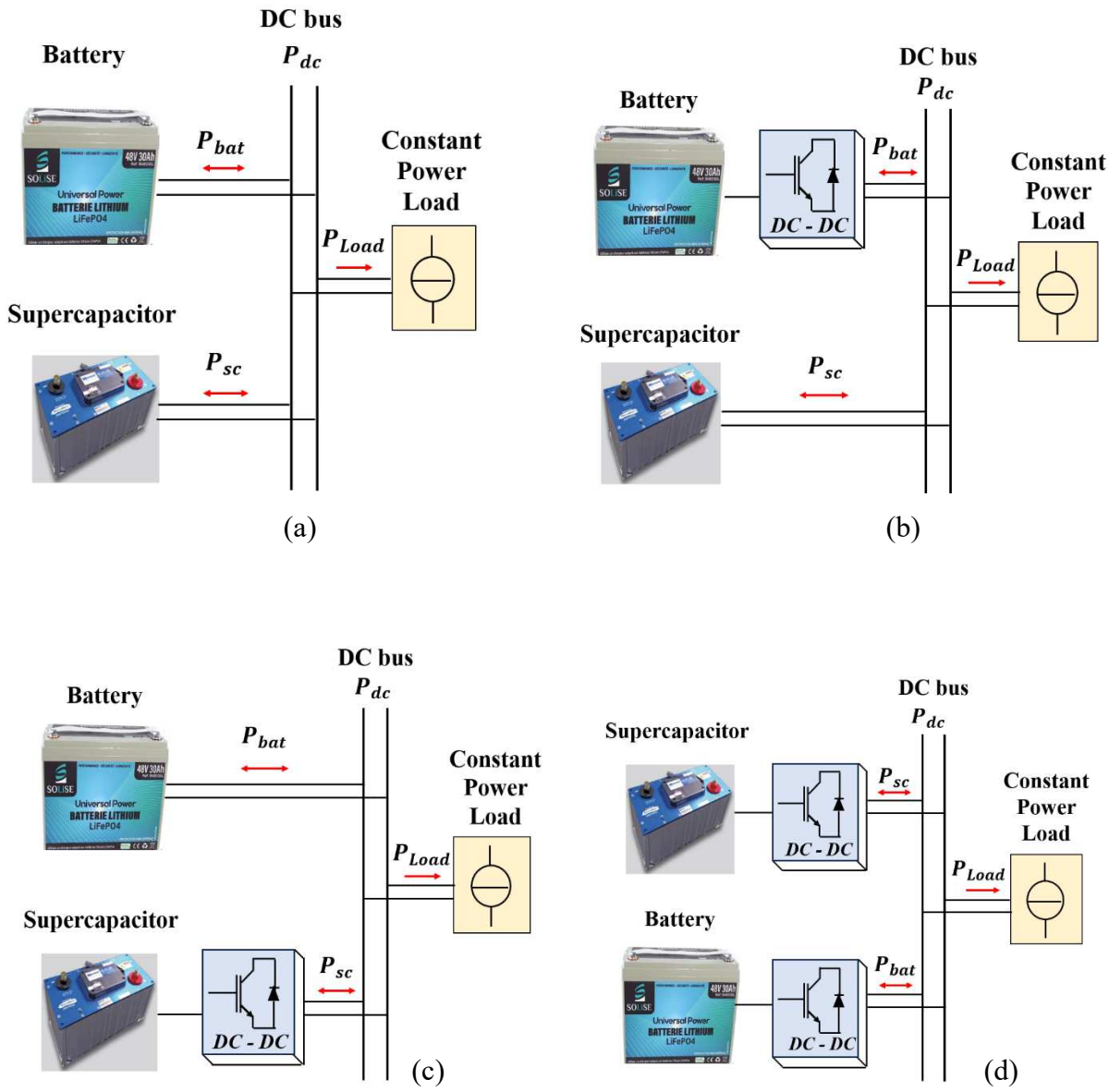

Figure 1-8: Topologies of HESS: (a) passive, (b-c) semi-active, (d) active

1.5 Review on microgrids control strategies

Several research works have highlighted the importance of incorporating control strategies for reliable and robust operation of MG systems taking into consideration the nature of installed RES, storage systems, and their interconnection to the electrical power grid. Fig. 1.9 presents an architecture of MG systems according to each MG system's level. However, the most significant challenge of this new MG system's architecture is the development and the deployment of suitable control strategies. These latter are required for efficient energy balance while ensuring a high level of power quality and favoring the active integration of prosumers in its related emerging electricity market. In addition, within this new MG system architecture,

control strategies must account for multiple disturbance variables and constraints, which manisfist across different time scales. Recently, numerous approaches have been proposed and could be classified according to the MG system's layers, including primary, secondary and tertiary controls. This particular organization is referred to as a hierarchical control approach since the level N computes (according to a certain algorithm or control law) and provides the reference to the level N-1. Each control layer takes in charge different operation objectives with different response time constraints as illustrated on figure 1-9.

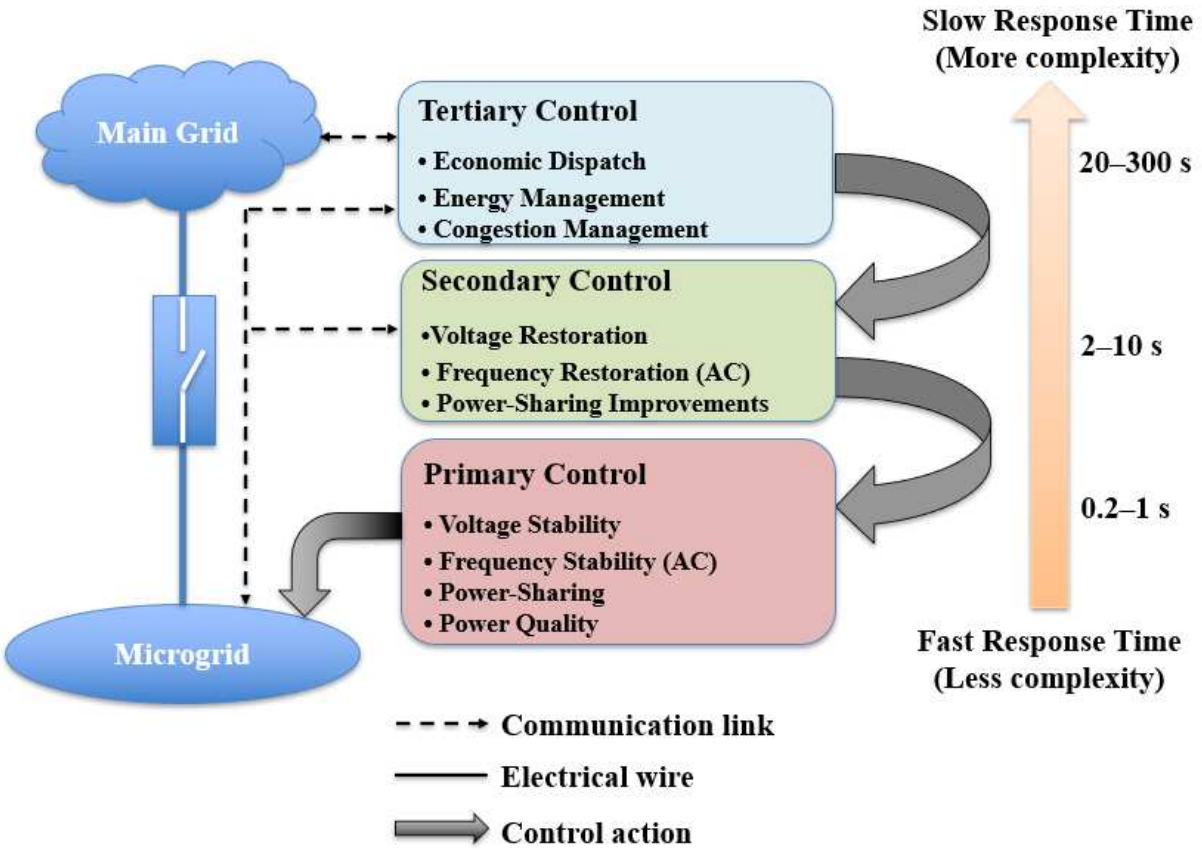

Figure 1-9 : Microgrid energy management levels [34]

As mentioned on figure 1.10, the primary control addresses each DGU output voltage regulation so that it reaches the reference value $v_{o,i}^{ref}$. This may be fulfilled by means of a single layer control (flatness [35], deadbeat [36]) or a two tiers control (linear controller [37,38], sliding mode control [39]) related to a power switching supply (boost, buck…) namely an inner loop that handles the current control (for component protection reason and output voltage stability) and an outer loop that stands for the DGU output voltage control.

Indeed, with the use of interface power converters, this type of control restores frequency for AC microgrid and amplitude of the voltage references feeding the inner current and voltage-control loops and reduces the circulating currents [40].

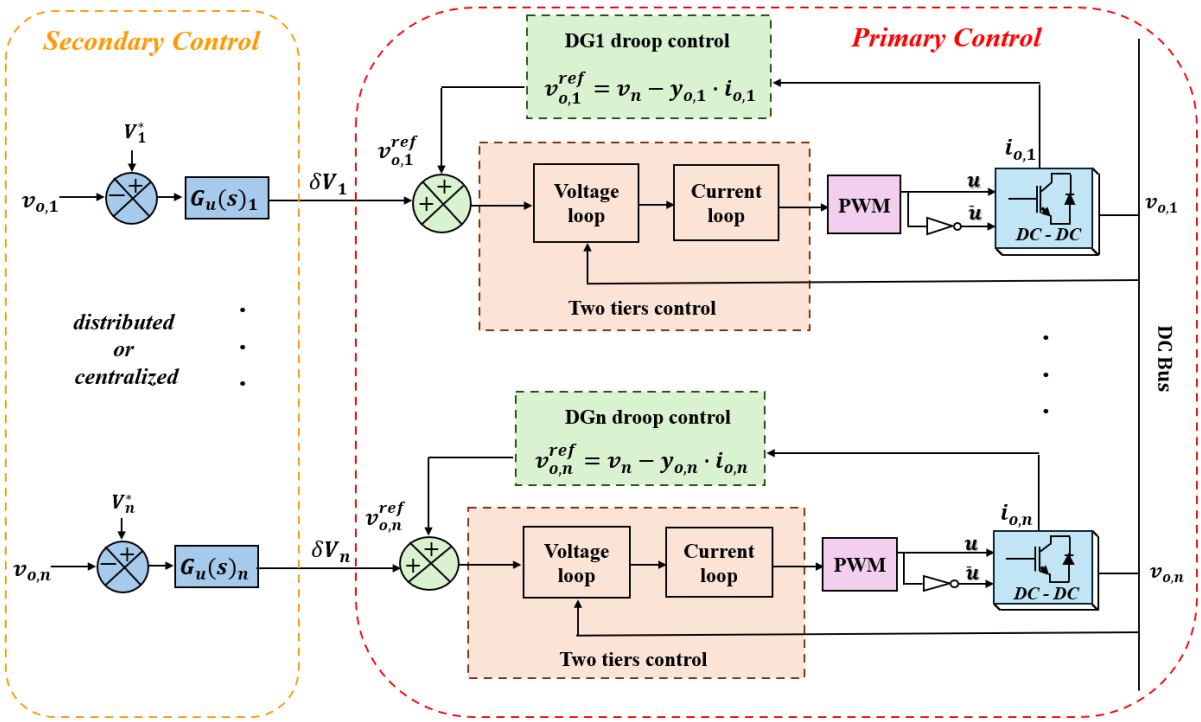

Figure 1-10 : Control structures of the primary (with two tiers controllers) and secondary levels.

The primary control operates in a decentralized way; thus, no communication is needed [41]. Besides, for scalability, service continuity and reconfiguration reasons, one benefit of any microgrid would be to provide plug and play feature, that is either add or remove any DGU at any time without interruption or manual reconfiguration requirement.

In modern power conversion systems, power supply stability and quality depend largely on the ability of power converters to respond rapidly to load variations. Moreover, since power converters are known for their fast dynamics, primary controllers must be fast, i.e. on time scales in the millisecond range [42].

Among the most popular strategies at the primary level to generate the reference value $v_{o,i}^{ref}$ is the droop control. The output voltage reference $v_{o,i}^{ref}$ is automatically adjusted depending on the power delivered, resulting in a slight drop (or "droop") in voltage as the load increases according to $v_{o,i}^{ref} = v_n - y_i \cdot i_{o,i}$ where v_n is the microgrid nominal bus voltage, $i_{o,i}$ is the current injected by the unit and y_i is the droop gain. This approach allocates the power in a decentralized manner between different sources (such as energy sources or storage units) without the need for complex communication [43]. A similar patten apply to AC microgrid [44].

Droop control is particularly popular in DC microgrids, as it simplifies system architecture, reduces communication requirements, and ensures efficient energy management when sources

are distributed or when rapid load variations occur [45]. Since the droop control principle is based on the introduction of a virtual impedance, similar to a resistor, it inevitably induces a slight deviation in voltage (or frequency in AC) from the nominal value.
Moreover, the droop control exhibits a second limitation, namely an unequal distribution of the per unit power between the sources, particularly when their characteristics differ (nominal power, rated current, line connection impedance between the DGU and the microgrid).

In a nutshell, when a constant gain y_i is used, a compromise arises between two contradictory objectives:

- a high y_i value enhances the current sharing but increases the voltage deviation,
- a small y_i value shrinks the voltage deviation but makes power sharing uneven.

To correct those deviations and restore nominal operating conditions, a secondary control is generally introduced upstream the primary control as illustrated on figure 1.10. As for the secondary control, it deals with frequency restoration (for AC grid), nominal voltage restoration (both AC and DC grids), microgrid synchronization to another grid (most often the main high power national grid from which the considered microgrid can be islanded as to operate autonomously) and power quality issues such as frequency and voltage deviations, loss of synchronization with the grid, as well as transient and harmonic effects linked to load fluctuations [46]. It coordinates primary control of microgrids and their subsystems within a few minutes [47]. Secondary control can be centralized, decentralized or distributed, and aims to correct deviations induced by the primary, i.e., restoring nominal microgrid operating conditions [48]. In centralized control, one supervisor manages the whole components of the system as shown in figure 1-11. The purpose of the central controller of the microgrid is to collect data from each DGU, and ensure load sharing between the different sources, and generating a voltage correction signal which it sends to all the converters in voltage mode. This correction compensates for the voltage drops introduced by the droop-type primary control, thereby restoring the nominal voltage of the microgrid [49]. For a centralized strategy, the efficiency of the system is then larger, voltage and frequency regulations show better performance, and it is possible to have access to all information from all sources. However, this approach suffers from reliability problems due to single point of failure and lengthy response times due to communication delays and communication, not to mention, cost increase and

complexity of the system in terms of communication infrastructure, centralized data processing and overall coordination, leading to increased costs and hardware requirements [46].

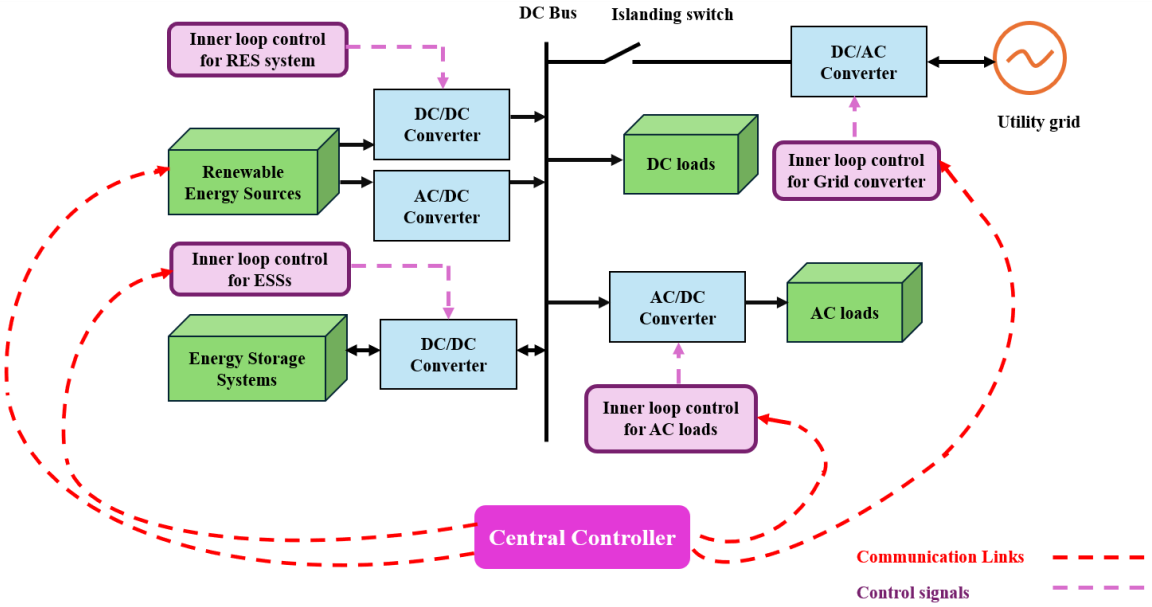

Figure 1-11 : Centralized control topology [48].

However, given the limitations of centralized control, the decentralized control approach emerges as a more flexible and resilient alternative. Indeed, the latter manages each MG unit using a local controller separately from the other neighboring, as shown in figure 1-12.

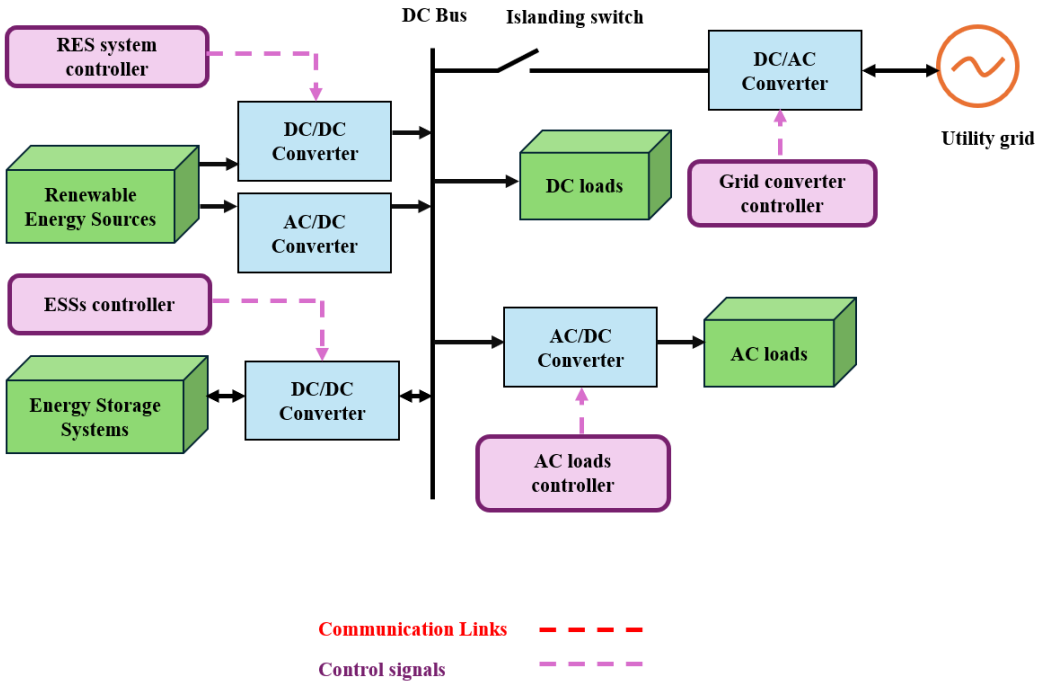

Figure 1-12 : Decentralized control topology [48].

Nevertheless, this type of control may suffer from limited coordination, which can cause deviations in DC bus regulation. This is where distributed control comes in, enabling interaction between local controllers, achieving a faster and more accurate response to deviations and leading then to greater stability and reliability of the microgrid, as demonstrated in [50].

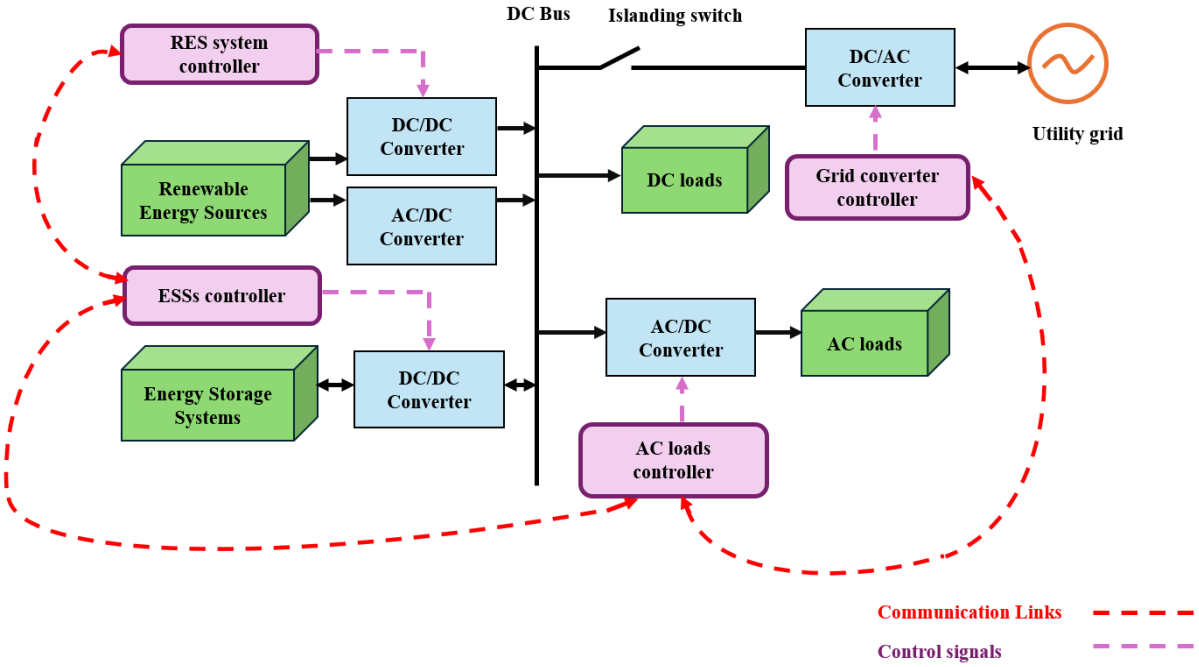

Figure 1-13 : Distributed control topology [48].

In the distributed architecture, each element of the MG has its own controller and exchanges information with its neighbors over a communication network, as shown in figure. 1.13. The best-known strategies of this technique are consensus-based and agent-based distributed control.

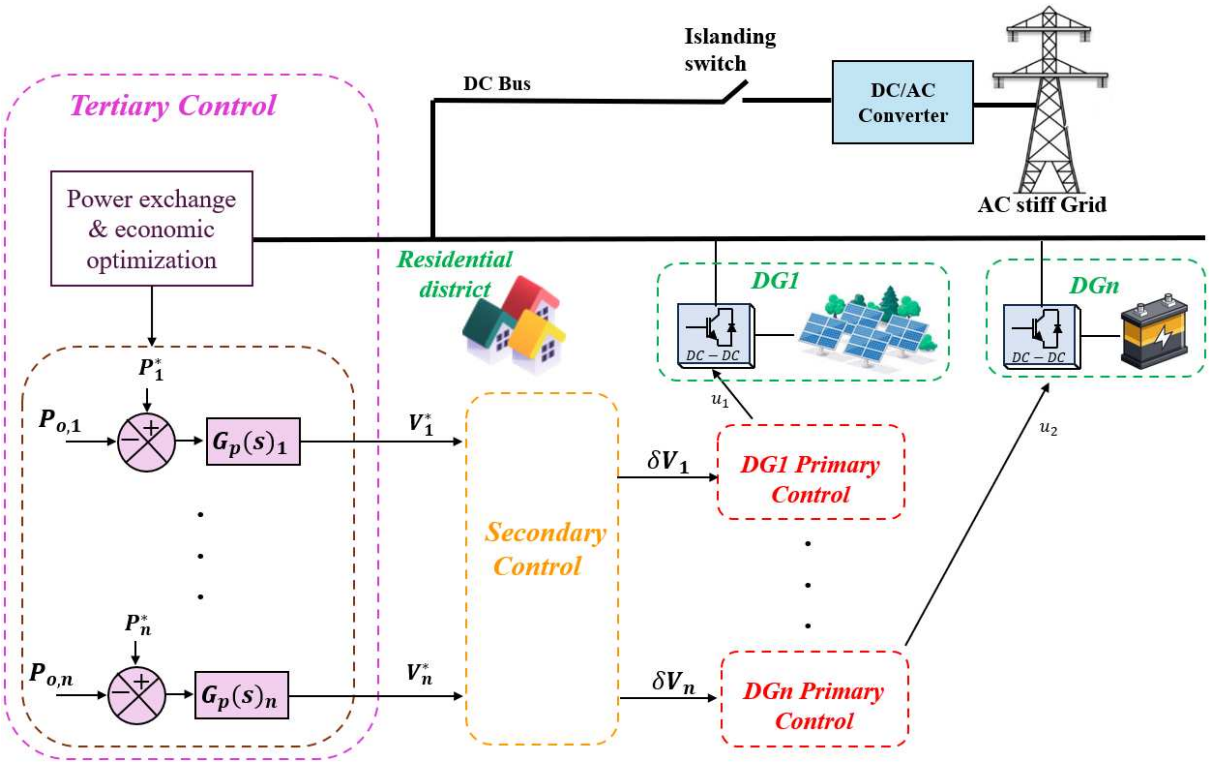

Figure 1-14 : Control structure of the tertiary level.

The tertiary control is located at the top of the hierarchical architecture. This high-level supervision is only activated in grid-tied mode, i.e. when the microgrid is connected to the main grid (also referred as stiff grid in the literature), and it manages the optimal distribution of energy flows on a larger scale in time (planning) and space (coordination between distributed units or microgrids), ensuring a consistent and stable power flow [44, 51, 52, 34] as described in figure 1-14 This global control leads and supervises both planning and optimization of microgrid operation over a longer time horizon. It is responsible for ensuring the economic optimization of the cost-operation system, optimizing the flow of energy between the microgrid and the main grid (or between several microgrids), and coordinating the management of resources according to demand and production forecasts. This level of control can be implemented on a centralized or distributed basis [34].

In a centralized manner, a global controller - such as a grid operator or SCADA system - collects data from all the equipment, then solves an optimization problem based on a predefined cost function, to determine the optimum operating points (voltage, power, frequency, etc.). These references are then transmitted to the local units to ensure coordinated and efficient operation of the system.

In a distributed way: Each local unit participates in the optimization via limited exchanges with its neighbors. Indeed, this approach does not require central coordination and relies only on local interactions, which improves the resilience of the system. It also improves scalability, by making it easier to add or remove units without reconfiguring the whole system.

1.6 Additional microgrids issues

Microgrids are obviously prone to issues similar to stand-alone systems, to name a few dynamics stability [53-55] and state-of-charge management [56]. Those topics have been investigated in literature and are beyond the scope of the present study. Some work, particularly in the field of embedded DC systems for ships, proposes solutions based on flexible architecture and control strategies adapted to isolated and critical environments [57]. However, their application to terrestrial microgrids requires rigorous adaptation. These issues, although relevant, do not fall directly within the scope of this thesis.

1.7 Conclusion

This chapter provides a comprehensive overview of energy challenges in rural areas, with a focus on the Moroccan and African contexts. Even though the rural electrification in Morocco is almost complete at the present time, this far the case for the sub-Saharan Africa faces far less comfortable situation. Moreover, coal and oil remain the primary energy sources, although different projects are underway to promote RES integration into the energy mix. This chapter highlights the strategic role that microgrids can play in decentralized electrification, particularly in isolated villages and even agricultural areas. A review of microgrid's architecture, components and control approaches has established the technical foundations for their effective integration. These elements will serve as a basis for developing a solution adapted for rural areas (e.g., farming systems) energy needs in the following chapters.

CHAPTER 2. A Generic and Hierarchical Approach for Energy Management in HESS based DC Microgrid

This chapter focuses on energy management in a DC microgrid integrating several storage devices or source (flywheel, supercapacitor, battery, solar panels, fuel cell…) in a close vicinity. A centralized generic and hierarchical strategy is well suited for this situation and power management is, therefore, proposed to:

(i) Ensures power distribution compliant with the dynamic characteristics of each storage technology.

(ii) Guarantees a regulation of the DC bus voltage in the presence of non-deterministic loads' variations.

(iii) Ensures objectives control related to either state of charge (SoC) or energy.

This chapter is organized as follows. First, a state-of-the-art review is provided focusing on DC microgrid power management. Secondly, the proposed approach principle is developed in detail, both outer and inner loops are thoroughly investigated. Finally, the proposed strategy is implemented and validated on MATLAB/Simulink simulations and through experimental tests carried out on a 1Kw test bench.

2.1 Introduction

The combination of different distributed generators, such as photovoltaic (PV) modules, wind turbines, fuel cells (FCs), loads, and energy storage systems (ESSs), within a common DC bus, makes the control of the voltage as well as the power allocation a challenge that needs to be efficiently addressed [48]. In this context, different control approaches have been proposed in the literature to best manage energy within HESS-based microgrids. These control methods aim to tackle the issues related to DC microgrid operations, which are mainly related to power allocation and DC bus voltage regulation in the presence of fluctuating loads. In this regard, several strategies for energy management have been applied. These control methods can be centralized, decentralized or distributed. The approach proposed here, given the proximity of the various energy sources used, is a centralized control-based strategy. Indeed, it allows the

supervision unit to have access to all the system's information at a high sampling rate, which contributes to greater responsiveness and overall optimization of performance.

The centralized control strategies mentioned in the literature are mainly based on filtering approaches [58, 59,60, 61, 62]. For a system with two storage systems including a battery and a supercapacitor bank, the low pass and/or high pass filters-based methods are widely used, and their principle is described in figure 2.2. It consists in splitting the load power into two portions, the low frequency part and high frequency component for batteries and supercapacitors, respectively. Despite having the advantage of being simple and easy to implement, filtering approaches do not incorporate any decision logic about the state of the charge of the used storage systems, i.e., they attribute fast components to storage units, such as supercapacitors, and slow components to batteries, regardless of their actual SoC and with no intention to control it via a supervision process.

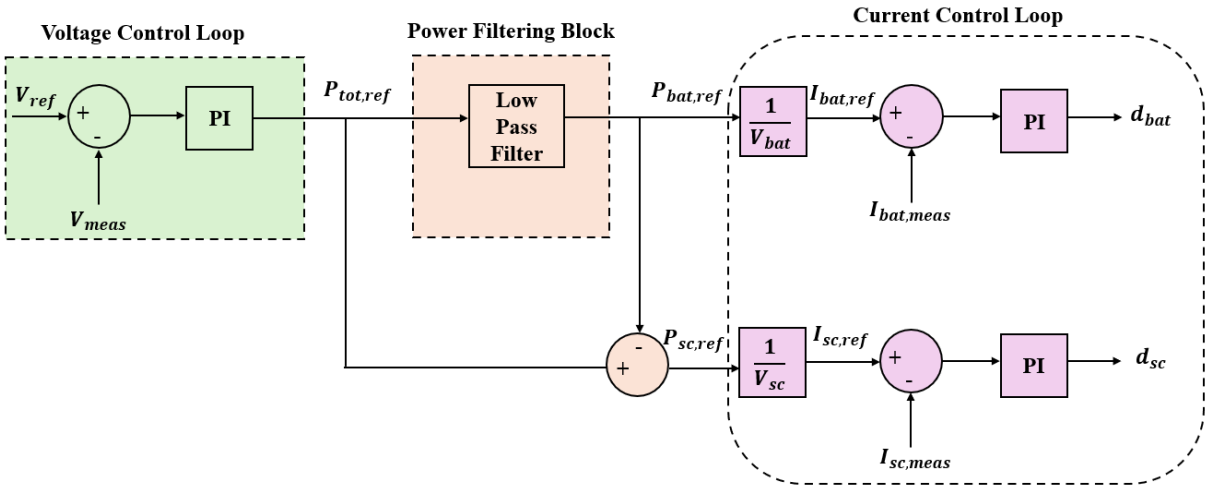

Figure 2-1 : Power allocation using filtering approach

Another method for power distribution was presented in [63], where quantitative power allocation is achieved considering the batteries and supercapacitors SoC and load constraints. By using the power spectrum, as depicted in figure 2-2, the authors studied the power level of each frequency point, and they calculated the split frequency by mapping the pre-allocated power to the low or high frequency parts of the power spectrum. The combination of the two data allows power to be distributed among the two storage devices involved.

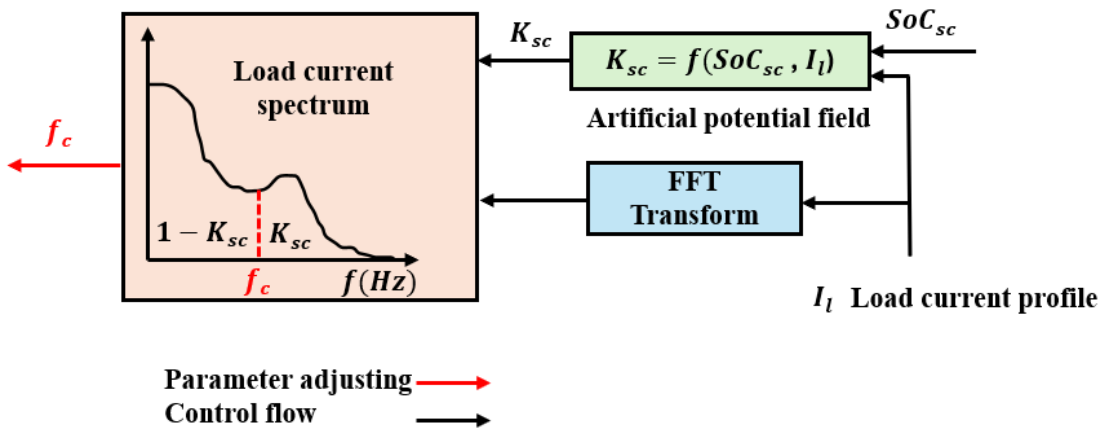

Figure 2-2: Adaptive power allocation using artificial potential field [63]

Systems with more than two energy storage devices have been extensively investigated [64, 65, 66, 67]. For instance, authors in [65] addressed the case of a fuel cell, a battery and a supercapacitor using the principle of frequency decoupling. As illustrated in figure 2-3, the load profile is first decomposed, for each storage device, into three frequency components. Then, a fuzzy logic control layer is deployed to keep the SoCs within a target range. However, the definition of rules and membership functions increases with the number of sources, whose number can become prohibitive to its implementation in large scale systems.

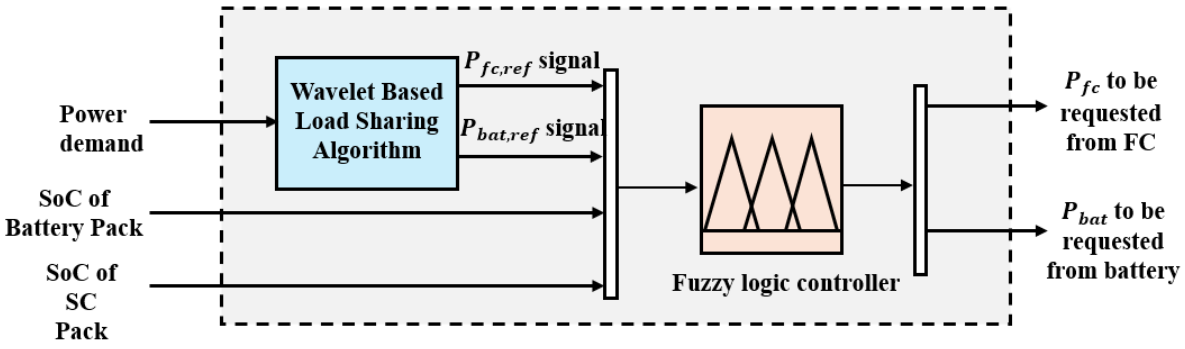

Figure 2-3 : A proposed energy management strategy using wavelet fuzzy logic control [65]

The proposed approach, in this thesis work, presents a new strategy for energy management in DC microgrid comprising a DC bus, a power source of energy (fuel cell, wind turbine, diesel generator, etc.), Ns storage devices whose SoC is to be controlled, and a Constant Power Load (CPL). Each source/ storage device must respond according to its own dynamic limits. They are connected to the DC bus via a bidirectional current converter. The control of each converter is based on a two-tier approach. The outer loop addresses the objective control, either an energy or a SoC, and it generates power reference (or current reference). The inner loop generates the

duty cycle through an input/output linearization. Experimental and simulation tests were carried out for the case of Ns = 2 (a battery and a supercapacitor bank) as storage devices and a fuel cell as an energy source.

The proposed strategy responds to the adaptability requirement by imposing a trajectory for each energy storage device involved. It can be applied to any power architecture including many storage systems, because of its systematic approach, which provides flexibility in easily integrating various kinds and quantities of storage devices.

Overall, the proposed hierarchical management of storage devices ensures DC bus regulation in the face of variable load. In this way, the supercapacitors handle fast fluctuations, reducing the charge-discharge cycles of the batteries, while the latter handle medium fluctuations, preserving the fuel cell for long-term energy needs within its dynamic limits. By respecting the specific features and constraints of each component, this approach contributes to extending their lifetime, guarantees optimum use of them, paving the way, then, towards a sustainable approach to modern energy systems. For instance, in a farming water pumping system, energy storage needs to typically hybridize in order to improve performance and extend the lifespan of batteries. Supercapacitors could be used to handle fast power fluctuations caused by sudden load changes, such as pump start-ups or variable motor demands. This might reduce the stress on the batteries, minimizing, therefore, the number of high-frequency charge–discharge cycles, preserving their lifetime.

2.2 Proposed strategy

2.2.1 Scope and objectives of the strategy

We consider a mono PCC (point of common connection) DC microgrid composed of Ns Energy Storage Systems (ESSs) and sources combined in close vicinity, as depicted in figure 2-4. The load is considered non-deterministic. Each storage device k, among the Ns ESS and sources, exhibits its own power density $P_{m,k}$ and energy density $E_{m,k}$.

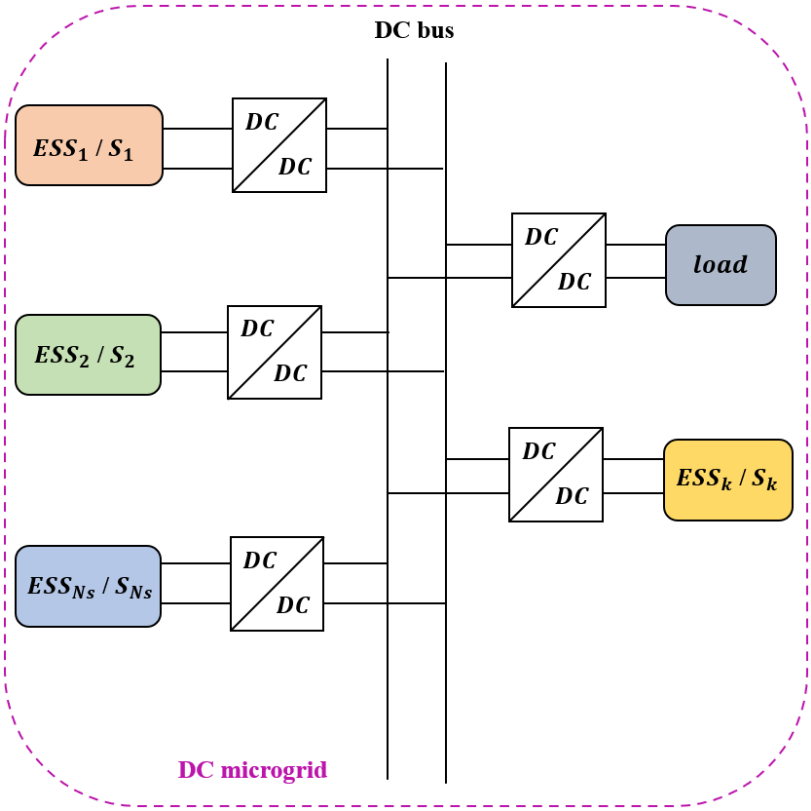

Figure 2-4: Structural architecture of a DC microgrid integrating several storage systems and sources

The Diagram of Ragone denoted in figure 2-5 shows the distribution of the most common energy storage devices (batteries, supercapacitors, fuel cells). Typically, the higher the power density, the faster the ESS or source can respond [68].

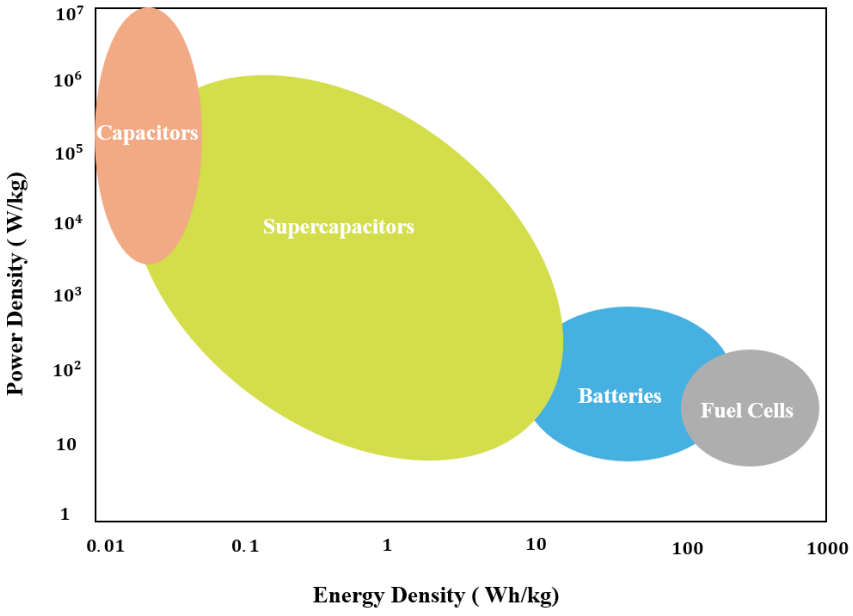

Figure 2-5: Diagram of Ragone [68]

2.2.2 Design of the inner loop

Each of the considered sources is connected to the DC bus by means of a DC/DC converter. If the source is compliant with regenerative mode, as in the case of SC or battery, a bidirectional converter is well suited. Such a power electronics device is depicted in figure 2-6, otherwise, as in the case of a fuel cell, a boost converter is more appropriate.

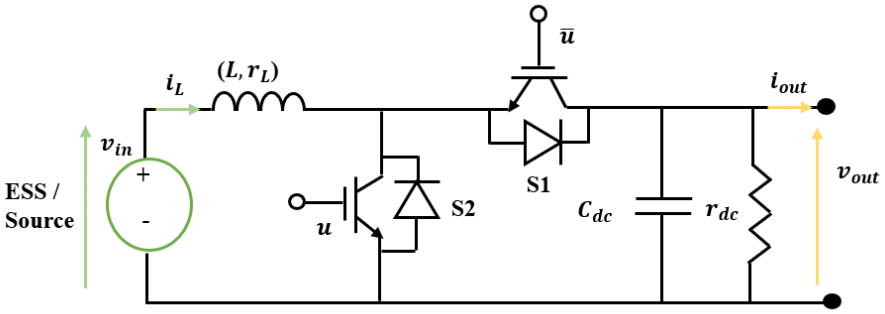

Figure 2-6: Bidirectional converter diagram

The current loop, in the proposed control strategy, generates references on the duty cycle. As depicted on figure 2-6, in continuous conduction mode, the converter's operation consists of two distinct sequences, which determine its behavior:

1. Sequence 1: $u = 1$, then S1 is OFF and S2 is ON.

$$L \cdot \frac{di_l}{dt} = v_{in} - r_l \cdot i_l \tag{2.1}$$

where v_{in} represents the input voltage, which can be v_{sc}, v_{bat} or v_{fc}, depending on the case, L the inductance of inductor, r_l the series resistor of the inductor and i_l is the current flowing through the inductor.

2. Sequence 2: $u = 0$, then S1 is ON and S2 is OFF, where v_{out} is the output voltage of the boost converter.

$$L \cdot \frac{di_l}{dt} = v_{in} - r_l \cdot i_l - v_{out} \tag{2.2}$$

For each variable g, the mean value $\bar{g}$ is computed over one switching period T_{pwm} as stated in Eq. 2.3:

$$\bar{g}(t) = \frac{1}{T} \cdot \int_{t}^{t+T_{pwm}} g(\tau) \cdot d\tau \tag{2.3}$$

Then, the mean model may be computed according to the Middlebrook approach [69], which (i) assumes equivalence between the instantaneous value and the mean value, and (ii) consists in replacing the binary switch order $u \in \{0,1\}$ by its mean value, i.e. the duty cycle d. It is derived in Eq. 2.4 and simplified in Eq. 2.5. This approach is valid as long as the ripple components remain negligible enough compared to the mean value.

$$L \cdot \frac{d\bar{i}_L}{dt} = \left(\overline{v}_{in} - r_L \cdot \bar{i}_L\right) \cdot d + \left(\overline{v}_{in} - r_L \cdot \bar{i}_L - \overline{v}_{out}\right) \cdot (1 - d) \tag{2.4}$$

$$L \cdot \frac{d\bar{i}_L}{dt} = \overline{v}_{in} - r_L \cdot \bar{i}_L - \overline{v}_{out} + \overline{v}_{out} \cdot d \tag{2.5}$$

In order to impose the closed loop current dynamic, we propose to implement an input/output linearization. The first step consists in defining a control variable $\upsilon(t)$ stated in Eq. 2.6, where k_p and k_i being the proportional gain and integral coefficients are, respectively, where $i_{L,ref} = P_{ref}/v_{in}$, P_{ref} being $P_{sc,ref}$, $P_{bat,ref}$ or $P_{fc,ref}$ depending on the case.

$$L \cdot \upsilon(t) = L \cdot \frac{d\bar{i}_{L,ref}(t)}{dt} + k_p \cdot \varepsilon_{i_L} + k_i \cdot \int_{0}^{t} \varepsilon_{i_L} d\,\tau \tag{2.6}$$

$$\varepsilon_{i_L} = \bar{i}_{L,ref}(t) - \bar{i}_L(t) \tag{2.7}$$

Therefore, the duty cycle d is computed following Eq. 2.8:

$$d = \frac{1}{\overline{v}_{out}} \cdot \left(L \cdot \upsilon(t) + r_L \cdot \bar{i}_L - \overline{v}_{in} + \overline{v}_{out}\right) \tag{2.8}$$

By combining equations Eqs. 2.5, 2.6 and 2.8, comes the closed-loop current dynamic, represented by Eq. 2.9, which shows that it is independent of both the setpoint and the system parameters.

$$\frac{d}{dt}\varepsilon_{i_L}(t) + k_p \cdot \varepsilon_{i_L}(t) + k_i \cdot \int_0^t \varepsilon_{i_L}(\tau) \cdot d\tau = 0 \tag{2.9}$$

This gives the following expression for the duty cycle:

$$d = \frac{1}{\overline{v}_{out}} \cdot \left[L \cdot \frac{d}{dt}\overline{i}_{L,ref}(t) + L \cdot k_p \cdot \varepsilon_{i_L} + L \cdot k_i \cdot \int_0^t \varepsilon_{i_L} \cdot d\tau + r_L \cdot \overline{i}_L - \overline{v}_{in} + \overline{v}_{out} \right] \tag{2.10}$$

k_p and k_i are tuned according to Eq. 2.11, where f_{pwm} being the switching frequency, with a view to impose the current dynamic error, as stated in Eq. 2.13 in the Laplace domain.

$$\xi = \frac{\sqrt{2}}{2} \qquad \omega_i = \frac{2\pi \cdot f_{pwm}}{10} \qquad k_p = 2 \cdot \xi \cdot \omega_i \qquad k_i = \omega_i^2 \tag{2.11}$$

2.2.3 Design of the outer loop and objective definition

The controlled variable is referred to as the objective, and it deals with either a SoC , as $o_k(t) = soc_k(t)$ or an energy, as $o_k(t) = y_k(t)$. It is work noting that whatever the nature of the objective, the purpose here is to express its time derivative $\dot{o_k}(t)$ through a bijective law f_k in respect to the power delivered p_k by the source k according to Eq. 2.12 . This explains why the proposed approach is qualified as generic in nature.

$$\dot{o_k}(t) = f_k(p_k), \quad k \in \{1, \dots, N_s\} \tag{2.12}$$

$\varepsilon_k(t)$ is denoted as the error committed on the kth objective:

$$\varepsilon_k(t) = o_{k,ref,f}(t) - o_k(t), \quad \forall k \in \{1, \dots, N_s\} \tag{2.13}$$

The objective reference is subjected to follow a trajectory $o_{k,ref,f}(t)$ in order to comply with the intrinsic dynamics of the related source on one hand, and to comply with the following control law, which implies a derivative term, on a second hand. This is performed by applying a second-order filter so that the filtered reference signal $o_{ref,f}$ is performed according to Eq. 2.14, whatever the nature of the initial reference signal $o_{ref,f}$, continuous or not. For the sake of compactness, the relationship is stated in the Laplace domain as follows:

$$o_{ref,f}(s) = o_{ref}(s) \cdot \left(1 + \frac{2\xi_f}{\omega_{f,k}} \cdot s + \frac{s^2}{\omega_{f,k}^2} \right)^{-1} \tag{2.14}$$

The expected dynamics for each objective are formulated according to Eq. 15. ξ_k and ω_k are the desired damping and cut-off pulsation associated to the ESS k, respectively.

$$\dot{\varepsilon_k}(t) + 2 \cdot \xi_k \cdot \omega_k \cdot \varepsilon_k(t) + \omega_k^2 \cdot \int_0^t \varepsilon_k(\tau) d\,\tau = 0 \tag{2.15}$$

The bandwidth [0, ω_k] of the outer loop of each converter is related to the intrinsic kinetics or power density, thus:

$$P_{m,1} > P_{m,2} > \cdots > P_{m,N_s} \Rightarrow \omega_1 > \omega_2 > \cdots > \omega_{N_s} \tag{2.16}$$

As a result, the proposed approach is said to be hierarchical since the k^{th}objective, i.e. the one related to the storage device indexed $k \in [\![0, N_s - 1]\!]$, is supposed to be taken in charge by the source indexed $(k+1)^{th}$. Therefore, the system has N_s objectives.

In what follows, the control principle is specified for a limited number, namely three, a SC, a battery and a fuel cell. This is not a simplification but rather a way to explicitly determine the control law of each storage device based on their specificity. Moreover, this is performed with no loss of generality.

2.2.3.1 First objective management

The algorithm is initiated at rank $k = 0$ with a view to controlling the stored energy $y_{dc}(t)$ in the DC bus. The device with the fastest response time is the most appropriate for achieving this objective. Denoting p_{load} the power demanded by the load and p_k the power delivered by the device *k*; and summoning the energy conservation principle, the DC bus energy y_{dc} follows the following dynamics, where C_{dc} and v_{dc} are the capacitance of the DC bus and its corresponding voltage, respectively.

$$\dot{y}_{dc} = \sum_{k=1}^{N_s} p_k + p_{load} \tag{2.17}$$

$$y_{dc} = 0.5 \cdot C_{dc} \cdot v_{dc}^2 \tag{2.18}$$

The related SC power reference $p_{sc,ref} = p_{1,ref}$ is computed according to Eqs. 2.19 and 2.20.

$$\varepsilon_0(t) = y_{dc,ref,f}(t) - y_{dc}(t) \tag{2.19}$$

$$p_{sc,ref} = \dot{y}_{dc,ref,f}(t) + 2 \cdot \xi_0 \cdot \omega_0 \cdot \varepsilon_0(t) + \omega_0^2 \cdot \int_0^t \varepsilon_0(\tau) \cdot d\tau + p_{load} - \sum_{k=2}^{N_s} p_k \quad (2.20)$$

The derivative term $\dot{y}_{dc,ref,f}(t)$ is also the reason why the objective reference $y_{dc,ref,f}(t)$ should be a continuous derivative signal, hence the second order filtering principle stated in Eq. 2.14. Besides, the term p_{load} stands for the load power rejection while the term $\sum_{k=2}^{N_s} p_k$ corresponds to a decoupling term.

Figure 2-7. illustrates the cascaded loops structure used to control the DC bus objective.

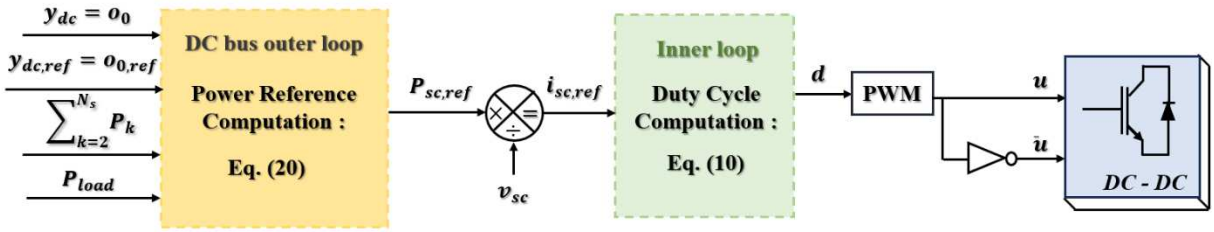

Figure 2-7 : Control block related to the first objective

2.2.3.2 Second objective management

The process is, then, carried out at rank $k = 1$ to control the SC SoC and the related error is defined as:

$$\varepsilon_1(t) = SoC_{sc,ref,f}(t) - Soc_{sc}(t) \quad (2.21)$$

The basic SC electric equivalent model consists of a series resistor r_{sc}, a parallel resistor R_p to account for the autodischarge, and a storage capacitor $C_{sc}$with q_c the store electrostatic charge stored on the plate, as depicted on figure. 2-8 and expressed in Eq. 2.22.

$$v_{sc}(t) = v_c(t) - r_{sc} \cdot i_{sc}(t) = \frac{q_c(t)}{C_{sc}} - r_{sc} \cdot i_{sc}(t) \quad (2.22)$$

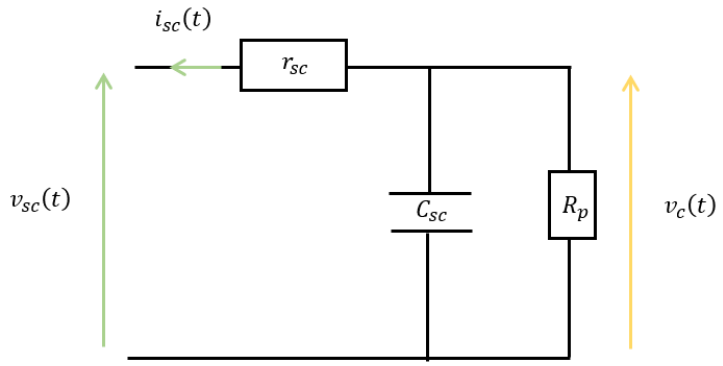

Figure 2-8 : Electrical diagram of the supercapacitor

The SoC may be evaluated either through voltage ratio under no load (Eq. 2.23) or coulomb counting method (Eq. 2.24) under current.

$$SoC_{sc}(t) = \frac{v_c(t)}{v_{c,max}} = \frac{v_{sc}(i_{sc} = 0)}{v_{sc,max}(i_{sc} = 0)} \tag{2.23}$$

$$SoC_{sc}(t) = SoC_{sc}(0) - \frac{\int_0^t i_{sc}(\tau) \cdot d\tau}{C_{sc} \cdot v_{sc,max}} \tag{2.24}$$

As a matter of fact, the measurement v_{sc} from the external terminals under load does not give access to the capacitor voltage v_c, indeed it also includes the ohmic drop voltage related to the series resistor. Yet, this is this very voltage that reflects the SoC. As a result, the former approach suffers from inaccuracy under current. Online estimation through high frequency stimulation may be an avenue. Then the latter method was preferred.

The bijective relationship between the SC SoC denoted SoC_{SC} and the SC power p_{sc} is formulated through Eq. 2.25.

$$\dot{SoC}_{SC}(t) = \frac{\dot{q}_{sc}}{q_{sc,max}} = \frac{-i_{sc}}{q_{sc,max}} = \frac{-p_{sc}}{v_{sc} \cdot q_{sc,max}} \tag{2.25}$$

where q_{sc} stands for the electrostatic charge stored in the SC capacitor, which is denoted by C_{sc}:

$$q_{sc,max} = C_{sc} \cdot v_{sc,max} \tag{2.26}$$

Based on the frequency separation, one can assume that the dynamic related to the DC bus is ended in comparison to the SC time frame. Then, the reduced order model, related to the DC bus, is formulated according to Eq. 2.27:

$$\dot{y}_{dc}(t) = 0 = -p_{load}(t) + p_1(t) + p_2(t) + \sum_{k=3}^{N_s} p_k(t) \tag{2.27}$$

As a result, it comes the reference power $p_{2,ref}$ related to the battery according to Eq. 2.28.

$$p_{bat,ref}(t) = p_{2,ref}(t) = -p_1(t) + p_{load}(t) - \sum_{k=3}^{N_s} p_k(t) \tag{2.28}$$

Combined with Eqs. 15 and 20, $p_{2,ref}$ is computed following Eq. 2.29.

$$p_{bat,ref}(t) = \dot{o}_1(t) \cdot v_{sc} \cdot q_{sc,max} + p_{load}(t) - \sum_{k=3}^{N_s} p_k(t) \tag{2.29}$$

To consider the limited dynamic of the battery, the load power $p_{load}(t)$ should be smoothed. For the sake of simplicity, it was decided to apply the filter identified in Eq. 2.14. Thus, Eq. 2.29 becomes:

$$p_{bat,ref}(t) = \left(S\dot{o}C_{sc,ref,f}(t) + 2 \cdot \xi \cdot \omega_1 \cdot \varepsilon_1(t) + \omega_1^2 \cdot \int_0^t \varepsilon_1(\tau)d\tau\right) \cdot v_{sc} \cdot q_{sc,max} + p_{load,\omega_{f,1}} - \sum_{k=3}^{N_s} p_k \tag{2.30}$$

$$p_{load,\omega_{f,1}}(s) = p_{load}(s) \cdot \left(1 + \frac{2 \cdot \xi_f}{\omega_{f,1}} \cdot s + \frac{s^2}{\omega_{f,1}^2}\right)^{-1} \tag{2.31}$$

The derivative term $SoC_{sc,ref,f}(t)$ is also the reason why the objective reference $SoC_{sc,ref,f}(t)$ should be a continuous derivative signal, hence the second order filtering principle stated in Eq. 14. Besides, the term P_{load} stands for the load power rejection and the term $\sum_{k=3}^{N_s} P_k$ corresponds to a decoupling term.

Figure 2-9. summarizes the outer/inner loops structure used to control the SoC of SC.

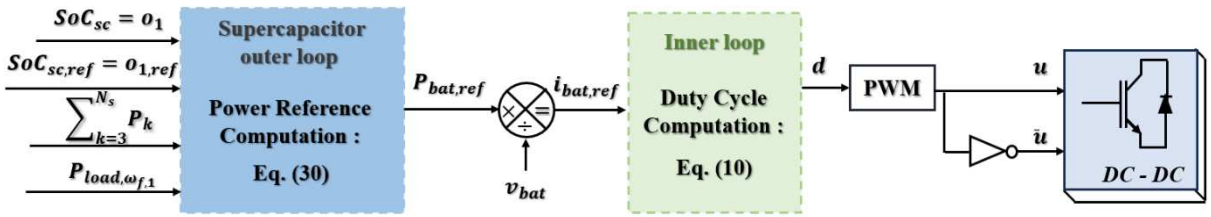

Figure 2-9 : Control block related to the second objective

2.2.3.3 Third objective control

Then, the process of objectives control is further derived at rank $k = 2$ in order to control the battery SoC. The related error is defined as:

$$\varepsilon_2(t) = SoC_{bat,ref,f}(t) - SoC_{bat}(t) \tag{2.32}$$

The battery SoC is evaluated according to a coulomb counting method [70]:

$$SoC_{bat}(t) = SoC_{bat}(0) - \frac{\int_0^t i_{bat}(\tau) \cdot d\tau}{C_{ah} \cdot 3600} \tag{2.33}$$

The initial value is set thanks to the Open Circuit Voltage (OCV) measured at rest prior proceeding to the experimental test, which is then compared to the static characteristic $ocv(SoC_{bat})$, provided by the manufacturer.

Since the capacity can decrease over time and may also depend on the temperature and current solicitation, estimating SoC is a problem in itself. However, this is beyond the scope of this work. Manufacturers can provide a battery management system (BMS) with accurate indicators of (SoC) and State of Health (SoH).

The bijective relationship between the battery SoC, denoted SoC_{bat} , and the battery power p_{bat} is formulated through Eqs. 2.34 and 2.35.

$$SoC_{bat}(t) = \frac{q_{bat}(t)}{q_{bat,max}} = \frac{q_{bat}(t)}{C_{ah} \cdot 3600} \tag{2.34}$$

$$\dot{SoC}_{bat}(t) = \frac{\dot{q}_{bat}(t)}{q_{bat,max}} = -\frac{i_{bat}(t)}{C_{ah} \cdot 3600} = -\frac{-p_{bat}}{C_{ah} \cdot 3600 \cdot v_{bat}} \tag{2.35}$$

$q_{bat} = C_{ah} \times 3600$ is the coulomb charge that the battery is supposed to deliver based on its ampere-hour capacity C_{ah}

By the same token, since the fuel cell is supposed to recharge the battery, the FC reference power $p_{fc,ref} = p_{3,ref}$ must be:

$$p_{fc,ref} = C_{ah} \cdot 3600 \cdot v_{bat} \cdot \left(\dot{SoC}_{bat,ref,f}(t) + \xi \cdot \omega_2 \cdot \varepsilon_{2_{bat}}(t) + \omega_2^2 \cdot \int_0^t \varepsilon_{2_{bat}}(\tau) d\tau\right) + p_{load,\omega_{f,2}} \tag{2.36}$$

$$p_{load,\omega_{f,2}}(s) = p_{load}(s) \cdot \left(1 + \frac{2\xi_f}{\omega_{f,2}} \cdot s + \frac{s^2}{\omega_{f,2}^2}\right)^{-1} \tag{2.37}$$

Figure 2-10 overviews the whole structure of outer/inner loops structure, used to control the battery SoC.

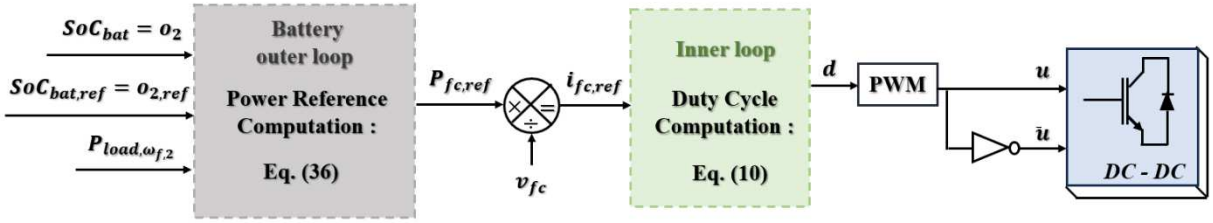

Figure 2-10: Control block related to the third objective

This principle can be extended to other storage devices, such as flywheel, as long as a bijective relationship between the objective, related to the storage device, and the power it delivers can explicitly be defined.

2.3 Controls parameter sizing

The proposed approach requires 4 parameters for each source:

- ξ and ω_k are the respective damping coefficient and cutoff frequency related to the input/output linearization control,
- $\xi_f$and $\omega_{f,k}$ are the respective damping coefficient and proper frequency related to the trajectory filtering,

2.3.1 Trajectory filter parameters $\xi_f$and $\omega_{f,k}$

In regard to $\xi_f$and $\omega_{f,k}$ parameters, the first one is set to $\xi_f = 1$ (whatever the storage device) to avoid any overshoot, which would possibly imply power saturation. As for $\omega_{f,k}$, it has an impact on the power derivative dp_k/dt delivered by the source k. Then, the designer should be attentive when it comes to dealing with the FC, as it is usually accepted that its current derivative should not exceed 5 to 10 A/s. The following consideration will demonstrate that $\omega_{f,2}$ is upperbound.

Let us consider a setup load Δp_{load} and do the math in the Laplace domain, then the storage device k is supposed to provide the following disturbance rejection power where $\xi = 1$:

$$p_{fc}(s) = \frac{1}{1 + \frac{2 \cdot \xi}{\omega_{f,k}} \cdot s + \frac{s^2}{\omega_k^2}} \cdot \frac{\Delta p_{load}}{s} \tag{2.38}$$

Basic Laplace to time transforms provides the transient expression, and assuming a null initial condition, i.e. $p_{fc}(t = 0) = 0$, the FC power is expressed as:

$$p_{fc}(t) = \Delta p_{load} \cdot \left(1 - \left(1 + \omega_f \cdot t\right) \cdot exp\left(-\omega_f \cdot t\right)\right) \tag{2.39}$$

The FC power derived from its voltage and current:

$$p_{fc}(t) = v_{fc}\left(i_{fc}\right) \times i_{fc}(t) \tag{2.40}$$

Basic computation leads to the FC current derivative:

$$\frac{di_{fc}(t)}{dt} = \frac{\Delta p_{load}}{v_{fc}\left(i_{fc}\right)} \cdot \frac{dg(t)}{dt} \cdot \left(1 + \frac{\Delta p_{load}}{v_{fc}^2\left(i_{fc}\right)} \cdot \frac{dv_{fc}}{di_{fc}} \cdot g(t)\right)^{-1} \tag{2.41}$$

where :

$$g(t) = \left(1 - \left(1 + \omega_f \cdot t\right) \cdot exp\left(-\omega_f \cdot t\right)\right) \quad and \quad \frac{dg(t)}{dt} = \omega_f^2 \cdot t \cdot exp\left(-\omega_f \cdot t\right)$$

Now, trying to solve explicitly $d^2 i_{fc}(t)/dt^2 = 0$ in order to express $max\left(di_{fc}(t)/dt\right)$ is not the most appropriate pathway. Indeed, nonlinear terms make it impossible. Instead, a numerical iterative process is far more suitable, and it consists of the consecutive steps:

1. Select an initial value for ω_f.
2. Determine the transient sequence end when $\xi = 1$ according to $t_{end} = 5/\omega_f$
3. For each $0 \le t \le t_{end}$ and based on the static characteristic interpolation $v_{fc}\left(i_{fc}\right)$, depicted in Fig. 2.11, determine $i_{fc}(t)$ value according to:

$$p_{fc}(t) = \Delta p_{load} \cdot \left(1 - \left(1 + \omega_f \cdot t\right) \cdot exp\left(-\omega_f \cdot t\right)\right) = v_{fc}\left(i_{fc}\right) \cdot i_{fc}(t) \tag{2.42}$$

4. For each $0 \le t \le t_{end}$, evaluate $di_{fc}(t)/dt$ according to:

$$\frac{di_{fc}(t)}{dt} = \frac{i_{fc}(t + dt) - i_{fc}(t - dt)}{2 \cdot dt} \tag{2.43}$$

5. If $max\left(di_{fc}(t)/dt\right)$ is reached for one $di_{fc}(t)/dt$, then stop the iterative process, if not, carry on.

The curves shown in figure 2-11 illustrate this method for $\omega_f = 1.8\,rad/s$ and $\Delta p_{load} = 800W$, for which $di_{fc}(t)/dt$ reaches 5.8A/s.

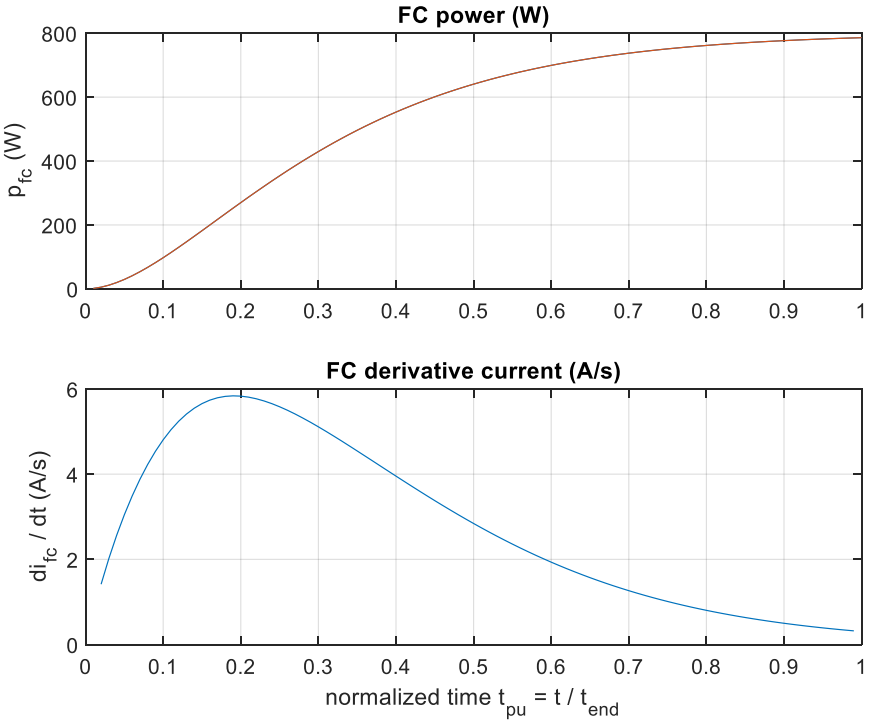

Figure 2-11: Evolution of fuel cell power and current derivative

In practice this predesign may be a bit optimistic because the FC is not only supposed to feed the load but also recharge the battery. As a result, one should introduce some margin.

2.3.2 input/output linearization control parameters $\boldsymbol{\xi}$ and $\boldsymbol{\omega_k}$

$\xi = \sqrt{2}/2$ was selected because it obviously provides the best tradeoff between the time response and overshoot. Besides, it is well established that the control cutoff frequency should be higher than the reference trajectory to ensure a null tracking error. It was decided to select $\omega_k = 2 \cdot \omega_{f,k}$.

2.4 Implementation and test bench

2.4.1 Experimental set up and test bench

The proposed approach was implemented on a test bench consisting of two storage devices, namely one SC (165F – 48V) one $LiFePO_4$ battery (30 A.h – 48V) and one unidirectional source, specifically a FC (800W – 40V). For the sake of convenience, the FC was actually emulated by means of a stabilized voltage control source. To limit cumbersome time computation, a rather basic zero order model was implemented in which the FC voltage is

confused with its static characteristic (Figure 2-12.) with no overvoltage (ohmic, charge transfer, concentration).

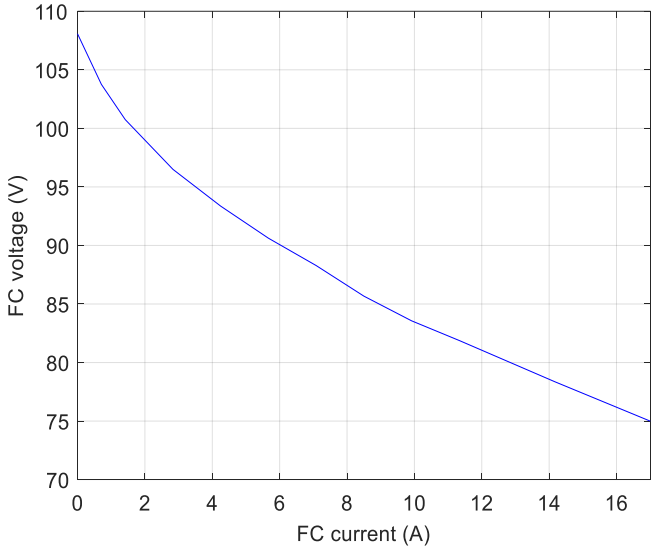

Figure 2-12 : FC static characteristic $v_{fc} = f\ (i_{fc}\ )$

The 200V DC link leans on a 940µF capacitor and feeds a resistive load and a CPL. The former is not mandatory but provides some safeguards by limiting the DC link voltage increase rate in case the control fails. The latter enables to conduct both discharge and regenerative modes, it is practically made from a bidirectional buck-boost converter supplied by a SC (165F – 48V) and associated to a larger bandwidth compared to the other converters. The overview setup is depicted on figure 2-13 and a picture is provided on figure 2-14. Each converter is actually one leg of a 1.2kV-59A SiC MOSFET six-pack module from Cree manufacturer.

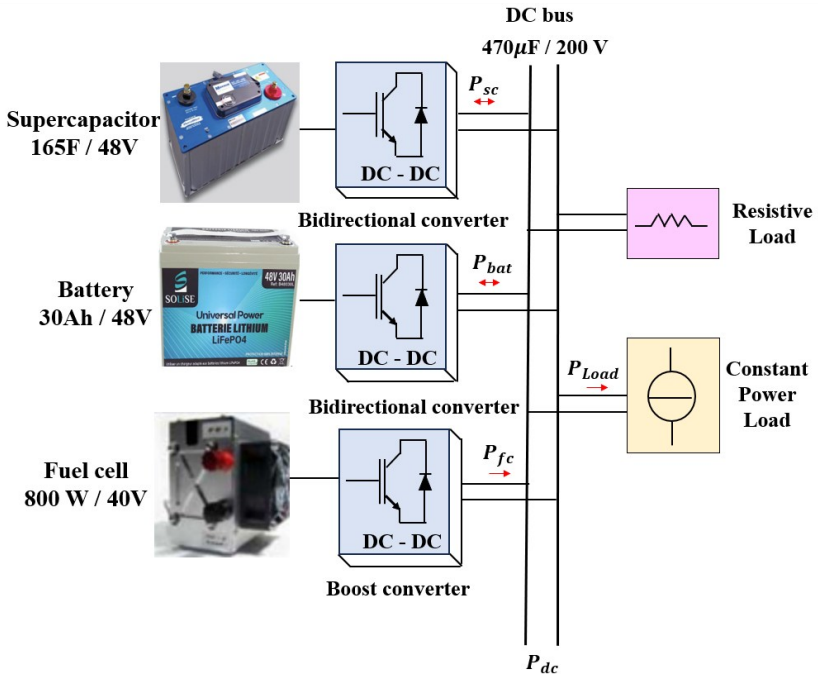

Figure 2-13 : Architecture of the studied microgrid

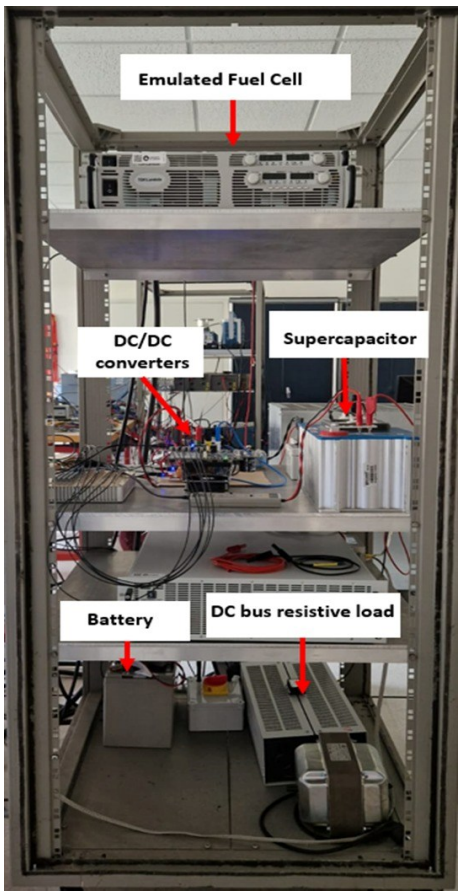

Figure 2-14 : Experimental testbench

The proposed control was first evaluated on Matlab/Simulnik prior to compiling it on the rapid prototyping dSPACE 1202 platform. The card interface issues the duty signals, which are connected to the driver through optic fibers. The measurement are samples at each half switching period, meaning that the control gets automatically the mean current values. The dynamic handle and supervision of the system (reference setting, PWM inception or interruption, load step configuration, measurements display, recordings) was performed, thanks to an interface developed on ControlDesk, as shown in figure 2-15.

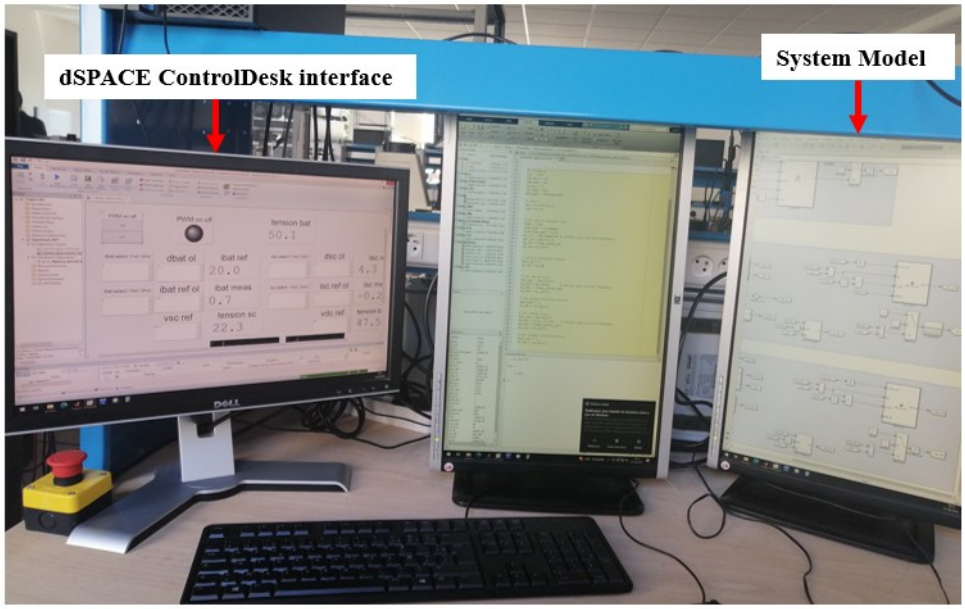

Figure 2-15: Real-time control setup

The control parameters are selected based on theoretical considerations. However, as a virtue of either phenomenon difficult to model or behaviors challenging to predict, (disturbances that affect the measurement probes and the control board, converter efficiency, SC and battery real capacity and inner impedance...), the control parameters are to be fine-tuned on the test bench. Eventually, the most suitable control parameters were the one mentioned in table 2-1.

Table 2-1 : System and control parameters

Parameter name	***symbol***	***value***
battery and SC converter inductor	L	600µH
FC converter inductor	L	100µH
dc bus capacitor	C_{dc}	940µF
dc bus resistive load	R_{load}	333 Ω
PWM frequency	F_{PWM}	50 kHz
inner loop cutoff frequency	ω_i	10 krad/s
o_0 outer loop cutoff frequency	$\omega_{c,0}$	400 rad/s

Parameter name	*symbol*	*value*
o_1 outer loop cutoff frequency	$\omega_{c,1}$	2 rad/s
o_2 outer loop cutoff frequency	$\omega_{c,2}$	0.7 rad/s
o_0 trajectory cutoff frequency	$\omega_{f,0}$	200 rad/s
o_1 trajectory cutoff frequency	$\omega_{c,1}$	1 rad/s
o_2 trajectory cutoff frequency	$\omega_{c,2}$	0.35 rad/s

In the upcoming sections, three scenarios are to be investigated to illustrate the appropriate behavior of the system.

2.4.2 Normal mode

The first test being conducted addresses the normal mode in which the CPL, combined to the resistive load, do not exceed the FC maximum power, i.e., $p_{Rload} + p_{cpl} \leq p_{fc,max}$. As for the power allocation, the experimental results are shown on figure 2-16. The CPL steps up at t=0 from 0W to 400W. Chronologically, the SC is the first one to counter this load increase, followed by the battery, and finally the FC takes in charge the complete load. The FC power overshoot at t=5s stems from the battery recharge. A similar behavior is observed when the step down happens at t=25s.

As for the objective regulation, the results are depicted in Fig. 2-17 by means of normalized values. To begin with, one can appreciate the DC link voltage that only encounters small deviation from its reference value at the very steep variation (t=0 and t=25s). As for the storage devices, it can be observed that they fully recover their soc reference, which was chosen to maintain a safety margin relative to the full charge or discharge.

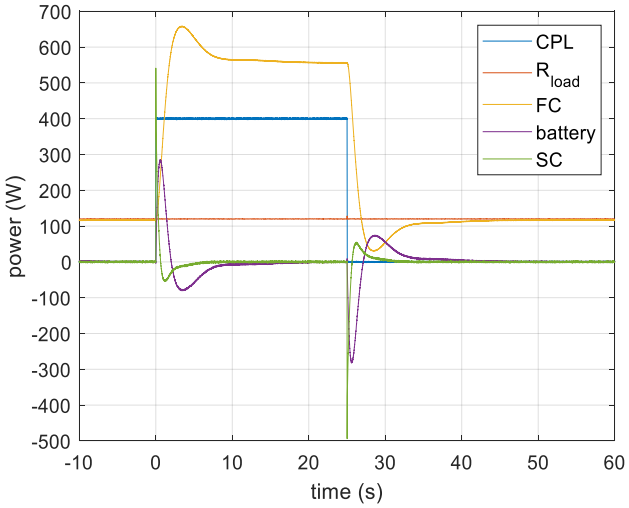

Figure 2-16 : Normal mode – power allocation

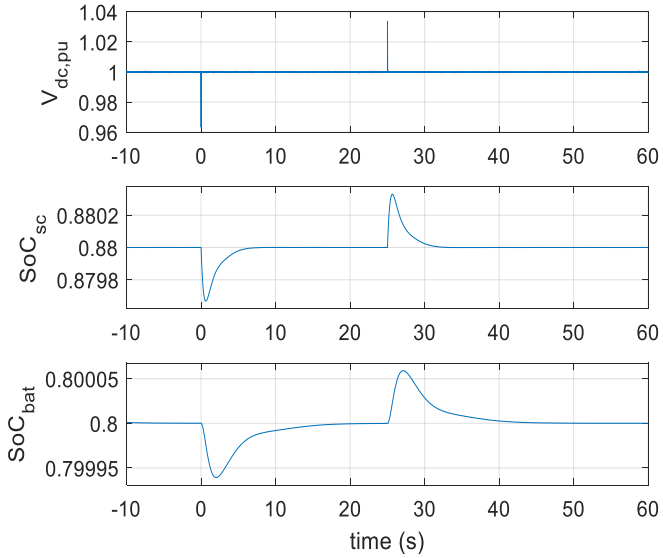

Figure 2-17 : Normal mode – objectives regulation

2.4.3 Overcharge mode

One should keep in mind the main characteristic of any hybrid source, namely that it includes a primary source, the FC in our case, which exhibits a rated power lower than the load peak power, and so with a view to cost reduction. Then, any extra power should be taken in charge by the auxiliary sources, in our case the SC and the battery.

The following scenario is an illustration of this feature. The power allocation is depicted in figure 2-18. Up to t=25s, the system encounters normal mode of operation. However, at t=25s, the system enters the overcharge situation since the FC reaches its maximum power (800W) and the SC combined with the battery must step in. At t=50s, the system should resume the normal mode of operation since the CPL has decreased enough and $p_{Rload} + p_{cpl} \leq p_{fc,max}$. However, this is not the case because the FC still has to recharge the battery. This is why the system only resumes normal mode at t=60s. The smooth transition at t=60s was made possible by introducing an algorithm like an anti-windup system, if not, the system encounters a sequence during which the FC power is null and the battery takes charge of the full load power. This is obviously not how the system is supposed to operate. In practice, the integral term in $p_{fc,ref}$, depicted in Eq. 25, is forced to stay constant as soon as $p_{fc,ref} \geq p_{fc,max}$. Note that this tweak is not to be confused with the integral term saturation, moreover it was observed to provide the best performances.

As for the objective regulation, apart from the similar remarks related to the normal mode, a large deviation on the battery SoC regulation all along the overcharge sequence is examined

from t=25s to t=50s, as shown in figure. 2-19. This was expected since the FC cannot simultaneously feed the load and recharge the battery as soon as it reaches its maximum power.

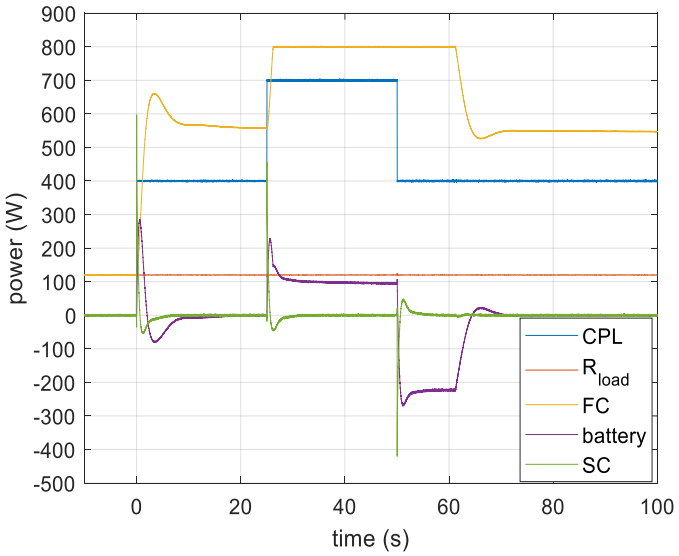

Figure 2-18 : Overcharge mode – power allocation

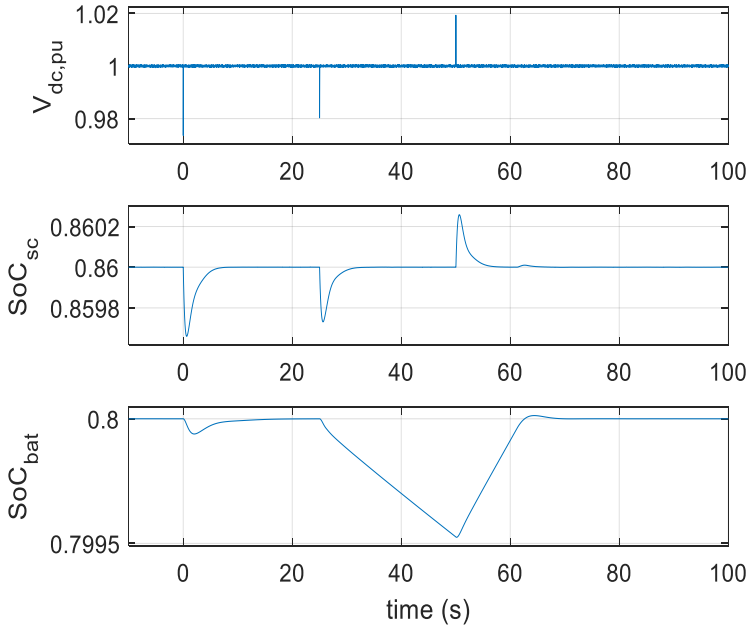

Figure 2-19 : Overcharge mode – objectives regulation

2.4.4 Regenerative mode

The CPL is a way to emulate any kind of electrical power chain conversion, motor or generator alike. Therefore, this study would not be complete without investigating regenerative sequence for which the CPL inject power towards the DC link. This scenario is illustrated in figures. 2-20 and 2-21. As for the power allocation, the system operates in normal mode up to t=30s, the time at which the system enters the regenerative sequence since the CPL power becomes

negative. Since the FC cannot absorb power, the SC combined with the battery must step in. At t=50s, the system should resume the normal mode of operation since the CPL becomes positive again and $p_{Rload} + p_{cpl} \leq p_{fc,max}$. However, this is not the case, as the battery still needs to recover its SoC reference. This is accomplished when the battery is discharging while feeding the load between t=50s and t=65s. The system returns to the normal mode only at t=65s.

As for the objective regulation, it is worth noting the large deviation on the battery SoC regulation all along the regenerative sequence from t=30s to t=50s. To avoid overshoot on the FC cell power, it is necessary to limit the integral term without penalizing the control linear domain range, a good compromise is to set this saturation according to:

$$sat = \frac{0.7 \cdot p_{fc,ref,max}}{k_i \cdot C_{ah} \cdot 3600 \cdot v_{bat,min}} \tag{2.44}$$

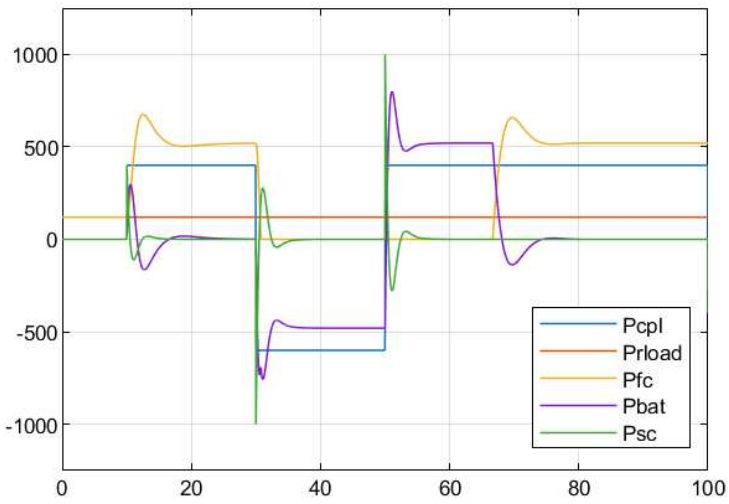

Figure 2-20 : Regenerative mode – power allocation

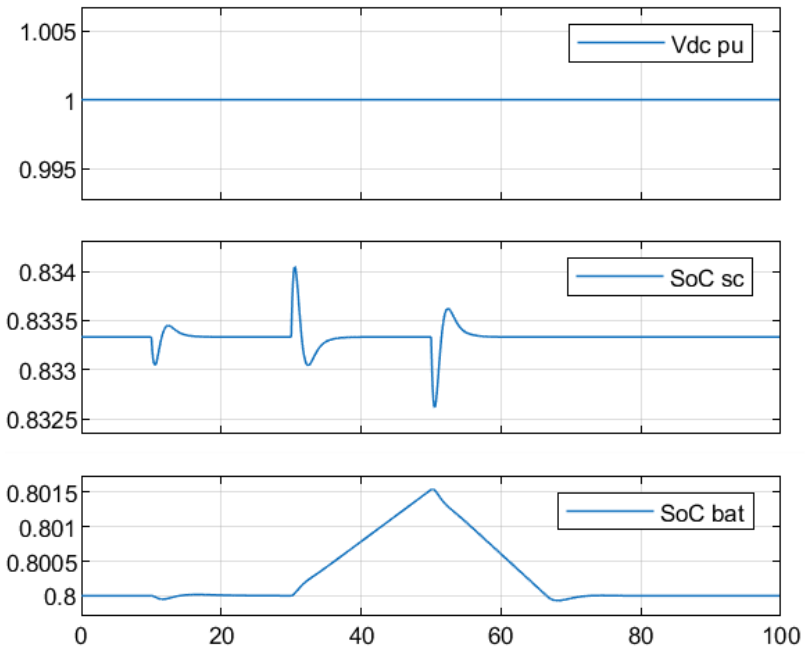

Figure 2-21 : Regenerative mode – objectives regulation

2.5 Conclusion

In this chapter, a new generic hierarchical strategy for a DC microgrid with multiple storage devices, is presented. The aim of this strategy is, firstly, to make the DC bus regulated in case of variable load demand, and secondly, to control the objective related to either the SoC or the energy of the studied energy storage units. The originality of the proposed method compared to others from literature lies in its generalized formalism combined with objectives. Indeed, this strategy can be applied to Ns storage elements. To demonstrate its effectiveness, a case study involving three devices, namely a supercapacitor, a battery and a fuel cell, under various load conditions using MATLAB/Simulink and a test bench equipped was presented for system analysis and validation. Three scenarios were investigated to illustrate control compliance with the expected goal.

CHAPTER 3. A Control Strategy for DC Microgrids with Integrated Distributed Generators

In the previous chapter, a centralized control strategy for a DC microgrid integrating closely located storage devices was proposed. In contrast, this chapter adopts a different approach tailored to a distributed architecture, suitable for DC microgrids where Distributed Generators (DGs) are geographically dispersed and require local coordination. The proposed controller provides the following key features:

(iv) Simultaneous proportional current sharing and precise regulation of average voltage.

(v) Minimal exchange of information between neighboring DGs to limit the communication load.

(vi) Robustness in the face of load variations and communication failures.

3.1 Introduction

In the context of increasing decentralization of production through renewable energies, control systems must be capable of guaranteeing both equitable power sharing between distributed DGs and reliable voltage regulation through the electrical grid, while considering communication process, cyber security, scalability and reliability constraints.

The proposed control approach comes to address the above-mentioned requirements, while minimizing implementation heaviness and complexity and communication burdens. Before describing how the proposed controller works, it is, nevertheless, worth reviewing the main existing methods that have been explored in the literature.

To begin with, the droop control strategy is one of the widely used methods for current sharing in DC microgrids, due to its fully decentralized nature and ease of implementation. Its principle is based on a simple law as depicted in figure 3-1. The output voltage $v_{o,i}$ of the ith DGU decreases in proportion to the current $i_{o,i}$ it supplies according to (1), where v_n is the grid nominal DC voltage, ΔV is the maximum authorized voltage deviation, and $I_{max,i}$ is the maximum output DC current for the ith DGU. The droop coefficient y_i is evaluated based on the grid constraint according to $y_i = \Delta V / I_{max,i}$.

$$v_{o,i} = v_n - y_i \cdot i_{o,i} \tag{3.1}$$

This strategy enables automatic current balancing without the need for communication between DGUs [71], [72]. However, this approach has significant limitations. On the one hand, it does not ensure accurate current sharing, especially in the presence of line impedance differences. Secondly, it offers no guarantee of effective bus voltage regulation to the rated value v_n, which can be a problem for system stability and the protection of sensitive loads. Moreover, it is well established that higher droop grain improves the current sharing but in return increases the voltage deviation and improves stability (since it increases the output impedance) [73].

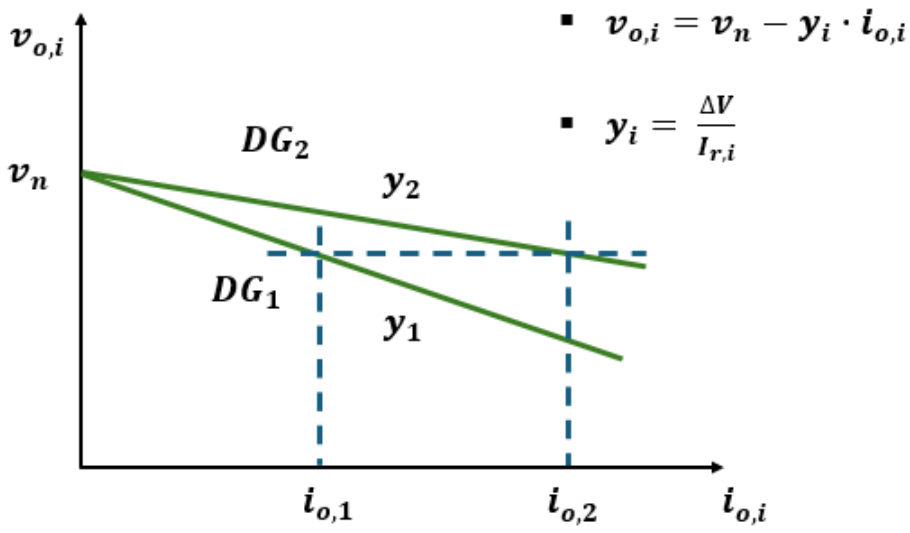

Figure 3-1 : Conventional droop controller

To overcome these limitations, many variants of droop control have been developed. Among these, non-linear droop approaches [74] propose dynamically adapting the voltage-current relationship as a function of the operating point, allowing flexibility in power sharing. Other methods, known as adaptive [75], adjust the droop coefficient in real time according to network conditions. For instance, the strategy, proposed in [75], allows local adaptation of the droop coefficient, nevertheless, it is based on a cost function defined at the system level, which inherently introduces a centralized approach. The dynamic droop adjustment also requires an optimization problem to be solved, implying a certain intensive computation. Hence, although these strategies partially improve performance, they introduce additional complexity into the controller design.

Droop-based strategies can be sorted out into three categories: those that modify the droop coefficients, those that adjust the reference voltage, and finally hybrid approaches that combine

these two mechanisms. In a distributed environment, each DGU has to adjust its parameters locally while exchanging information only with its direct neighbors. This enables efficient coordination without overloading the communication network.

A current trend is to combine droop-based primary control with distributed secondary control, responsible for correcting deviations generated by the primary layer. However, some of these strategies require each DGU to have access to all the data in the microgrid, which leads to a dependency on high-capacity communication. For example, the work of [76] assumes that each unit has access to the voltages, currents and the droop coefficient of its neighbors. These requirements make the system more vulnerable to communication failures or attacks, while increasing the complexity of implementation. Moreover, the strategy was experimentally validated with only two DGUs. To decrease this dependency, reduced communication approaches - where only neighbor information is exchanged - have emerged as a relevant alternative [77]. In this context, consensus algorithms have emerged as powerful tools for achieving distributed coordination based on local information [78]. For example, in [79], the authors propose a controller based on two loops: one to correct the voltage, while the other to adjust the droop coefficients, both driven by a consensus algorithm. Another adaptive method, presented in [80], uses two (Proportional Integrator) PI controllers to dynamically adjust the voltage and the coefficients according to the consensus established on the reference current. Figure 3.2 illustrates its whole control strategy. This combines a primary layer (PI + PWM) for local regulation, a secondary layer comprising two PI regulators for voltage restoration and dynamic adjustment of the droop coefficient, and a consensus layer enabling each DGU to estimate the reference current via exchanges with its neighbors. Although these approaches achieve objectives effectively, their layering-based approach complicates the design of the system and requires delicate adjustment of the parameters of each loop to guarantee satisfactory performance.

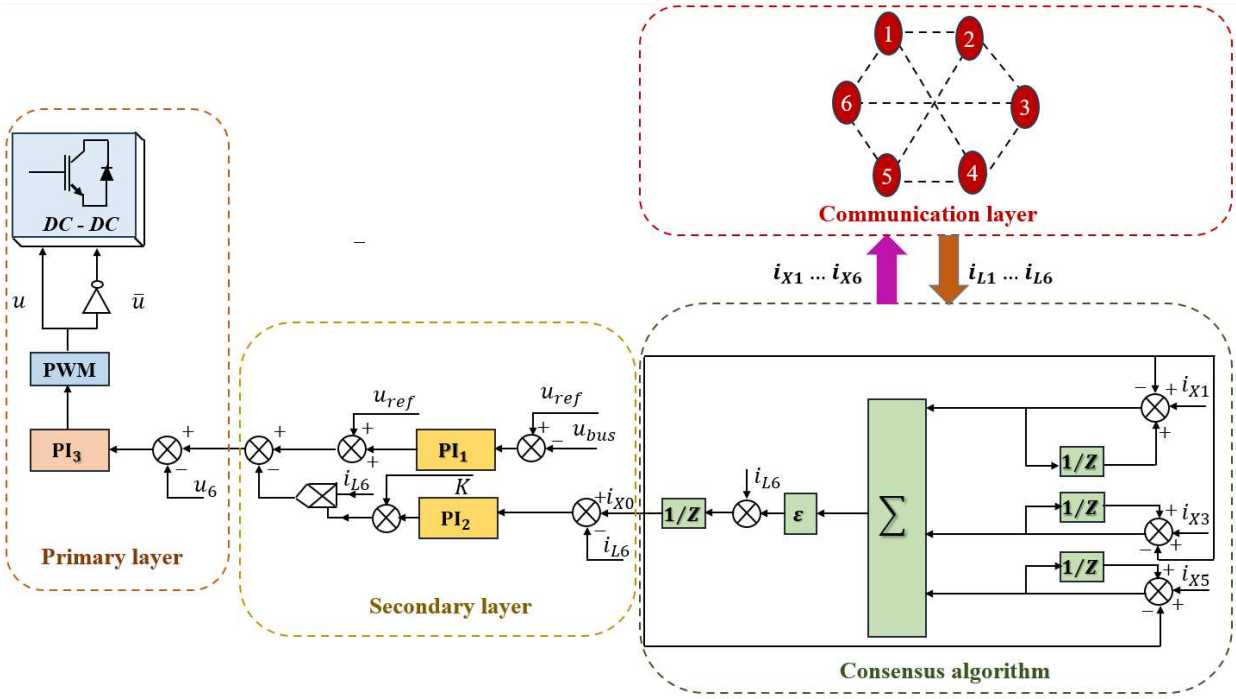

Figure 3-2 : Principle of distributed hierarchical control strategy used in [80]

Similarly, the two-voltage shifting terms strategy proposed in [81], although effective, presents a complexity of tuning noted in [82], where a simplified version with unified control has been suggested.

Overall, the majority of recent distributed strategies rely on several regulators acting in parallel to ensure voltage stability and current sharing. However, this multi-layered structure results in significant design and tuning complexity. In addition, the communication load required by some of these controllers can affect network stability and pose security risks.

This chapter proposes a new approach to distributed cooperative control aimed at automatically adjusting the droop coefficients of DGUs in a unified manner. Unlike some existing solutions, such as [82] whose proposed strategy is depicted in figure 3-3., the method presented here requires neither a voltage observer nor the fine-tuning of several parameters.

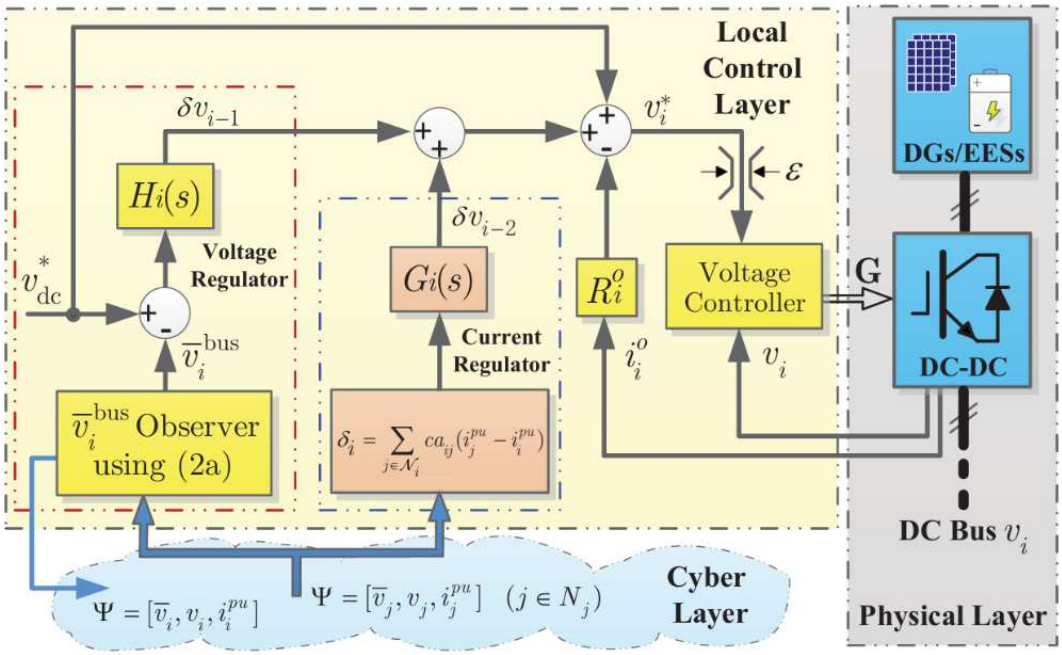

Figure 3-3 : The proposed unified distributed cooperative strategy in [81].

The rest of the chapter will present the mathematical structure of the proposed controller, the details of its implementation, and the results of simulations validating its performance compared with existing strategies.

3.2 Theoretical Foundations of Distributed Control

In this chapter, we will first introduce the fundamental concepts of graph theory and consensus algorithms, which form the mathematical and conceptual basis of our cooperative control approach. These tools enable interactions between DGU to be modelled efficiently by representing communication links, and serve as a foundation for designing robust, adaptive and scalable distributed control strategies.

3.2.1 Graph Theory

A directed graph with N nodes is defined as a pair $\mathcal{G} = (\mathcal{V}, \mathcal{E})$, where $\mathcal{V} = \{1, \ldots, N\}$ is the set of nodes (or agents), and $\mathcal{E} \subseteq \mathcal{V} \times \mathcal{V}$ is the set of edges (or communication links). An edge $(j, i) \in \mathcal{E}$ means that agent j sends information to agent i. In an undirected graph, information exchanges are bidirectional, i.e. $(j, i) \in \mathcal{E} \Leftrightarrow (i, j) \in \mathcal{E}$.

The graph can be represented by an adjacency matrix $\mathcal{A} = [a_{ij}]$, where a_{ij}>0 if $(i, j) \in \mathcal{E}$, and a_{ij}= 0 otherwise. The degree matrix $\mathcal{D}$ is a diagonal matrix such that $d_i = \sum_{j \neq i} a_{ij}$. The Laplacian matrix of the graph is then defined as:

$$\mathcal{L} = \mathcal{D} - \mathcal{A} \tag{3.2}$$

The Laplacian matrix is a key element to analyzing the connectivity and the dynamics of multi-agent systems.

3.2.2 Distributed Consensus Protocol

A consensus algorithm allows a set of agents, each with local information, to reach a common agreement only through exchanges with their neighbors. The aim is to achieve global coordination using only local interactions, making it a key tool for distributed systems.

Expressly, each agent i has a local state variable $x_i(t)$ which we wish to converge towards a common value $\bar{x}$. The desired collective behavior is then formulated as follows:

$$\lim_{t\to\infty} x_i\,(t) = \bar{x} \quad \forall i \in \mathcal{V} \tag{3.3}$$

In our context, x_i may refer for instance to the per unit DGU current, or the local mean voltage. Where $\mathcal{V}$ denotes the set of agents in the network. The evolution of x_i is governed by continuous dynamics, usually expressed as:

$$\dot{x}_i(t) = -\sum_{j\in\mathcal{N}_i} a_{ij} \cdot \left(x_i - x_j\right) \tag{3.4}$$

Here, $\mathcal{N}_i$ is the set of neighbors of agent i and a_{ij} is a positive weight associated with communication between DGUs i and j.

3.3 DC microgrid configuration

The DC microgrid studied in this work is a mono-PCC one, its architecture is shown in figure 3-4. This grid consists of four distributed generation units (DGU1 to DGU4), each coupled to a DC-DC converter and supplying a local load (Load 1 to Load 4). Each DGU is connected to the PCC through a line exhibiting an impedance z_i. Besides, a common load is fed at the PCC. Each DGU is equipped with a local controller to regulate the output voltage while ensuring current sharing between the different units. Communications between the DGs are limited to exchanges between direct neighbors according to figure 3-5.

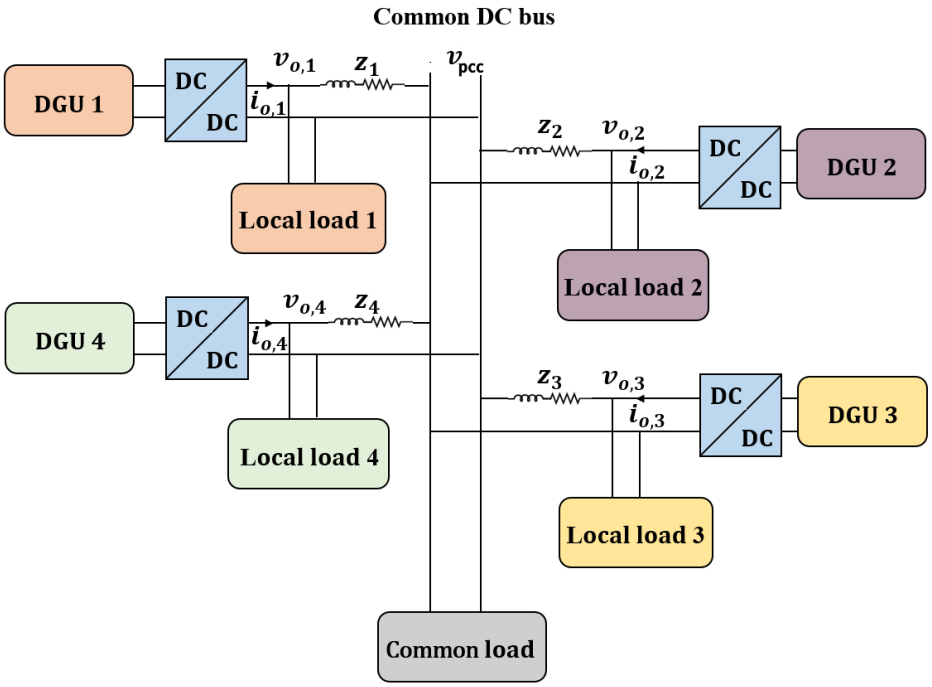

Figure 3-4 : The considered DC microgrid architecture

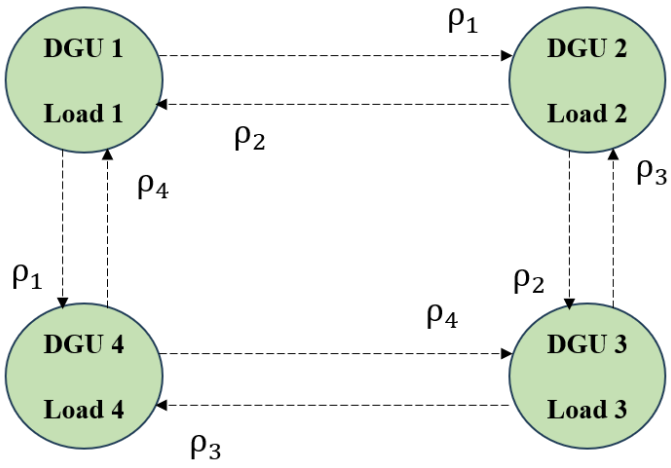

Figure 3-5 : Communication layer related to the considered electrical grid

3.4 Proposed Distributed Cooperative Control strategy

3.4.1 Control objectives

In order to ensure a stable, safe and reliable DC microgrid operation with multiple DGUs, effective coordination between these units is essential. This coordination relies on a distributed control architecture capable of guaranteeing both the correct sharing of loads and the maintenance of voltage within its setpoint. Thus, the control proposed in this work aims to satisfy two main objectives:

- Proportional load sharing

The first objective is to ensure a fair distribution of output currents between the different units according to their rated capacity. Specifically, each DGU must inject a current proportional to its rated current. Mathematically, this means that the ratio between the injected current $i_{o,i}(t)$ and its rated current $i_{r,i}$ must be equal for all units in steady state:

$$\lim_{t\to\infty} \frac{i_{o,i}(t)}{i_{r,i}} = \lim_{t\to\infty} \frac{i_{o,j}(t)}{i_{r,j}}, \quad \forall i,j \in \mathcal{V} \tag{3.5}$$

- Average voltage regulation

The second objective is to regulate the common DC bus voltage. Due to the distributed nature of the system, it is difficult to impose an identical voltage at all points. Instead, the objective is to converge the average output voltages of the different units to a nominal value v_n defined for the microgrid:

$$\lim_{t\to\infty} \sum_{i=1}^{N} v_{o,i}(t) = v_n \tag{3.6}$$

3.4.2 The proposed controller

In this work, a droop-based control strategy was implemented for which the output reference voltage $v_{ref,i}$ is generated following Eq. 3.7:

$$v_{ref,i} = v_n - y_i \cdot i_{o,i} \tag{3.7}$$

where v_n is the nominal bus voltage, $i_{o,i}$ is the current injected by the unit and y_i is the droop gain. However, when a constant gain y_i is used, a compromise arises between two often contradictory objectives:

- a high y_i value enhances the current sharing but increases the voltage deviation,
- a high y_i value enhances the system stability as a virtual resistance damping,
- a small y_i value shrinks the voltage deviation but makes power sharing uneven.

To overcome this limitation, the proposed cooperative controller is developed, in a distributed manner, based on a dynamic adaptation of droop gains. The idea is that each DGU dynamically adjusts its gain taking into account both its own local situation and information shared with its

neighbors. The coordination process is based on a distributed consensus protocol applied to the gains themselves.

The droop gain evolves according to the following law:

$$\dot{y}_i(t) = -\sum_{j \in \mathcal{N}_i} a_{ij} \cdot (\rho_i - \rho_j) \tag{3.8}$$

where ρ_i is a local coordination variable specific to each agent, exchanged between neighbors, and a_{ij} represents the communication weight in the graph. This structure makes it possible to synchronize the dynamics of gains in a fully distributed framework.
This law is based on a consensus-type principle, in which each DGU dynamically adjusts its droop coefficient according to the differences observed with its neighbors. Intuitively, if a unit injects more current than its neighbors (i.e. its variable ρ_i is higher), it reduces its droop gain to decrease its contribution, and vice versa (according to relation 3.9).

Based on (3.8) and the specific value of a_{ij} it is clear that $\sum_{i=1}^{N} \dot{y}_i(t) = 0$ at any time. Then, $\sum_{i=1}^{N} y_i = 0$ as soon as the variable are initiated with null initials conditions, i.e. $y_i(t_0) = 0$.

Each variable ρ_i is updated dynamically as follows, where α is the control parameter, $i_{pu,i} = i_{o,i}(t)/i_{r,i}$ is the per unit current, i.e. output current of each DGU with respect to its nominal value $i_{r,i}$.

$$\dot{\rho}_i = v_n - \alpha \cdot \rho_i \cdot i_{pu,i} \tag{3.9}$$

The whole architecture of this cooperative controller, including the structure of the observers, the internal control loops and their integration into the overall system, will be detailed in the next section, along with a representative diagram in figure 3-6.

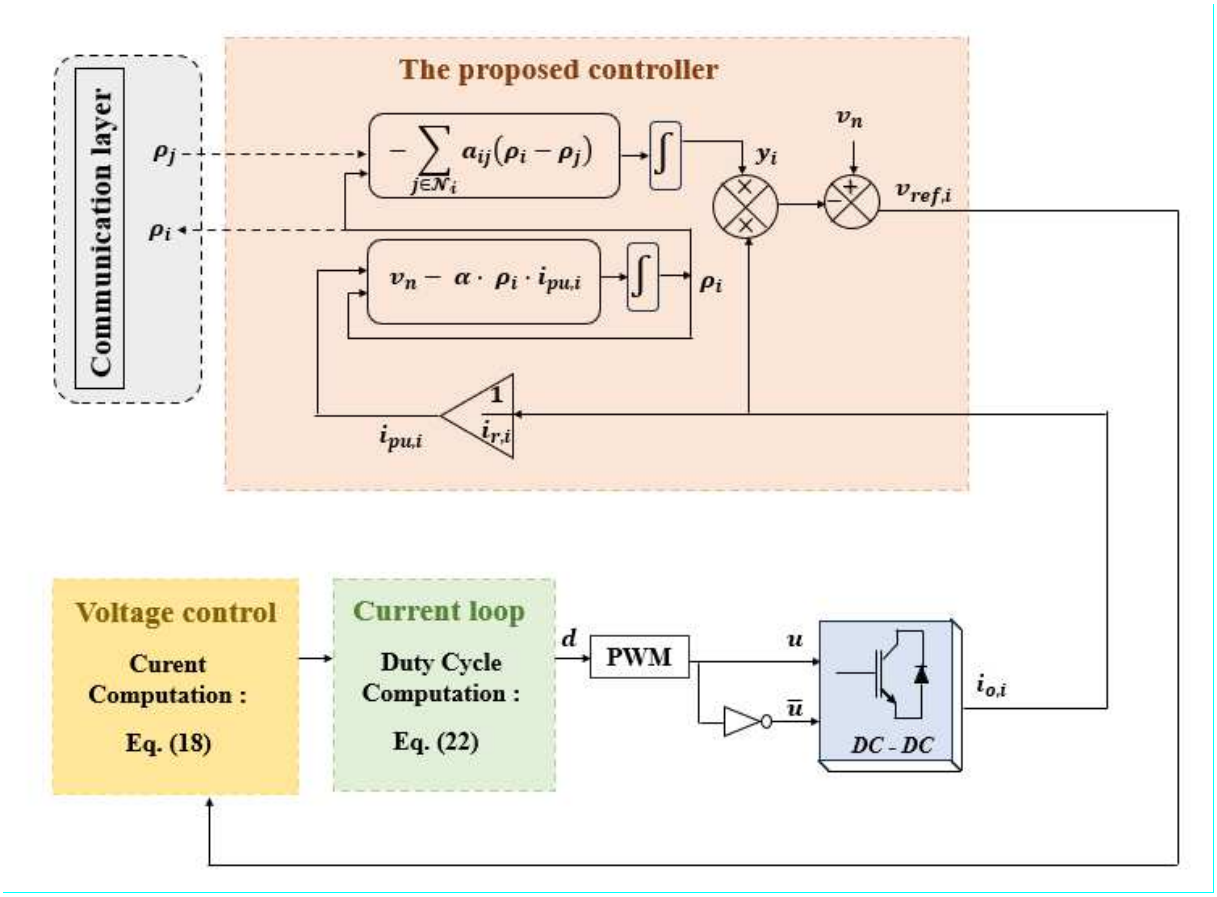

Figure 3-6 : Multi-layer diagram of the proposed strategy

3.4.3 Steady state analysis

Studying the steady-state behavior of the proposed distributed controller results in demonstrating its ability to simultaneously satisfy the abovementioned objectives, proportional current sharing and average voltage regulation. By expressing the operating Eqs (3.7), (3.8) and (3.9) in matrix form, we can formally analyze the system's equilibrium conditions. The dynamic equations of the system are grouped in the following form:

$$V_{ref} = V_n - Y \cdot I_o \tag{3.10}$$

$$\dot{Y} = -\mathcal{L} \cdot P \tag{3.11}$$

$$\dot{P} = V_n - \alpha \cdot P \cdot I_{pu} \tag{3.12}$$

where:

$V_{ref} \in R^N$ is the reference voltage column vector,

$V_n = v_n \cdot \mathbf{1_{N\times 1}}$ is the nominal voltage column vector,

$Y = diag(y_1, \dots, y_N)$ is the diagonal matrix of droop gains,

$\mathcal{L} = D - A$ is the Laplacian matrix of the communication graph,

$P = diag(\rho_1, \dots, \rho_N)$ contains the synchronized consensus variables,

$I_{pu} = [i_{pu,1}, \dots, i_{pu,N}]^T$ is the per unit current vector,

$\alpha \in R_+^*$ is a global control parameter.

In steady state, it is assumed that the derivatives become zero, i.e. $\dot{Y} = 0$ and $\dot{P} = 0$. Under these conditions, Eqs. (3.11) and (3.12) become:

$$-\mathcal{L} \cdot P = 0 \quad \Rightarrow \quad \rho_1 = \rho_2 = \cdots = \rho_N = \bar{\rho} \tag{3.13}$$

In other words, thanks to the consensus protocol implemented via the Laplacian matrix, all the units converge towards a common value of the variable ρ_i. Injecting this condition into Eq 3.12, it gives:

$$0 = V_n - \alpha \cdot P \cdot I_{pu} \quad \Rightarrow \quad i_{pu,i} = \frac{v_n}{\alpha \cdot \rho_i} = \frac{v_n}{\alpha \cdot \bar{\rho}} \tag{3.14}$$

The obtained Eq 3.14 shows that all the agents inject an equal per unit current, thus ensuring perfectly balanced current sharing between the different DGUs.

It is worth noting that all DGUs are synchronized, i.e. set in operation at the same time, and $\sum_{i=1}^{N} y_i(t) = 0$ is maintained by setting the initial condition as $y_i(t_0) = 0$ for each DG. By multiplying Eq 3.10 by $\mathbf{1}_{1\times N}$ and dividing by N, the average voltage v_{avg} is determined:

$$V_{ref} = V_n - Y \cdot I_o \qquad \Rightarrow \qquad v_{avg} = \frac{1}{N} \cdot \sum_{i=1}^{N} v_{ref,i} = v_n - \frac{1}{N} \cdot \sum_{i=1}^{N} y_i \cdot i_{o,i} \approx v_n \tag{3.15}$$

$\sum_{i=1}^{N} y_i = 0$ but $\sum_{i=1}^{N} y_i \cdot i_{o,i} \neq 0$, nonetheless this quantity is small in comparison to v_n . The full prove are developed in appendix A and B and consist of basic operations. Thus, we can conclude that the average reference voltages of all DGUs almost converges towards the nominal setpoint $v_n$without the need to implement a secondary control to compensate the voltage deviation. In this way, the two objectives of secondary control are achieved simultaneously, namely current sharing proportional to the rated capacity and regulation of the average voltage.

3.4.4 Voltage and current loops control

In order to follow the reference voltage V_{ref}, generated by the distributed cooperative controller, each boost converter, whose scheme is presented in figure 3-7, is regulated using a hierarchical

structure, which is made up of two nested control loops: an outer loop dedicated to regulating the voltage, and an internal loop responsible for regulating the inductive current.

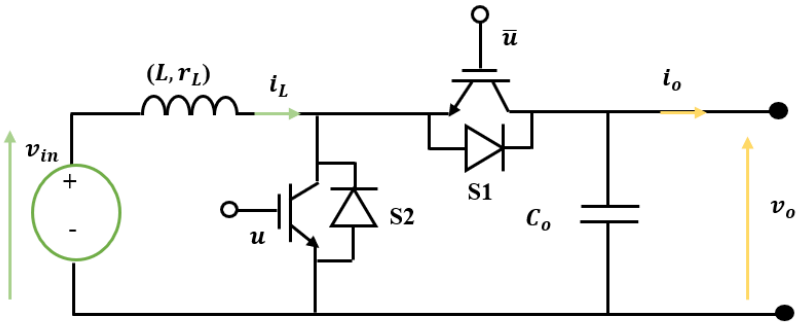

Figure 3-7 : Boost converter

As for the outer loop, the regulation of the output voltage v_o to $v_{ref,i}$ relies on an approach based on the electrostatic energy stored e in the output capacitor C_o, whose expression is given by:

$$e = \frac{1}{2} \cdot C_o \cdot v_o^2 \tag{3.16}$$

Instead of directly comparing the measured voltage with the setpoint, the actual energy is compared to the reference one. The energy error is thus defined as:

$$e_v = \frac{1}{2} \cdot C_o \cdot (v_{ref}^2 - v_o^2) \tag{3.17}$$

The proposed approach is similar to the one introduced in chapter 2, the voltage source v_{in} reference power p_{ref} is computed according to Eq 3.18 where $P_o = v_o \times i_o$ represents a local estimate of the power supplied to the load, used here as a decoupling term to mitigate disturbances.

$$p_{ref} = P_o + C_o \cdot v_{ref} \cdot \dot{v}_{ref} + k_{pv} \cdot e_v(t) + k_{iv} \cdot \int_0^t e_v(\tau) \cdot d\tau \tag{3.18}$$

The controller gains $k_{pv} = 2 \cdot \xi_v \cdot \omega_v$ and $k_{iv} = \omega_v^2$ are then selected to set the error dynamic according to Eq 3.19.

$$\dot{e}_v(t) + k_{pv} \cdot e_v(t) + k_{iv} \cdot \int_0^t e_v(\tau) \cdot d\tau = 0 \tag{3.19}$$

As a result, the current reference $i_{L,ref}$ is computed following $i_{L,ref} = p_{ref}/v_{inf}$.

As for the inner loop, the inductor current i_L regulation is based on the average dynamics model, as follows, where r_L is the parasitic series resistance of the inductor L,, d is the duty cycle applied to the converter, v_{in} is the input voltage, and v_o is the output voltage.

$$\frac{di_L}{dt} = \frac{1}{L} \cdot (v_{in} - r_L \cdot i_L - (1-d) \cdot v_o) \tag{3.20}$$

The current error is defined as:

$$e_i = i_{L,ref} - i_L \tag{3.21}$$

Following an input/output linearization approach, the duty cycle is generated according to Eq 3.22

$$d = 1 + \frac{L}{v_o} \cdot \left(\frac{r_{Lb}}{L} \cdot i_L - \frac{v_{in}}{L} + \frac{di_{L,ref}}{dt} + k_{pi} \cdot e_i + k_{ii} \cdot \int_0^t e_i(\tau) \cdot d\tau \right) \tag{3.22}$$

The controller gains k_{pi} and k_{ii} are determined from dynamic specifications (cut-off pulsation ω_i , damping factor ξ_i) via $k_{pi} = 2 \cdot \xi_i \cdot \omega_i$, $\quad k_{ii} = \omega_i^2$ so much so that the error e_i dynamic is imposed according to :

$$\dot{e}_\iota + k_{pi} \cdot e_i + k_{ii} \cdot \int e_i \, dt = 0 \tag{3.23}$$

3.4.5 Stability analysis

This section focuses on the stability assessment of the DC microgrid when the proposed distributed cooperative controller is applied. The main objective is to ensure that the overall behavior of the system remains stable, even in the presence of local load variations or changes in control parameters. Two types of analysis are carried out: steady-state stability analysis of the overall system and sensitivity analysis related to the control parameter α.

In this study, it is assumed that the local control loops of each DGU (i.e. current $i_{L,i}$ and voltage $v_{o,i}$) are significantly faster than the distributed coordination loop. In other words, their poles are assumed to be stable and far enough apart that their dynamics do not interfere with that of

the consensus protocol. Consequently, the output voltage of each converter $v_{o,i}$ is assumed to follow its reference perfectly $v_{ref,i}$.

The system is then modelled in compact form by a vectorial differential equation, such that:

$$\dot{x} = f(x) \tag{3.24}$$

where $x = [P, Y, I_b]^T$ is the state variables vector:

- $P = \text{diag}(\rho_1, \dots, \rho_N)$, the consensus variables,
- $Y = \text{diag}(y_1, \dots, y_N)$, the diagonal matrix of droop gains,
- $I_b = \text{diag}(i_{b,1}, \dots, i_{b,N})$, the currents in the interconnection lines.

To analyze stability around the equilibrium point x_0, we linearize the system by calculating the Jacobian matrix:

$$J = \nabla f(x_0) \tag{3.25}$$

The poles of the system are then determined by calculating the eigenvalues of this Jacobian matrix.

- Case study

A simulation involving $N = 4$ DGUs was conducted to illustrate the stability of the system. The evolution of the eigenvalues was observed when the local loads varied between:

$R_{local} = [80, 50, 40, 20]\Omega$ and $R = [200, 125, 100, 50]\Omega$

The results obtained are shown in figure 3-8. Whatever the load's configuration, all the eigenvalues of the system keep a strictly negative real part, attesting to the stability of the system. This demonstrates that the distributed control algorithm is robust to large variations in local load conditions.

- Sensitivity to control parameters.

A second analysis was carried out to study the impact of the control parameter α on the dynamics of the system. By varying α from 40 to 400, figure 3-9 shows how the poles evolve in the complex plane. We observe that:

- An increase in α shifts the poles to the left of the complex plane.
- This shift reflects faster damping and improved system response speed.

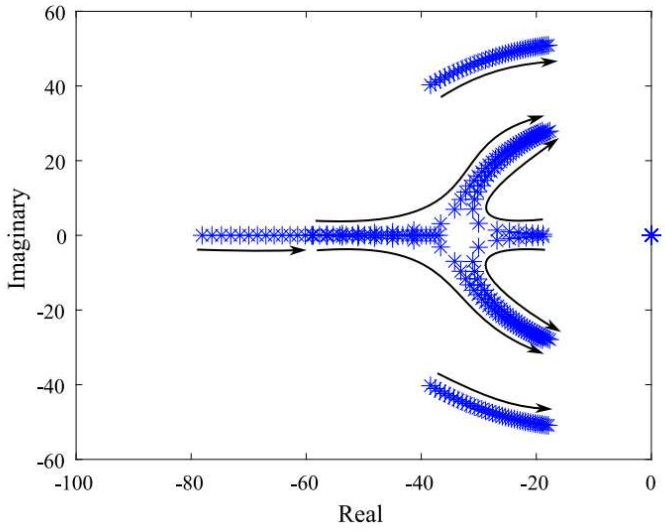

Figure 3-8 : Eigenvalues evolution of the system under local load variation

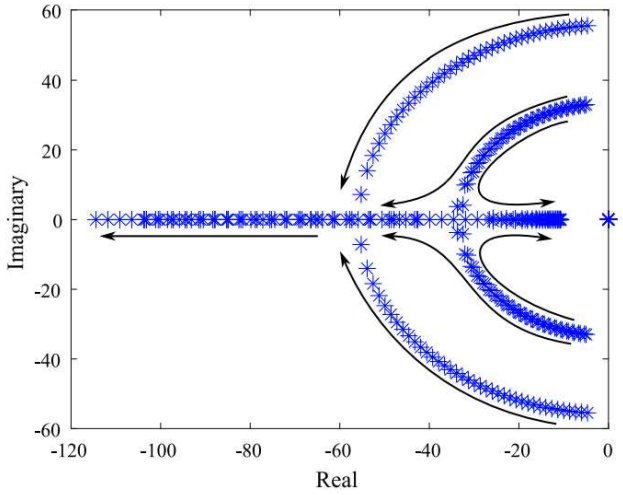

Figure 3-9 : Movement of the poles of the system during an increase of α from 40 to 400

3.5 Simulation results

This section presents the transient simulation results obtained to validate the performance of the distributed control strategy applied to a DC microgrid. The study focuses on the evaluation of voltage regulation and current sharing between DGUs in the presence of disturbances, such as load variations and communication delays. The simulations were carried out in the MATLAB/Simulink environment, considering an architecture with four interconnected DGUs. The parameters used to model the physical system, and the control loops are summarized in Table 3-1. The results make it possible to analyze the robustness and stability of the controller under different operating conditions.

Table 3-1 : System and Controller parameters

Symbol	Description	Value
v_{in}	Input DC source voltage	$100\ V$
L_b	Boost inductor	$1.25\ mH$
C_b	Boost output capacitor	$2\ mF$
r_i	Line resistance	$\{0.5, 0.2, 0.3, 0.4\}\ \Omega$
l_i	Line inductance	$\{150, 80, 100, 120\}\ \mu H$
v^*	Voltage reference	$200\ V$
ξ_i, ω_i	Current loop parameters	$1, 2000\ rad/s$
ξ_v, ω_v	Voltage loop parameters	$1, 200\ rad/s$
i_r	DGU rated current	$\{15, 25, 20, 30\}\ A$
f_{sw}	Switching frequency	$40\ kHz$
T_c	Control period	$25\ \mu s$
α	Controller coefficient	300

3.5.1 Comparison between Classic Droop Control and the proposed controller

A comparative study was first carried out between conventional droop control and the distributed secondary control strategy to highlight the limitations of the classical controller and the significant advantages of the latter. Up to $t = 1.5s$, only droop control is active, providing acceptable voltage regulation, thanks to low slope coefficients, but with unbalanced current sharing between the different units. Each DGU adjusts its output independently, leading to uneven power distribution. From $t = 1.5s$, activation of distributed control enables coordination between the units via a consensus mechanism, leading to convergence of voltages towards the reference value and gradual balancing of injected currents. As illustrated in figure 3-10, the average voltage of the common bus is better regulated, and the accuracy of current sharing is considerably improved. The proposed strategy thus demonstrates clear superiority in terms of overall performance, ensuring stability and fairness in the operation of the microgrid. One may note the small discrepancy between $v_{avg} = 199.7V$ and $v_n = 200V$, which stems from the non-strictly null quantity $\sum_{i=1}^{N} y_i \cdot i_{o,i} \neq 0$.

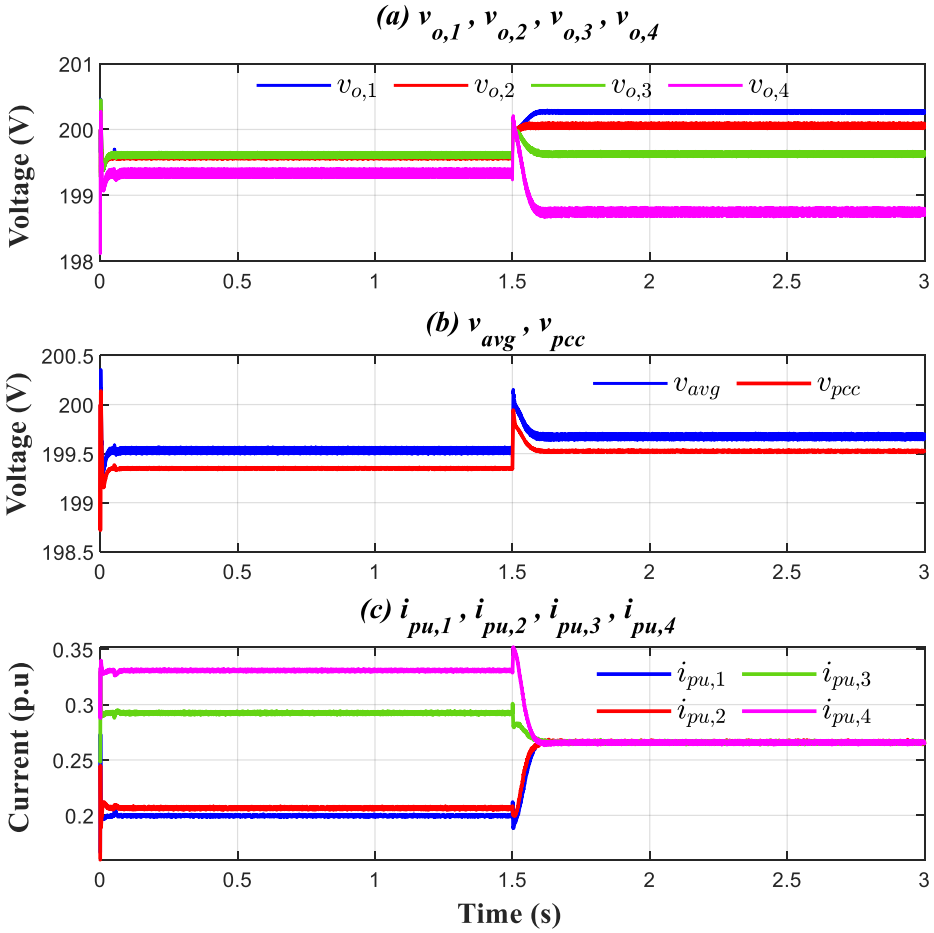

Figure 3-10 : Comparison of the proposed cooperative control with the conventional droop control

3.5.2 Effect of common load changes on the common DC bus

In this scenario, the common load R_{cl} on the DC bus is suddenly reduced from 90 Ω to 20 Ω at $t = 1s$, then restored to its initial value at $t = 2s$. This disturbance causes a sudden increase in current demand, resulting in a transient drop in the common dc bus voltage v_{pcc} , visible in figure 3-11 (b). The local voltages $v_{o,i}$, shown in figure 3-11. (a), react differently depending on the DGUs, but return to equilibrium after each event.

The injected currents $i_{pu,i}$, depicted in figure 3-11 (c), increase coherently with the drop in resistance, demonstrating an effective distribution of effort between the units. Their gradual return to normal after $t = 2s$ attests to the system's ability to absorb global variation while maintaining good stability. These results highlight the responsiveness and robustness of the controller to changes in common load.

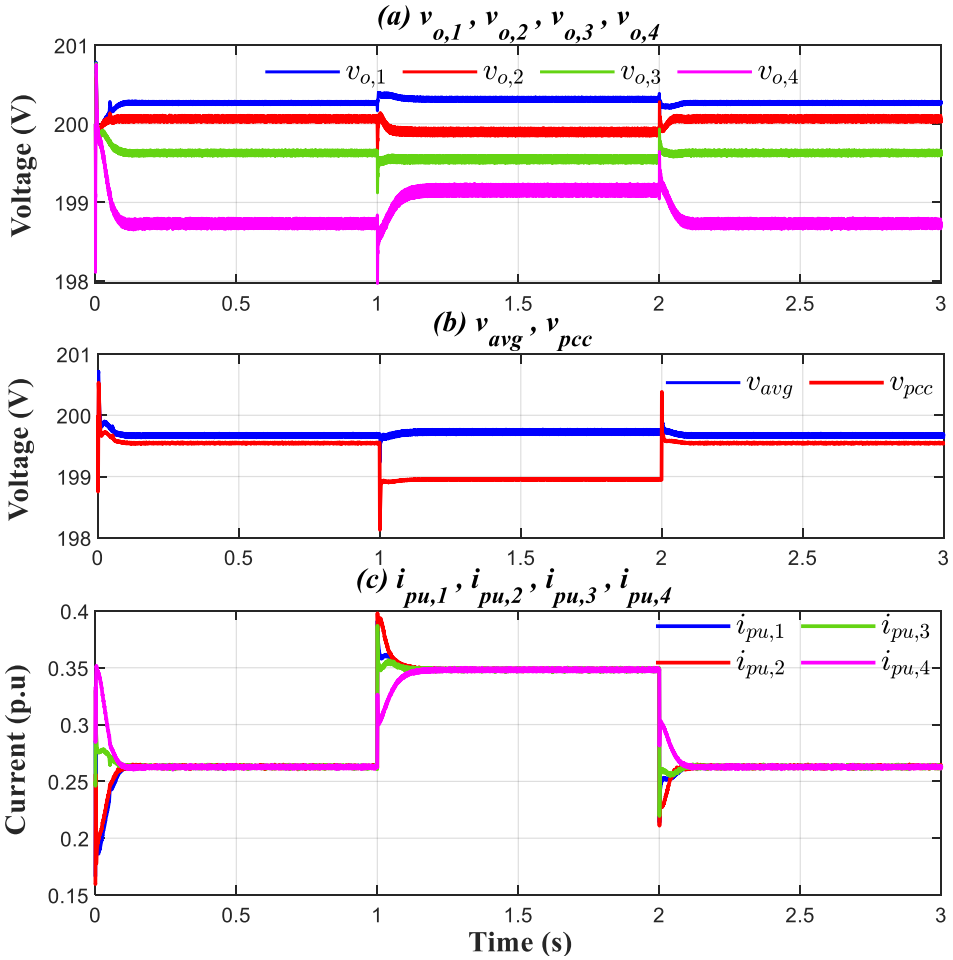

Figure 3-11 : Response of the DC microgrid under common load variation

Figure 3-12 illustrates the evolution of the droop gains and state variables of the DGUs in response to the variation in the common load. During disturbances at $t = 2s$, the droop gains (graph (a)) adjust dynamically, reflecting an adaptive redistribution of effort between the units. In parallel, the variables, (graph (b)) react with a brief divergence followed by rapid convergence towards a common value, demonstrating the effectiveness of the consensus mechanism. These dynamics show that the proposed controller succeeds in maintaining the coordination and balance of the microgrid in the face of load variations.

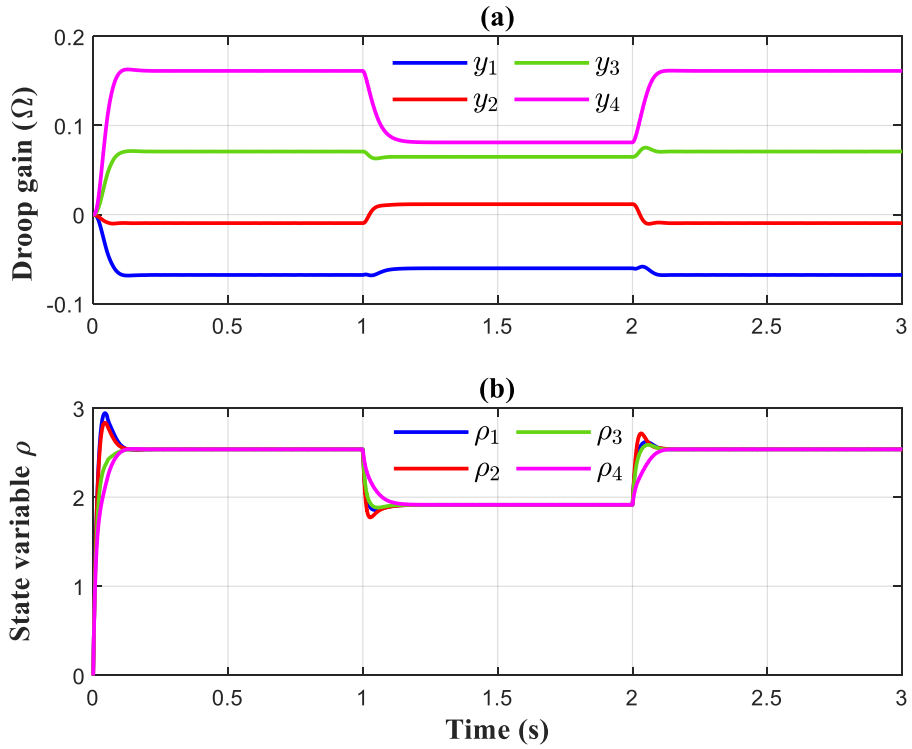

Figure 3-12 : Evolution of droop gains and state variables during common load variation

3.5.3 Effect of local load changes on the local buses

In this test, the initial local loads are defined as follows: R_{local}= [80Ω, 50Ω, 45Ω, 30Ω]. Each load undergoes a change at a specific time:

- R_1 and R_2 are halved at $t = 1s$ and $t = 2s$, respectively.
- R_3 and R_4 are doubled at $t = 3s$ and $t = 4s$, respectively.

These variations mainly affect the DGUs concerned, without significantly disturbing the network as a whole. Figure 3-13 (a) shows that the local voltages react individually to each disturbance. When a load is reduced, the associated local voltage falls slightly, reflecting an increase in current. Conversely, when the load is doubled, there is an increase in local voltage. Figure 3-13 (b) highlights that the average voltage v_{avg} and the common bus voltage v_{pcc} remain stable overall, showing that these local disturbances only slightly affect the system as a whole. This stability reflects the effectiveness of the controller in containing the impact of load variations at the local level. Finally, Figure 3-13 (c) clearly illustrates the responses of the injected currents. Each DGU sees its current vary precisely at the same time as the other DGUs.

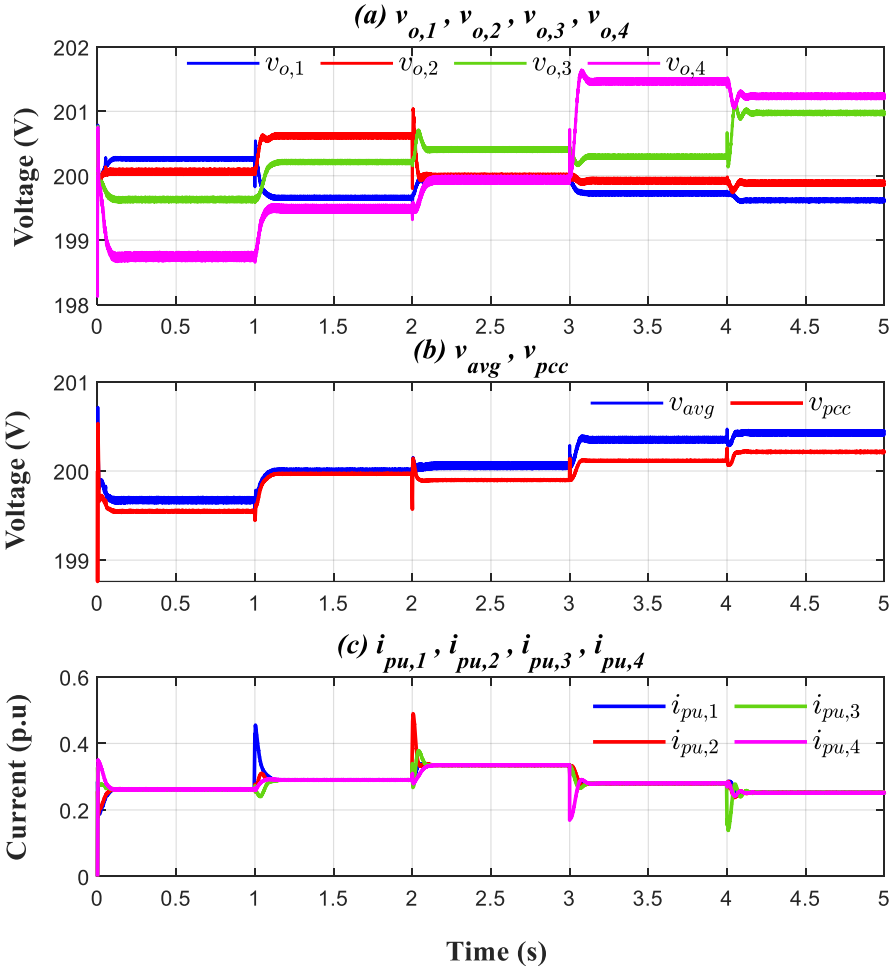

Figure 3-13 : Response of the DC microgrid under local loads' variation

3.5.4 Communication failure assessment

This scenario evaluates the robustness of the proposed distributed controller to a partial loss of communication and several load disturbances. At $t = 0.5$, a failure of the communication link between DGU2 and DGU3 is introduced. This interruption is detected using a "handshake mechanism", which allows each DGU to temporarily exclude a neighbor from the consensus process, thus ensuring continuity of control despite the failure.

Subsequently, several load variations are applied: between $t = 1s$ and $t = 2s$, $R_{cl}$is reduced from 90 Ω to 20 Ω, then restored to 90 Ω between $t = 2s$ and $t = 3s$. Finally, at $t = 3s$ R_1 is decreased from 80 Ω to 20 Ω. Figure 3-14. shows that the system responds effectively to these disturbances. The local voltages and the bus voltage remain stable, and the current injected by each DGU adjusts coherently. Despite the loss of communication between two units, voltage regulation is maintained, and current sharing remains balanced, demonstrating the resilience and adaptability of the proposed controller.

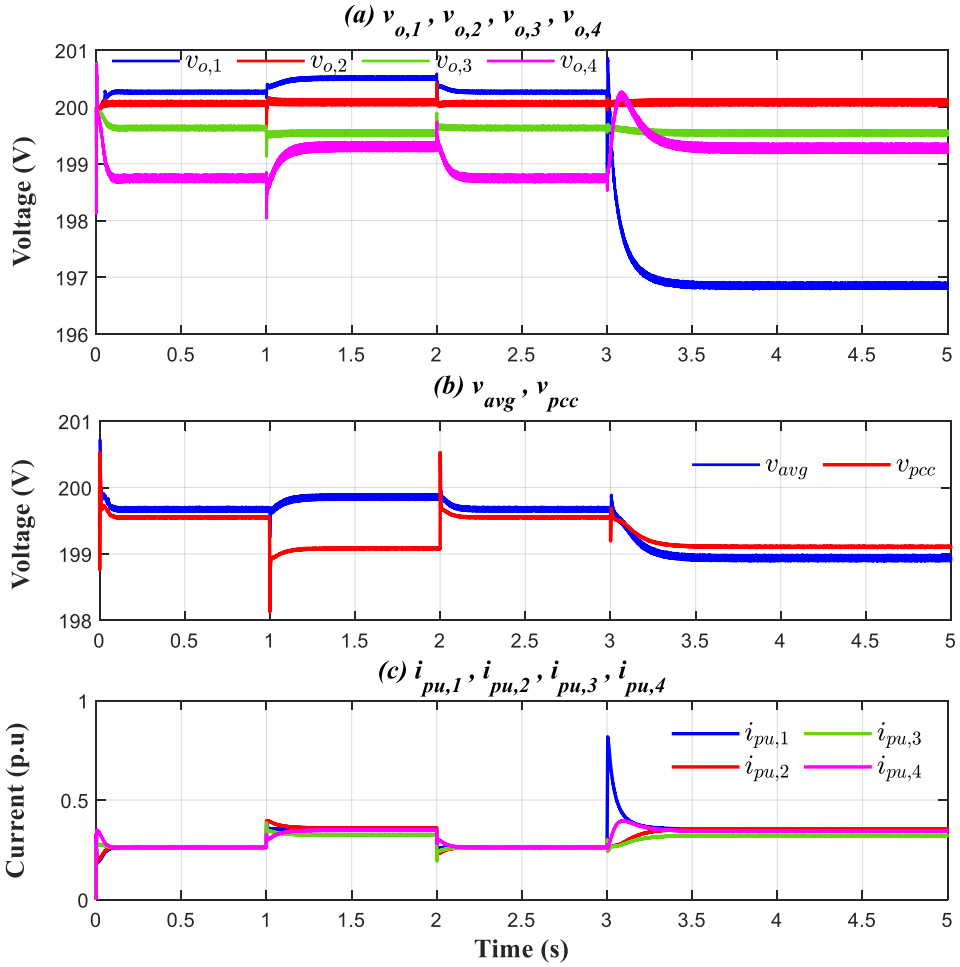

Figure 3-14 : Evolution of voltages and currents under link 2-3 communication failure

3.5.5 Performance evaluation under communication delays

In distributed control systems for DC microgrids, communication delays can occur and affect coordination between units. In order to assess the impact of communication delays, a τ delay was applied to the controllers as follows:

$$\dot{y}(t) = -\sum_{j \in \mathcal{N}_i} a_{ij} \left(\rho_i(t) - \rho_j(t-\tau) \right) \tag{24}$$

To evaluate the robustness of the proposed controller, two scenarios with delays of 15ms and 30ms were tested. The results presented in figures 3-15 and 3-16 show that the controller maintains stable regulation despite the presence of these delays. For instance, with 15 ms, performance remains virtually unchanged. Even with 30 ms, although the transients are slightly more pronounced, the system maintains good stability, balanced current sharing and controlled bus voltage. This confirms the controller's ability to tolerate moderate communication delays without compromising efficiency. The aforementioned approach was also applied to a mesh-

grid, however the results are not as satisfying. Indeed, the current sharing is perfectly achieved, but the voltage deviation is quite significant and a secondary control would be relevant.

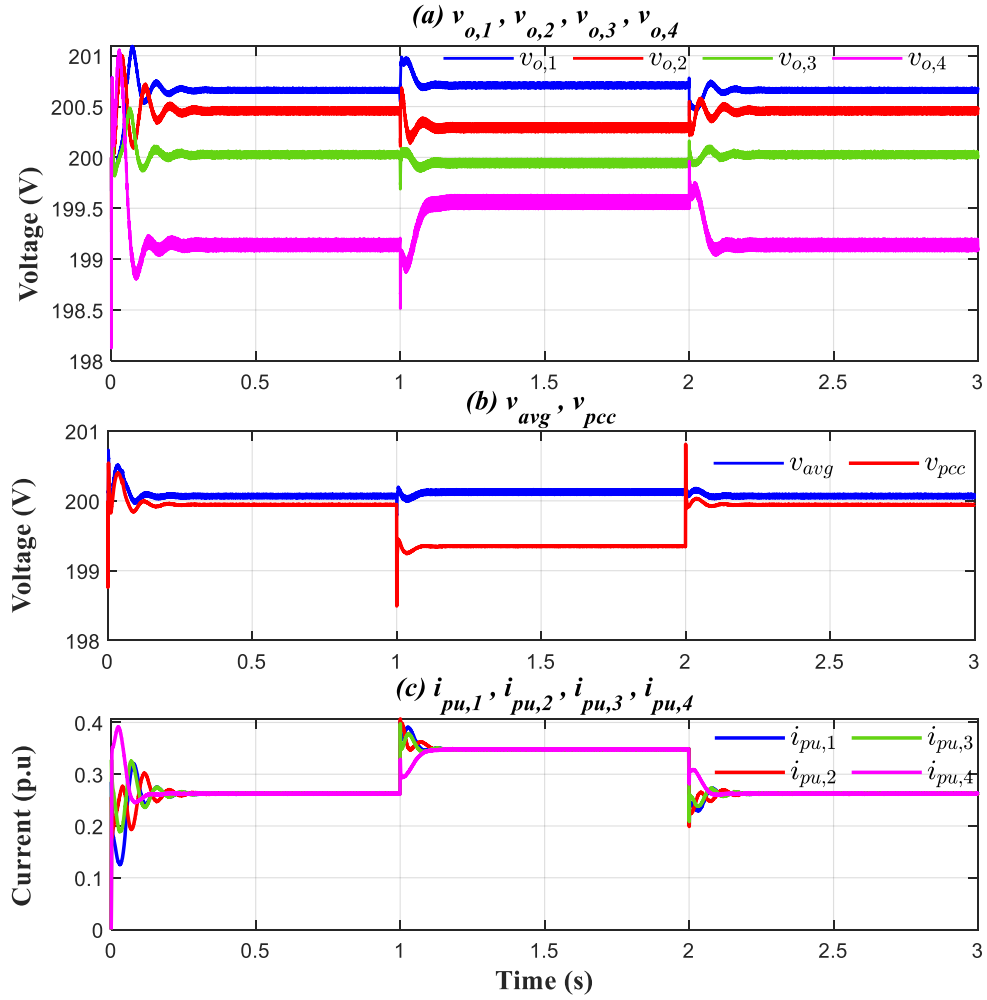

Figure 3-15 : Evolution of voltages and currents under communication delay of 15 ms

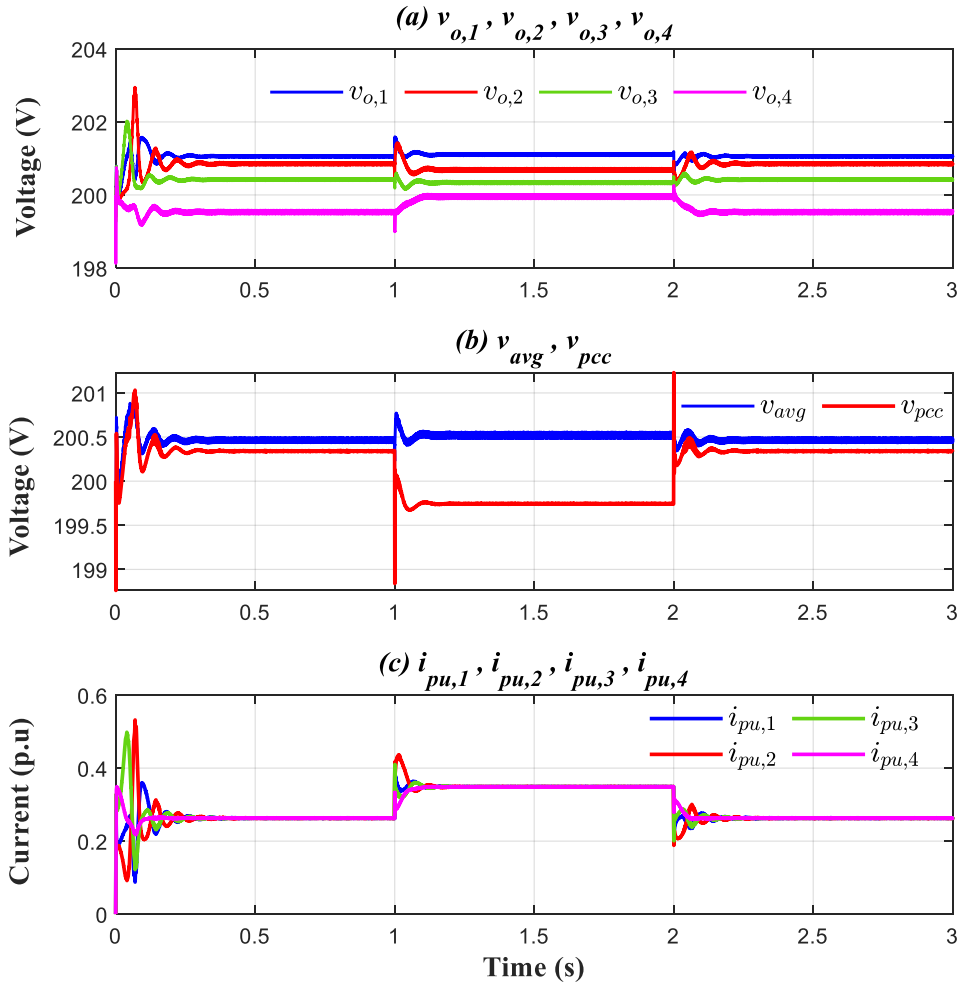

Figure 3-16 : Evolution of voltages and currents under communication delay of 30 ms

3.6 Conclusion

This chapter proposed a cooperative distributed control strategy for DC microgrids whose sources are geographically scattered. This strategy allows both efficient mean voltage regulation and accurate load sharing. The method is based on simplified control, avoiding the need for complex control structures or multiple hierarchical layers. It relies only on local exchanges between neighbors via one single communication variable, reducing the burden on the communication layer. This approach also hinges on one single control parameter, making it easy to size and design, not to mention that this favors scalability to large number of DGU.

Simulations and tests, including realistic disturbances, such as load variations (local and common), communication interruptions and delays, have confirmed the robustness and efficiency of the proposed controller. As a result, this solution represents a reliable, lightweight and high-performance alternative for the autonomous control of DC microgrids. Following on

from this logic of improving energy management, the next chapter looks at the tertiary level, dealing specifically with the coordination of energy exchanges between microgrids.

CHAPTER 4. Cooperative Tertiary Control for Energy Management in Multi DC Microgrids

This chapter presents an energy management strategy dedicated to the tertiary level of distributed DC microgrids. The objective is to coordinate energy exchanges between microgrids while guaranteeing local autonomy and the security of storage devices. To achieve this, a Predictive Functional Control (PFC) method is deployed within each microgrid to anticipate load and generation dynamics. A distributed power exchange algorithm is then applied, based on several indicators - notably local consumption, the SoC of the batteries and the energy produced by PV panels. Simulation results obtained in Matlab/Simulink demonstrate the effectiveness of this approach for optimizing energy flows in a multi-microgrid system.

4.1 Introduction

Tertiary control is the highest level in the hierarchical architecture of microgrid management. It is mainly used to coordinate energy flows between several interconnected microgrids, but also with the main grid where possible. This level of overall supervision aims to optimize the use of available RESs and/or ESSs, considering economic criteria, resources and storage constraints. In a system of distributed microgrids, it enables cooperative or competitive management of energy exchanges. This strengthens the overall resilience of the system while ensuring greater energy autonomy.

In this context, several research works focused on energy coordination between DC microgrids, through distributed and adaptive tertiary control strategies [83]. Another control strategy about distributed hierarchical cooperative and on a cluster of islanded microgrids has been presented in [84]. Authors in this work proposed a control strategy that aims to regulate the frequency/voltage of all RESs within each MG and to achieve the active/reactive power sharing among MGs focusing on the discontinuous communication issue in the distributed MGs. Another interesting work is presented in [85], the work proposed a review on Multi-Agent System (MAS) strategies in microgrid as well as in microgrid clusters. The benefits of the MAS-based distributed coordinated control and optimization strategies are presented with the

framework of stabilization of power and energy, as well as voltage and frequency within the MGs and Multi-MGs (MMGs). Furthermore, the authors in this research work review different control strategies, which are dedicated to reducing the effect of communication delays namely, the generalized predictive control (GPC), the weighted average predictive control and the sliding mode control for the random communication delay scenarios. Moreover, one of the challenging difficulties that are met around MMGs is the difficulty in achieving power dispatch optimization. On this matter, in [86] a hybrid interactive communication optimization solution using hierarchical architecture-based communication has been proposed. This strategy provides the possibility for the microgrids in MMGs to plug-in or plug-out depending on the state of each one.

Model Predictive Control (MPC) is another optimization-based technique being used for MG control [87]. MPC incorporates a dynamic model of the system to be controlled. The internal dynamic model enables the MPC to predict the sequence of future system's states and outputs. In fact, the basic idea of MPC is to predict the future behavior of the system over a finite time horizon and then compute the optimal control input while taking into account some constraints. The control input is calculated by solving at each sampling instant a finite horizon optimal control problem. The first control input is applied to the system while the other control inputs are ignored. The horizon is shifted and the whole procedure is repeated. For instance, authors in [88] presented robust adaptive current predictive control (RPCC) for three-phase inverters connected to the grid. Error correction is performed by means of an adaptation strategy that works in parallel with the algorithm deadbeat, thus preserving the fast response characteristic of the prediction law. Authors in [89] presented a predictive deadbeat control strategy direct power (DPC) with improved voltage vector sequences for a network connected to a VSI (Voltage Source Inverter). In [90] and [91] deadbeat control is used to minimize the prediction error (predict the action effect of the control) so that the reference current can be followed correctly without any mistake. Authors in [92] have proposed different methods and algorithms for hysteresis control in order to obtain a fixed switching frequency. Depending on the method used, the complexity of the control unit can be increased considerably.

Other advanced techniques have been also investigated and studied. For instance, GPC and PFC have shown their control efficiency for MG systems control. Unlike MPC, the GPC is compatible with non-minimum phase systems, but due to its simple implementation, using linear controller, it is more popular in power electronics control system. It uses a discrete

transfer function model for the process and of the disturbance, hence, fewer sensors are needed if compared to PFC, which uses a state space model [93]. It is worth noting that the PFC was not implemented for single MG system's control, despite that it is considered as the most used predictive control technique in industry [94,95,96]. In the field of control in microgrids, it was used only in [97], in which the authors have designed a PFC controller based on a tertiary control strategy. The aim was to manage the power flow in DC microgrid clusters. This was achieved by solving the cost function in the finite receding horizon and computing, in real-time, voltage set points in order to create bus voltage difference.

The approach, proposed in this work is part of tertiary-level control which plays an overall role in multi-microgrid systems. For instance, in [98], a study on distributed tertiary control-based approaches has been investigated. This topology has been applied to microgrid clusters, and it is based on a multi-agent concept. In this approach, intelligent agents, representing various components in a microgrid, interact with each other according to certain rules. Each agent, as an entity, has a localized knowledge base and is characterized by its autonomy, which excludes the idea of centralizing the control of the overall system [99]. Furthermore, based on energy and load consumption forecasting [100], power generation from DERs, historical loads, and weather/season factors, an energy management system provides commands and information about the state of each MG to each physical device, in order to interact and respond accordingly.

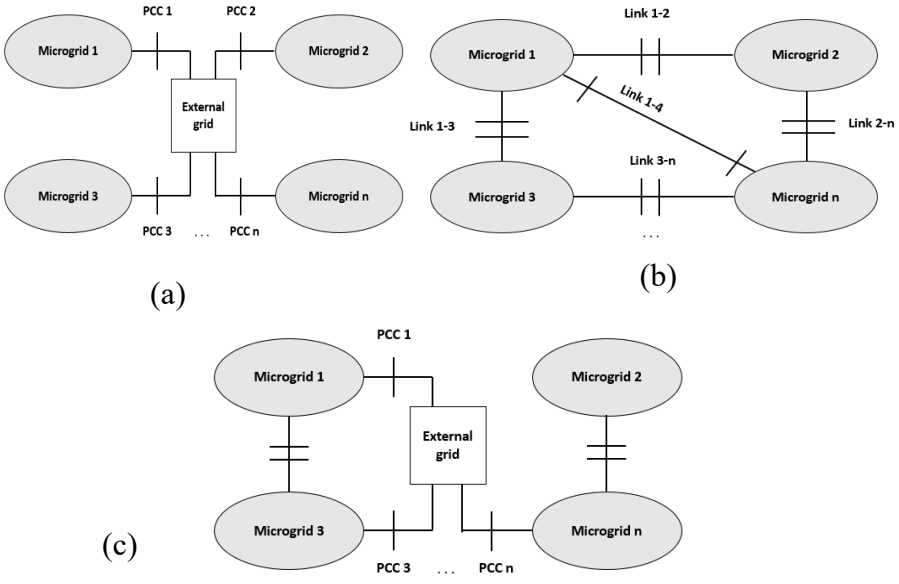

Figure 4-1 : a) the PCM, b) GSIM, and c) MPSC

In addition, it is essential to consider the physical interconnection architecture of microgrids, as the efficiency of energy exchanges and the quality of overall coordination depend directly on it. In this context, authors in [101] explored a holistic study of multi-microgrids, with

particular emphasis on the different possible architectures to form a grid of micro-grids. Indeed, those architectures have been investigated in terms of their layout. This latter gives an idea about how the microgrids are interconnected, their line technology, which defines how the electricity is transmitted, and finally the interconnection technology, which can be linked either to conventional power transformers or to power electronics devices. The architectures are as follows: i) the Parallel Connected Microgrids (PCM) with an external grid, ii) the Grid Series Interconnected Microgrids (GSIM) and the Mixed Parallel-Series Connection (MPSC). As shown in figure 4-2 (a), the PCM architecture consists on connecting all the MGs concerned to the same external grid by giving the possibility for each MG to have a one single PCC. This is in terms of layout, however, when it comes to line technologies, the PCM architecture as well as the other ones, which are going to be investigated in the next few lines, have the same line technology, namely DC or AC. In order to ensure a high level of controllability of the MGs, the usage of power converters remains the best choice for all the architectures that are being addressed. In the GSIM architecture, as shown in figure 4-2 (b), the MGs are all interconnected between each other as well forming then a grid of MGs. The difference here is there is no external grid linking them in contrast to the PCM architecture. Regarding the MPSC, all MGs are connected directly to the external grid or forming clusters of series interconnected MGs allowing mutual support, especially when a disconnection or an overload of external network occurs figure 4-2 (c).

The work presented in this chapter proposes to use the GSIM architecture for forming multi-MG systems including a simple power flow management between its MGs.

4.2 Energy Management Strategy

The energy management within the studied MG systems consists first of predicting future production and consumption using ARIMA model as described in figure 4-2. This model makes it possible to estimate a SoC reference that the battery will have to follow. To control the SoC reference, the PFC controller is then synthesized. It acts on a bidirectional converter whose two switches are PWM-controlled, allowing energy to be injected into or extracted from the battery. The aim is to ensure that the battery's actual SoC dynamically follows the reference trajectory derived from the prediction module. The control strategy is depicted in figure 4-3.

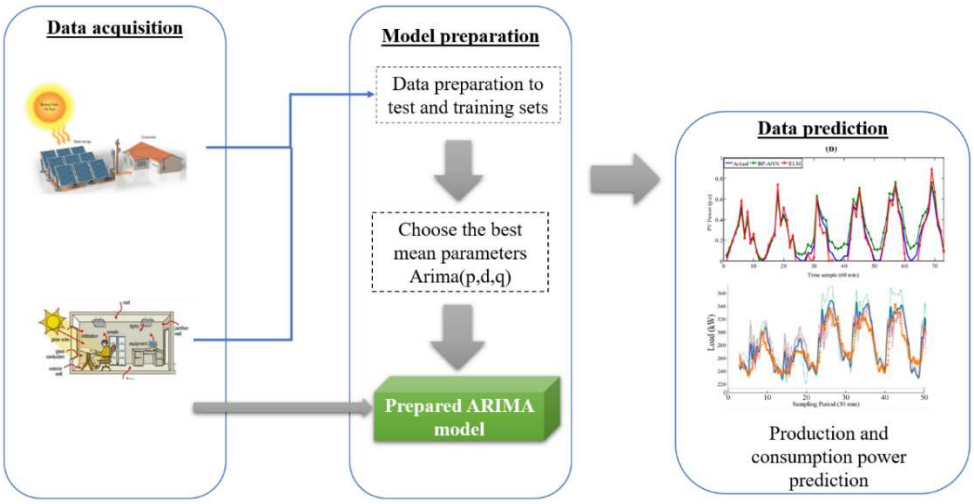

Figure 4-2 : ARIMA-based data prediction framework

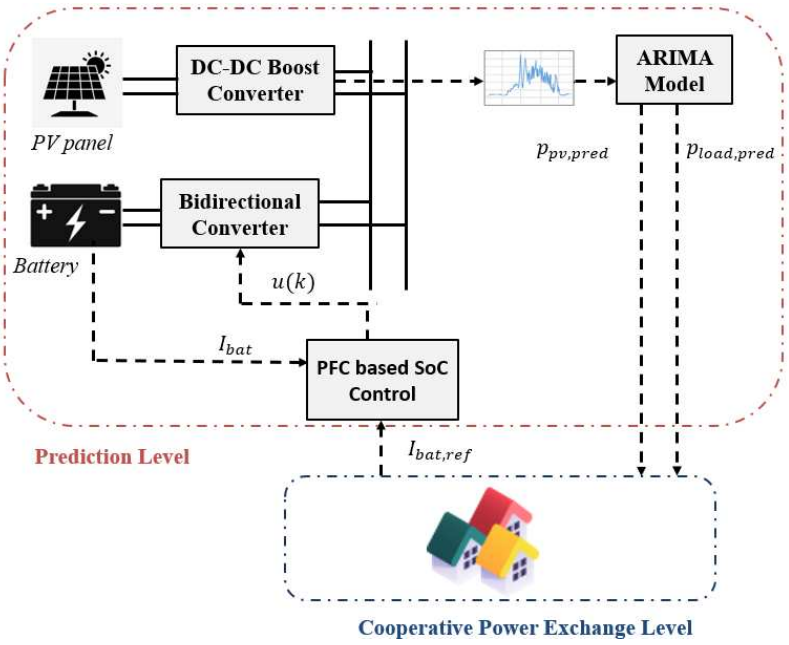

Figure 4-3 : Microgrid configuration and control strategy

The control of SoC within each microgrid is realized using a PFC approach. The required battery power is computed at each instant $(k+i)$ as:

$$P_{Bat}(k+i) = P_{load}(k+i) - P_{PV}(k+i) \tag{4.1}$$

This power must satisfy the battery operating constraints:

$$SoC_{min} < SoC(k+i) < SoC_{max} \tag{4.2}$$

Since the SoC is considered as the integral image of the battery current, I_{bat}, it is controlled indirectly by making it track a predicted reference trajectory:

$$I_{bat_p} = \left[I_{bat_p}(k+1), I_{bat_p}(k+2), \dots, I_{bat_p}(k+n)\right] \tag{4.3}$$

The PFC computes the control signal $U(k)$ so that the output of the system y=I_{bat} reaches the reference $y_r = I_{bat_p}$within a finite prediction horizon n_p. The structure of the PFC control loop is illustrated in figure 4-4. A first-order exponential model is adopted as the internal prediction model due to its simplicity and effectiveness. The discretized transfer function of the model is written as follows, where $I_{bat_m}(z)$ is the Z-transform of the predicted battery current, $U(z)$ is the Z-transform of the control signal, k_m is the static gain of the model, Te is the sampling period of the controller, τ_m is the time constant of the model.

$$\frac{I_{bat_m}(z)}{U(z)} = \frac{k_m\left(1 - e^{\frac{-Te}{\tau_m}}\right)}{z - e^{\frac{-Te}{\tau_m}}} \tag{4.4}$$

Let's consider that $a_m = e^{\frac{-Te}{\tau_m}}$ and $b_m = (a_m - 1)$, the model in its recurrence form becomes, where $I_{bat_m}$is the predicted battery current at time k, $U(k-1)$ is the control signal at previous time step.

$$Ibat_m(k) = -a_m Ibat_m(k-1) + k_m(1+a_m)U(k-1) \tag{4.5}$$

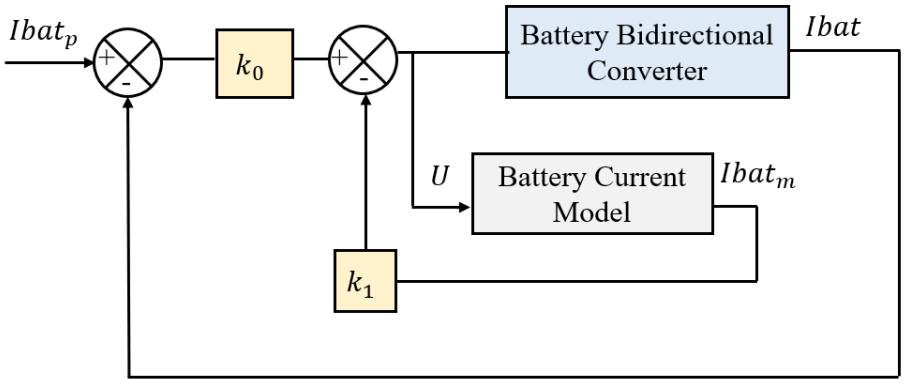

Figure 4-4 : Battery current regulation via PFC and predictive estimation

The predicted increment is:

$$\Delta I_{bat_m}(k) = I_{bat_m}(k + n_p) - I_{bat_m}(k) = [1 - (-a_m)^{n_p}]\left[k_m U(k) - I_{bat_m}(k)\right] \quad (4.6)$$

From this expression, the control law is derived as:

$$U(k) = k_0\left(Ibat_p - Ibat(k)\right) + k_1 Ibat_m(k) \quad (4.7)$$

where $Ibat_p$ is the reference battery current (from prediction), $Ibat$ is the actual battery current measured, $Ibat_m$ is the predicted battery current from the internal model, k_0 is the gain applied to the tracking error, k_1 is the gain applied to the model output prediction.

$$k_0 = \frac{1-\lambda_r^{n_p}}{k_m[1-(-a_m)^{n_p}]} \quad \text{and} \quad k1 = \frac{1}{k_m}$$

Regarding cooperative energy exchange, we consider a distributed MG system as a cluster of *N* MGs, which are interconnected with each other based on the GSIM architecture. Formally, an MG can be defined by a 4-tuple, as follows: $MG_j = \{SoC_j, SOC_{jmax}, SOC_{jmin}, P_j\}$, where SoC_j is its battery state of charge, SOC_{maxj} is the maximum value of the state of charge allowed for its storage system, SOC_{minj} is the minimum value of state of charge allowed, below this value, the MG could not meet any eventual future demand of energy, $P_j = P_{production} - P_{consumption}$, when this value is negative the MG is supplied from other MGs, otherwise the MG is supplying power to the other MGs. In this case, a microgrid MG_j can either receive or supply the energy depending on the sign of P_j. More specifically, depending on the values and the limits of the SoC and the Power P_j, the following sets can be classified and defined into 4 categories as follows:

$$S1 = \{\cup\, MG_j / SoC_j > SOC_{jmin}\,,\, P_j > 0\} \quad (4.8)$$

$$S2 = \{\cup\, MG_j / SoC_j < SOC_{jmin},\ P_j < 0\} \quad (4.9)$$

$$S3 = \{\cup\, MG_j / SoC_j > SOC_{jmin}\ P_j < 0\} \quad (4.10)$$

$$S4 = \{\cup\, MG_j / SoC_j < SOC_{jmin}\,,\, P_j > 0\} \quad (4.11)$$

The class of currents P_{Mk} can be defined as follows:

$$P_{M_k}=\{\Sigma P_j \ / MG_j \in M_k\}, \text{ for } k \in [|1,4|] \qquad (4.12)$$

In this approach, the microgrids are dynamically classified at each instant according to their state of load and power flow. In order to ensure priority management of requirements, energy exchange is organized by giving priority to critical MGs, then to MGs with a partial deficit in accordance with the logic implemented in the exchange algorithm below in figure 4-5.

Algorithm: Cooperative power flow and exchange

Function [SoC_updated, Pavailable_updated] = power_exchange (P_available, SoC_available)
Initialize outputs
Classify MGs into sets S1–S4:
S1: Main producers with enough SoC
S2: Critical consumers
S3: Moderate consumers
S4: Unstable producers
Energy flows management
Case 1: Distribute power from S1 to S2
Pexch= min(P_available (S1), abs(P_available (S2)))
Pavailable_updated (S1) = Pavailable_updated (S1) – Pexch
Pavailable_updated (S2) = Pavailable_updated (S2) +Pexch
Case 2: Distribute remaining power from S1 to S3
Pexch= min(P_available (S1), abs(P_available (S2)))
Pavailable_updated (S1) = Pavailable_updated (S1) – Pexch
Pavailable_updated (S3) = Pavailable_updated (S3) +Pexch
Case 3: S4 contribute to power supply for S2 and S3 when necessary
Pexch= min(P_available (S4), abs(P_available (S2 ∪ S3)))
Pavailable_updated (S4) = Pavailable_updated (S4) – Pexch
Pavailable_updated (S2 ∪ S3) = Pavailable_updated (S2 ∪ S3) +Pexch
Update SoCs
Return SoC_updated and Pavailable_updated

Figure 4-5 : An energy management algorithm for the studied MMGs

4.3 Simulation results

The technical characteristics of the four microgrids (MG1 to MG4) are designed to represent a realistic diversity of energy profiles, as depicted in figure 4-6, while ensuring complementarity that facilitates efficient energy exchange. MG1, with a large PV surface area of 350 m² (20% efficiency) and a maximum solar power output of 1000 kW, coupled with a 5000-kWh battery, has a potential production surplus in relation to its moderate requirement (~15 kW), making it an ideal candidate for the role of supplier in the system. MG2 and MG3, despite having large batteries (7000 kWh each), have relatively low solar production (100 m² and 200 m² of PV respectively), against large loads (~20 kW and 18 kW), placing them in a position of net consumers, often dependent on external input to avoid critical SoC situations. The more balanced MG4, with 300 m² of PV, 6,500 kWh of battery and an average load of 14 kW, acts

as a buffer, able to contribute punctually to the overall balance. All MGs share a battery efficiency of 90%, guaranteeing consistent modelling of energy conversions. This choice of architecture enables us to faithfully represent a distributed energy ecosystem, combining producer, consumer and mixed profiles. The aim is to assess the value of decentralized energy exchange mechanisms in a realistic and varied context.

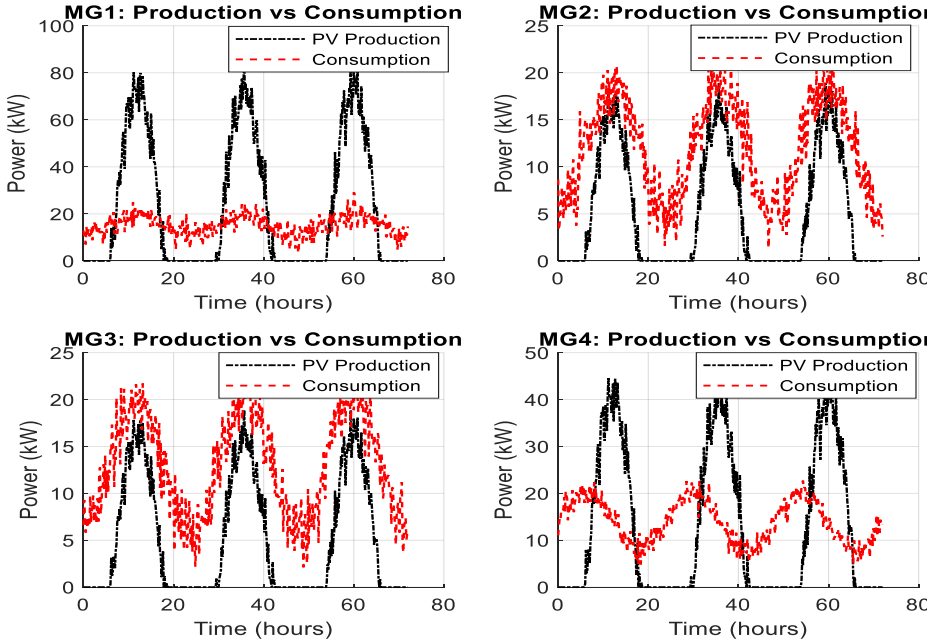

Figure 4-6 : PV production and consumption profiles for the considered MGs

The PFC controller was first compared to the PI controller in order to figure out which one follow the reference predicted current, via a bidirectional grid following converter. Since the SoC is considered as an image of the battery current, the control of this latter turned out to be easier compared to the control of the SoC and still can give a clear indication of its behaviour. The results clearly show, as depicted in figure 4-7, that the PFC controller consistently outperforms the PI controller in terms of battery current tracking accuracy, with superior performance in terms of both root-mean-square error (RMSE) and relative error in all the microgrids analysed. For instance, in MG1, the RMSE drops from 16.78 (PI) 9.81 A (PFC), with a relative error reduced from 2.14% to 0.64%, i.e. an improvement by a factor of ~3.3. MG2 shows a similar improvement, with an RMSE of 3.90 for the PI versus 2.29 for the PFC, and a relative error dropping from 2.44% to 0.75%, confirming a more than 3-fold reduction. For MG3, the results are even more marked, the PFC reduces the RMSE from 3.57 to 2.09 and the relative error from 1.60% to 0.36%, i.e. a performance gain of around 4.4 times. Finally,

MG4 has an RMSE of 6.05 (PI) vs. 3.54 (PFC) and a relative error of 1.15% vs. 0.32%, an improvement factor of ~3.6. Overall, the PFC controller provides more precise and stable dynamic control, reducing the relative error by a factor of 3 to 4 compared to the PI in all cases. These results confirm the superiority of the PFC and fully justify its adoption in standalone MG control, in particular to guarantee more reliable current tracking, limit SoC drops and prevent overloads in an interconnected multi-microgrid system.

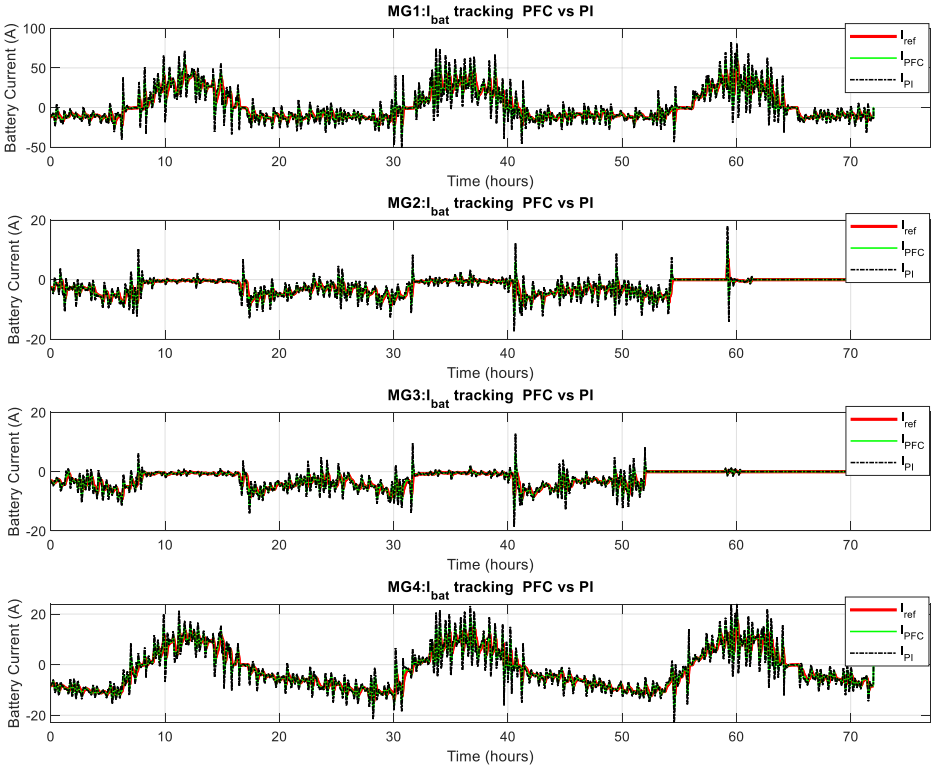

Figure 4-7 : Simulation results for each MGs using the PFC and PI controllers

In order to analyze the performance of the two controllers thoroughly, figure 4-8 zooms in on the time between 10am and 11am. This time slot corresponds to a period of high microgrid disturbance, characterized by high photovoltaic production, sustained consumption and intense power exchanges between microgrids. The curves clearly show that the PFC controller (red line) follows the battery current reference much more accurately than the PI controller (dotted black line). Across all the microgrids (MG1 to MG4), the PFC shows better dynamics, faster response and less oscillation than the PI. This translates into a better attenuation of transient overcurrent's, a more effective ability to react to sudden fluctuations in net power, a better alignment with the reference throughout the critical period. These results then reinforce the conclusion that PFC is a more robust and accurate solution for power management under complex dynamic conditions.

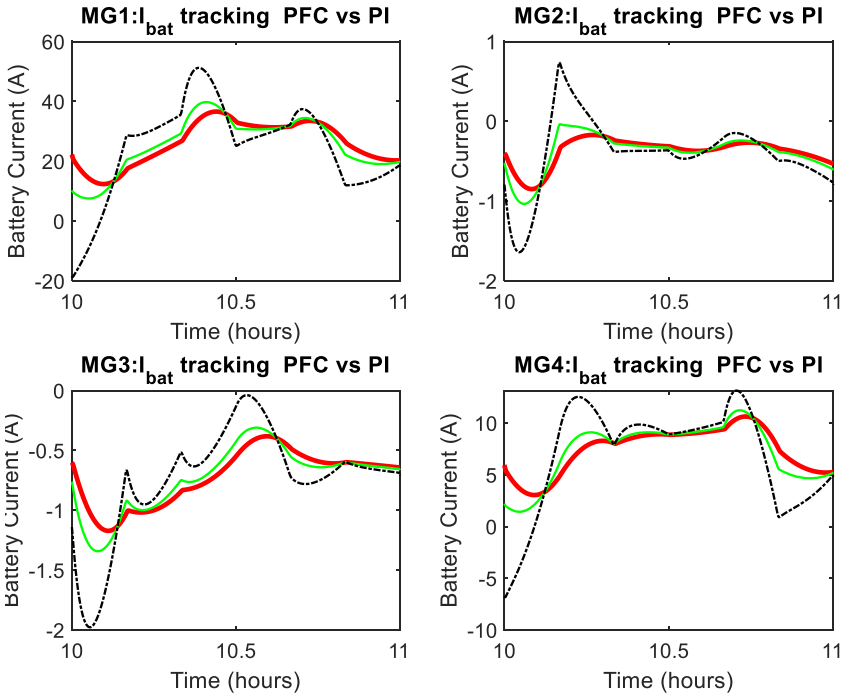

Figure 4-8 : Zoomed-in comparison of battery current tracking performance between PFC and PI controllers over the time interval between 10 h and 11 h

After validating the PFC for each single MG, we then conducted simulations using four MGs, which are linked according to the GSIM architecture. Analysis of the SoC curves, as depicted in figure 4-9, clearly confirms the beneficial impact of energy exchanges between microgrids. For MG1, without exchange, the SoC reaches 100% on several occasions (around hours 20, 40 and 65), resulting in a loss of around 500 to 800 kWh/day due to the lack of additional storage capacity. With exchange, its SoC is regulated between 60% and 90%, enabling efficient redistribution, of up to 800kWh/day. MG2, in a critical situation, sees its SoC fall to 20% from hour 35 without exchange, then stagnate until hour 75, reflecting a near-blackout. Thanks to exchanges, this drop is delayed until hour 70, ensuring prolonged operation and an external input estimated at 700 and 1200 kWh/day. Similarly, MG3, which reaches 20% SoC at around hour 60 without exchange, is maintained above the critical threshold until hour 75 when it is powered, with an intake of up to 1100 kWh/day. Lastly, MG4 is more stable, fluctuating between 40% and 60% in both cases. Without exchange, it occasionally loses 200 to 500 kWh/day, whereas with exchange, it becomes a moderate contributor, transferring 200 to 300 kWh/day to the other MGs. These observations confirm the effectiveness of the exchange mechanism in avoiding blackouts, reducing losses and optimizing collective energy autonomy.

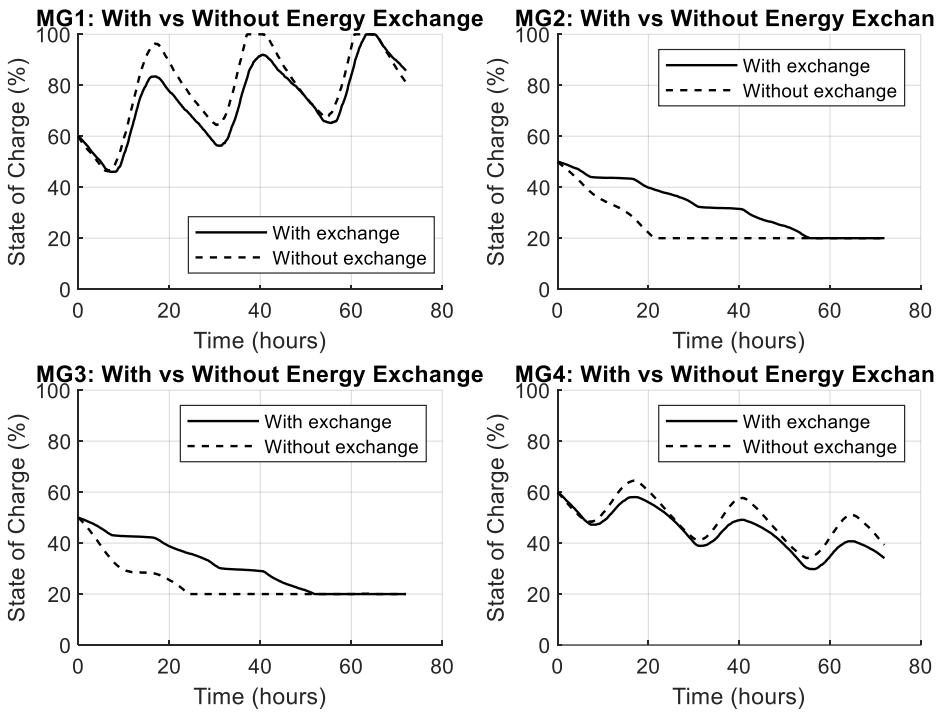

Figure 4-9 : SoC values with and without energy exchange

In addition to these quantitative results, the evolution of SoCs shows a trend towards rebalancing between microgrids when an exchange mechanism is active. While some MGs reach their maximum capacity or fall below a critical threshold in isolated mode, the introduction of exchanges enables the whole system to operate within a more homogenous safety range (between 20% and 90%). This collective stabilization is a strong indicator of energy resilience, particularly for vulnerable microgrids, such as MG2 or MG3, whose ability to maintain service is extended thanks to external contributions. These results underline the value of a cooperative approach, which reduces the need to oversize individual systems, while ensuring optimised continuity of service at cluster level.

In order to clearly illustrate the efficiency and economic benefits of a local energy exchange system, we have measured the amount of the exchanged power, as depicted in figure 4-10. For instance, MG1 acts as the main supplier, injecting up to -20 kW for around 10 hours a day, contributing by an estimated 360 kWh over 3 days, valued at €54 (at €0.15/kWh) - a surplus that would otherwise have been lost. MG2 and MG3, with peaks of up to +10 kW, act as the main beneficiaries, each receiving around 300 kWh over the period, equivalent to a saving of €45 per microgrid, or €90 in total. MG4, which is more neutral, exchanges an average of ~3 kW, representing around 75 kWh transferred over 3 days, for an estimated value of €11.25. All in all, the system delivers an overall economic gain of around €155 over 3 days, while ensuring

greater energy resilience, particularly for vulnerable microgrids, such as MG2 and MG3, which benefit from MG1's contribution. This exchange mechanism promotes optimization of resources, limits energy losses, and demonstrates the relevance of cooperative energy management in a distributed MMG.

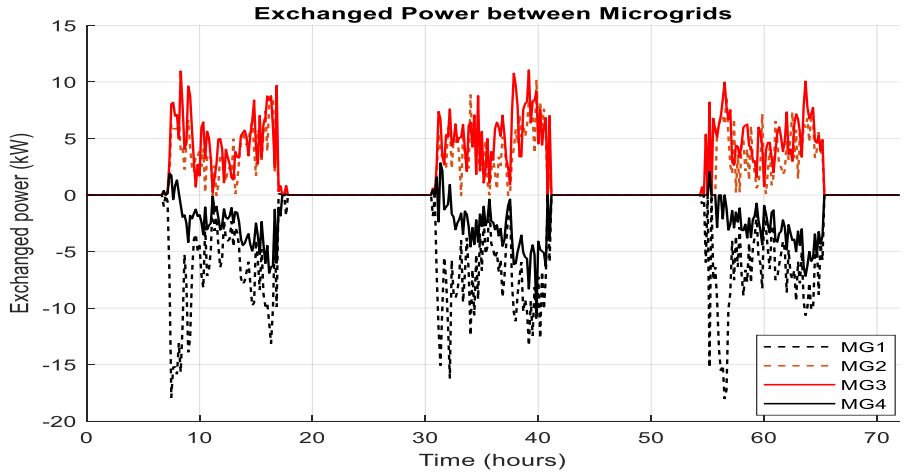

Figure 4-10 : Power exchanged between MGs

This power exchange analysis shows a regular alternation of energy injection and absorption cycles, following typical daily dynamics (daytime PV production, night-time consumption). This cyclical behaviour demonstrates the system's ability to regulate itself intelligently, by assigning each MG an adaptive role depending on the period: supplier, receiver or buffer. MG1 thus acts as an energy core, while MG4 adopts a moderating role, confirming the possibility of a flexible and dynamic distribution of roles. It is worth mentioning that this power exchange mechanism maintains an overall balance of exchanged power, with input and output distributed consistently between the microgrids. This ensures that the net sum of energy exchanged over a given period is close to zero, avoiding any prolonged overloading or under-supply. These results confirm the scalability of the proposed rule-based algorithm. Indeed, by increasing the number of MGs, it becomes possible to build robust local energy ecosystems, capable of adapting to variations in production, consumption or prices, without depending exclusively on the main grid.

4.4 Conclusion

In this chapter, a holistic control approach for energy management in distributed MMGs is introduced. It was designed at the highest level in hierarchical control of microgrids to perform power exchange between the microgrid and external networks. First, a control strategy based on predictive function control was proposed to manage the power flow in a standalone

DC microgrid. The PFC-based control strategy was evaluated through simulations. Results are promising and show the efficiency of the PFC against the PI controller. The proposed distributed cooperative approach for energy exchange was also evaluated and preliminary results showed its capability in handling potential power exchanges scenarios promoting the optimization of resources, limiting energy losses, while demonstrating the relevance of cooperative energy management in distributed MMGs.

General Conclusions and Perspectives

This manuscript is part of a research project aimed at proposing an integrated approach to intelligent energy management in (DC) microgrids, with a particular focus on applications in rural areas, especially in the Moroccan context. Through four complementary chapters, this work successively explored socio-energetic issues, local hierarchical control strategies, distributed cooperative regulation mechanisms, and finally the upper layers of energy optimization at the scale of a set of interconnected microgrids.

The first part of the study provided an in-depth overview of the energy challenges in rural areas. While Morocco has made considerable progress with its rural electrification program, a large part of sub-Saharan Africa is still faced with a lack of access to electricity, persistent dependence on fossil fuels and low penetration of renewable energies in the energy mix. This analysis has highlighted the strategic role that decentralized microgrids can play, particularly in isolated localities (e.g., farming systems), where extensions to the centralized grid are technically or economically hard to achieve. An examination of their architecture, components and control structures formed the technical basis for the following chapters.

Secondly, a generic hierarchical control strategy was developed, capable of simultaneously managing DC bus voltage regulation and managing the energy levels of several storage units. This approach, which can be applied to any number of devices, is based on a unified formulation that allows electrical stability objectives (voltage stabilization) and energy objectives (SoC balancing, autonomy management, etc.) to be expressed in parallel. Simulations and experimental tests carried out on a microgrid integrating a battery, a supercapacitor and a fuel cell enabled this strategy to be validated in various dynamic load scenarios, demonstrating its flexibility, genericity and ability to take account of the heterogeneous nature of storage devices.

The third part of the study focused on distributed control strategies, with a view to scalability and resilience. A simplified cooperative approach was proposed, based on local exchanges between neighboring units. This structure avoids the complexities of multiple centralized or hierarchical systems, while ensuring reliable regulation of the average bus voltage and a fair distribution of the load. This method is distinguished by its lightweight algorithm, which makes it easy to deploy on embedded devices or in environments where computing and communication resources are limited. The results obtained under various disturbances - local

or global load variations, communication outages, delays - confirm the robustness and effectiveness of the strategy.

Finally, a tertiary-scale energy management strategy has been proposed to organize energy flows between several distributed microgrids. This strategy is based on PFC, which offers the ability to anticipate future energy needs by integrating production (PV) and consumption predictions. The PFC controller was compared with a conventional PI controller, showing better reference tracking accuracy, improved dynamics and better transient management. In addition, a cooperative energy exchange method was developed to enable microgrids to share their energy surpluses or deficits intelligently, depending on their states of load. The results show an improvement in local autonomy, a reduction in losses and collective optimization of resources.

Other avenues of research may be explored following this work. Firstly, it would be useful to further develop the implementation of stabilization algorithms for the controls developed in Chapters 2 and 3, in particular through linearization approaches, Lyapunov criteria or frequency analysis. This would formally ensure the stability of the proposed solutions in dynamic multi-agent configurations.

At the microgrid cluster level, the cooperative approach developed could be extended to a non-cooperative framework based on game theory. The objective would be to develop an energy exchange strategy in which each microgrid acts as an autonomous player in the local market, deciding to buy or sell energy according to its own needs, constraints and economic interests. This strategy would take into account local production costs and battery state of charge, while promoting collective SoC balancing.

Finally, real-time experimental work, as well as studies on robustness in the face of communication failures and cybersecurity, would be necessary to validate the feasibility and resilience of the solutions proposed in this thesis.

Appendix A

1. convergence of the sum of $y_k(t)$

The starting point is the relation designated as (8) in chapter 3:

$$\frac{d}{dt}y_i = -\sum_{k\in N_i} a_{ik}\cdot(\rho_i - \rho_k) \tag{1}$$

We define the following vectors:

$$P = \begin{pmatrix}\rho_1\\ \vdots \\ \rho_k \\ \vdots \\ \rho_n\end{pmatrix} \qquad Y = \begin{pmatrix}y_1\\ \vdots \\ y_k \\ \vdots \\ y_n\end{pmatrix} \qquad 1_n = \begin{pmatrix}y_1\\ \vdots \\ y_k \\ \vdots \\ y_n\end{pmatrix} \tag{2}$$

Let us call A the adjacent matrix whose elements are a_{ik}.

Matrix L being the Laplacian matrix related to the adjacent matrix A. Then equation Eq. 1 is equivalent to Eq. 3:

$$\dot{Y} = -L\cdot P \tag{3}$$

L is also designated as the communication matrix in literature. Due to the undirected nature of communication between each DGU, the last line of L is the sum of the $(n-1)$ previous ones, so much so that 1_n is a left sided eigenvector associated to the eigen value $\lambda_1 = 0$.

$$(1_n)^t\cdot L = 0 \tag{4}$$

Then, it comes Eq. 4 :

$$\left(\sum_{k=1}^{n}\dot{y}_k(t)\right) = \frac{d}{dt}\left((1_n)^t\cdot\dot{Y}\right) = -\frac{d}{dt}((1_n)^t\cdot L\cdot P) = 0 \tag{5}$$

Eq. 5 proves that $\sum_{k=1}^{n} y_k$ stays constant over time.

In our case, each element has a null initial condition, so that Eq. 5 leads to the result Eq. 6:

$$\sum_{k=1}^{n} y_k\,(t) = \sum_{k=1}^{n} y_k\,(t=0) \tag{6}$$

Eq. 6 highlights that some of the droop gains are necessarily negative.

2. Convergence to v_n demonstration

In chapter 3, relation (6) asses that:

$$\frac{1}{n} \cdot \sum_{i=1}^{n} v_{ref,i} = v^* \tag{7}$$

This convergence is to be demonstrated in the present section.

The following variables and parameters are defined as follows:

n : number of DGU

v_n: microgrid nominal voltage

$v_{o,k}$: kth DGU output voltage

$v_{ref,k}$: kth DGU output voltage reference

$i_{o,k}$: kth DGU output current

y_k: kth DGU voltage droop gain

v_{pcc}: voltage at the PCC

$i_{l,k}$: current in the line between the kth DGU and PCC

ρ_k: control variable related to the kth DGU control layer. ρ_k enables the current sharing and it evolves according to relation (5)

$\bar{\rho}$: steady state value of $\rho_k \forall k$, i.e. the consensus value,

$I_{r,k}$: kth DGU rated output current

$L_{l,k}$: inductance of the line between the kth DGU and PCC

$R_{l,k}$: resistance of the line between the kth DGU and PCC

$R_{ld,pcc}$: resistive load connected at the PCC

$R_{ld,k}$: resistive load connected at the kth DGU output

The control and electrical variables dependency towards the time will not be mentioned for sake of clarity.

Preliminary :

$$\frac{d}{dt}\rho_k = v_n - \alpha \cdot \rho_k \cdot \frac{i_{o,k}}{I_{r,k}} \tag{2}$$

$$\frac{d}{dt}\rho_k = 0 \qquad \Longrightarrow \qquad v_n = \alpha \cdot \rho_k \cdot \frac{i_{o,k}}{I_{r,k}} \tag{3}$$

In steady state, the consensus is reached so that:

$$\frac{d}{dt}y_k = \sum_{k\in N_i} a_{ik}\cdot(\rho_i - \rho_k) = 0 \quad \Longrightarrow \quad \rho_k = \bar{\rho}\ \forall k \tag{4}$$

$$(3)+(4) \Longrightarrow \quad i_{o,pu,k} = \frac{i_{o,k}}{I_{r,k}} = \frac{v_n}{\alpha\cdot\bar{\rho}} \tag{5}$$

Droop control:

$$v_{ref,k} = v_n - y_k\cdot i_{o,k} \tag{6}$$

Single pcc voltage:

$$v_{pcc} = v_{ref,k} - R_{l,k}\cdot i_{o,k} \tag{7}$$

$$(6)+(7) \Longrightarrow \ v_{pcc} = v^* - (y_k + R_{l,k})\cdot i_{o,k} \tag{8}$$

$$\frac{v_{pcc}}{I_{r,k}} = \frac{v_n}{I_{r,k}} - (y_k + R_{l,k})\cdot i_{o,pu,k} \tag{9}$$

Fair sharing current:

$$(5)+(9) \Longrightarrow \ \frac{v_{pcc}}{I_{r,k}} = \frac{v_n}{I_{r,k}} - (y_k + R_{l,k})\cdot i_{o,pu} \tag{10}$$

Sum:

$$\sum_{k=1}^{n}\frac{v_{pcc}}{I_{r,k}} = \sum_{k=1}^{n}\frac{v_n}{I_{r,k}} - i_{o,pu}\cdot\sum_{k=1}^{n}(y_k + R_{l,k}) \tag{11}$$

Besides:

$$v_{pcc} = v_{ref,k} - R_{l,k}\cdot i_{o,k} \tag{12}$$

$$\frac{v_{pcc}}{I_{r,k}} = \frac{v_{ref,k}}{I_{r,k}} - R_{l,k}\cdot\frac{i_{o,k}}{I_{r,k}} = \frac{v_{ref,k}}{I_{r,k}} - R_{l,k}\cdot i_{o,pu} \tag{13}$$

$$\sum_{k=1}^{n}\frac{v_{pcc}}{I_{r,k}} = \sum_{k=1}^{n}\frac{v_{ref,k}}{I_{r,k}} - i_{o,pu}\cdot\sum_{k=1}^{n}R_{l,k} \tag{14}$$

$$(5)+(9) \Longrightarrow \ \sum_{k=1}^{n}\frac{v_{ref,k}}{I_{r,k}} - i_{o,pu}\cdot\sum_{k=1}^{n}R_{l,k} = \sum_{k=1}^{n}\frac{v_n}{I_{r,k}} - i_{o,pu}\cdot\sum_{k=1}^{n}(y_k + R_{l,k}) \tag{15}$$

$$\Rightarrow \sum_{k=1}^{n}\frac{v_{ref,k}}{I_{r,k}} = \sum_{k=1}^{n}\frac{v_n}{I_{r,k}} - i_{o,pu}\cdot\sum_{k=1}^{n}y_k \tag{16}$$

Assuming that the output control voltage is effective, the output voltage $v_{o,k}$ actually follows its reference $v_{ref,k}$:

$$v_{o,k} = v_{ref,k} \tag{17}$$

$$(17) + (4) \Longrightarrow \; y_k \cdot i_{o,k} = v_n - v_{o,k} \tag{18}$$

Thanks to The Kirchhoff's voltage, the transient dynamics of the kth line current is described as:

$$L_{l,k} \cdot \frac{d}{dt} i_{l,k} = v_{o,k} - v_{pcc} - R_{l,k} \cdot i_{l,k} \tag{19.a}$$

In steady state:

$$L_{l,k} \cdot \frac{d}{dt} i_{l,k} = 0 = v_{o,k} - v_{pcc} - R_{l,k} \cdot i_{l,k} \tag{19.b}$$

$$(18) + (19.b) \Longrightarrow \; y_k \cdot i_{o,k} = v^* - v_{pcc} - R_{l,k} \cdot i_{l,k} \tag{20}$$

The Kirchhoff's current law provides:

$$\sum_{k=1}^{n} \left(i_{o,k} - \frac{v_{o,k}}{R_{ld,k}} \right) = \frac{v_{pcc}}{R_{ld,pcc}} \tag{21}$$

$$(20) + (21) \Longrightarrow \; y_k \cdot i_{o,k} = v_n - R_{ld,pcc} \cdot \sum_{k=1}^{n} \left(i_{o,k} - \frac{v_{o,k}}{R_{ld,k}} \right) - R_{l,k} \cdot i_{l,k} \tag{22}$$

$$(18) + (22) \Longrightarrow \; y_k \cdot i_{o,k} = v^* + R_{ld,pcc} \cdot \sum_{k=1}^{n} \left(-i_{o,k} + \frac{v_n - y_k \cdot i_{o,k}}{R_{ld,k}} \right) - R_{l,k} \cdot i_{l,k} \tag{23}$$

Sorting out the terms provides (24):

$$y_k \cdot i_{o,k} + \sum_{k=1}^{n} \left(y_k \cdot i_{o,k} \cdot \frac{R_{ld,pcc}}{R_{ld,k}} \right) = v_n \cdot \left[1 + \sum_{k=1}^{n} \left(\frac{R_{ld,pcc}}{R_{ld,k}} \right) \right] - R_{ld,pcc} \cdot \sum_{k=1}^{n} (i_{o,k}) - R_{l,k} \cdot i_{l,k} \tag{24}$$

The control variable ρ_k is related to the kth DGU control layer. ρ_k enables the current sharing and it evolves according to relation (25).

$$\frac{d}{dt} \rho_k = v_n - \alpha \cdot \rho_k \cdot \frac{i_{o,k}}{I_{r,k}} \tag{25}$$

In steady state, the consensus is reached so that:

$$\frac{d}{dt} \rho_k = 0 \quad and \quad \rho_k = \bar{\rho} \; \forall k \tag{26}$$

$$(6) + (26) \Longrightarrow \quad \frac{i_{o,k}}{I_{r,k}} = \frac{v_n}{\alpha \cdot \bar{\rho}} \tag{27}$$

NB:

The approximative value of $\bar{\rho}$ may be literally determined thanks to a power balance. The approximation implies neglecting the resistive lines losses and results in $\bar{\rho}_{app} = 2.5$.

However, the exact value of $\bar{\rho}$ may only be numerically determined.

x standing for the state variables vector, it follows the dynamics $\dot{x} = f(x)$ where f is a nonlinear functions vector.

Numerically solving $f(x) = 0$ will provide the exact value, namely $\bar{\rho} = 2.505$.

$(24) + (27)$ enable to write:

$$y_k \cdot i_{o,k} + \sum_{k=1}^{n} \left(y_k \cdot i_{o,k} \cdot \frac{R_{ld,pcc}}{R_{ld,k}} \right) = v^* \cdot \left[1 + \sum_{k=1}^{n} \left(\frac{R_{ld,pcc}}{R_{ld,k}} \right) \right] - \frac{v_n \cdot R_{ld,pcc}}{\alpha \cdot \bar{\rho}} \cdot \sum_{k=1}^{n} I_{r,k} - R_{l,k} \cdot i_{l,k} \quad (28)$$

Sorting out the terms provides:

$$y_k \cdot i_{o,k} + \sum_{k=1}^{n} \left(y_k \cdot i_{o,k} \cdot \frac{R_{ld,pcc}}{R_{ld,k}} \right) = v_n \cdot \left[1 + \sum_{k=1}^{n} \left(\frac{R_{ld,pcc}}{R_{ld,k}} \right) - \frac{R_{ld,pcc}}{\alpha \cdot \bar{\rho}} \cdot \sum_{k=1}^{n} I_{r,k} \right] - R_{l,k} \cdot i_{l,k} \quad (29)$$

Summing (29) on the n DGU gives:

$$\sum_{k=1}^{n} y_k \cdot i_{o,k} \cdot \left(1 + \frac{n \cdot R_{ld,pcc}}{R_{ld,k}} \right) = v_n \cdot n \cdot \left[1 + \sum_{k=1}^{n} \left(\frac{R_{ld,pcc}}{R_{ld,k}} \right) - \frac{R_{ld,pcc}}{\alpha \cdot \bar{\rho}} \cdot \sum_{k=1}^{n} I_{r,k} \right] - \sum_{k=1}^{n} \left(R_{l,k} \cdot i_{l,k} \right) \quad (30)$$

$R_{l,k} \cdot i_{l,k}$ represent the voltage drop in each lin. A properly designed microgrid should comply with (31.a):

$$R_{l,k} \cdot i_{l,k} \ll v_n \quad (31.a)$$

Summing (31.a) on the n DGU gives:

$$\sum_{k=1}^{n} \left(R_{l,k} \cdot i_{l,k} \right) \ll v_n \cdot n \quad (31.b)$$

$$(30) + (31.b) \Longrightarrow \sum_{k=1}^{n} y_k \cdot i_{o,k} \cdot \left(1 + \frac{n \cdot R_{ld,pcc}}{R_{ld,k}} \right) = v_n \cdot n \cdot \left[1 + \sum_{k=1}^{n} \left(\frac{R_{ld,pcc}}{R_{ld,k}} \right) - \frac{R_{ld,pcc}}{\alpha \cdot \bar{\rho}} \cdot \sum_{k=1}^{n} I_{r,k} \right] \quad (32)$$

For any load $R_{ld,k}$:

$$\left(1+\frac{n\cdot R_{ld,pcc}}{R_{ld,k}}\right)\geq min\left(1+\frac{n\cdot R_{ld,pcc}}{R_{ld,k}}\right) \tag{33}$$

Let us call m this minimum value:

$$m=min\left(1+\frac{n\cdot R_{ld,pcc}}{R_{ld,k}}\right)=1+\frac{n\cdot R_{ld,pcc}}{max\left(R_{ld,k}\right)} \tag{34.a}$$

$R_{ld,k}$ is directly linked to the power consumed by the related load. It may be sensible to think that $R_{ld,k}$ and $R_{ld,pcc}$ are of the same order, so much so that:

$$m\cong 1+n \tag{34.b}$$

Thanks to $(eq.15.a)$, it comes:

$$y_k\cdot i_{o,k}\cdot\left(1+\frac{n\cdot R_{ld,pcc}}{R_{ld,k}}\right)\geq y_k\cdot i_{o,k}\cdot m \tag{35}$$

Summing (35) over the n DGU gives:

$$\sum_{k=1}^{n} y_k\cdot i_{o,k}\cdot\left(1+\frac{n\cdot R_{ld,pcc}}{R_{ld,k}}\right)\geq m\cdot\sum_{k=1}^{n} y_k\cdot i_{o,k} \tag{36}$$

Sorting out the terms provides:

$$\sum_{k=1}^{n} y_k\cdot i_{o,k}\leq\frac{1}{m}\cdot\sum_{k=1}^{n} y_k\cdot i_{o,k}\cdot\left(1+\frac{n\cdot R_{ld,pcc}}{R_{ld,k}}\right) \tag{37}$$

$$(32)+(37)\Longrightarrow\quad\sum_{k=1}^{n} y_k\cdot i_{o,k}\leq\frac{v_n\cdot n}{m}\cdot\left[1+\sum_{k=1}^{n}\left(\frac{R_{ld,pcc}}{R_{ld,k}}\right)-\frac{R_{ld,pcc}}{\alpha\cdot\bar{\rho}}\cdot\sum_{k=1}^{n} I_{r,k}\right] \tag{38}$$

Dividing (18) by n gives:

$$\frac{1}{n}\cdot\sum_{k=1}^{n} y_k\cdot i_{o,k}\leq\frac{v_n}{m}\cdot\left[1+\sum_{k=1}^{n}\left(\frac{R_{ld,pcc}}{R_{ld,k}}\right)-\frac{R_{ld,pcc}}{\alpha\cdot\bar{\rho}}\cdot\sum_{k=1}^{n} I_{r,k}\right] \tag{39}$$

Let us define ε as the bracket terms on the right-side member of (38).

$$\varepsilon=1+\sum_{k=1}^{n}\left(\frac{R_{ld,pcc}}{R_{ld,k}}\right)-\frac{R_{ld,pcc}}{\alpha\cdot\bar{\rho}}\cdot\sum_{k=1}^{n} I_{r,k} \tag{40}$$

ε may be numerically computed thanks to the system parameters. It appears that:

$$0 < \varepsilon \ll 1 \tag{41}$$

$$(39) + (40) \Longrightarrow \frac{1}{n} \cdot \sum_{k=1}^{n} y_k \cdot i_{o,k} \leq v_n \cdot \frac{\varepsilon}{m} \tag{41.a}$$

$$(32) + left\ side\ inequality\ of\ (41): \quad 0 < \frac{1}{n} \cdot \sum_{k=1}^{n} y_k \cdot i_{o,k} \tag{41.b}$$

$$(41.a) + (41.b) \Longrightarrow \quad 0 < \frac{1}{n} \cdot \sum_{k=1}^{n} y_k \cdot i_{o,k} \leq v_n \cdot \frac{\varepsilon}{m} \tag{41.c}$$

With the considered parameters set, the numerical application indicates that $\varepsilon = 0.7665$ and $m = 5$. The computation of ε is detailed in Appendix B. Consequently:

$$\frac{1}{n} \cdot \sum_{k=1}^{n} y_k \cdot i_{o,k} \cong 0 \tag{41.d}$$

Let us recall that:

$$v_{ref,k} = v_n - y_k \cdot i_{o,k} \tag{42}$$

Summing (42) on the n DGU and dividing by n gives:

$$\frac{1}{n} \cdot \sum_{k=1}^{n} v_{ref,k} = v_n - \frac{1}{n} \cdot \sum_{i=k}^{n} y_k \cdot i_{o,k} \tag{43}$$

$$(41.c) + (43) \Longrightarrow \quad v_n \cdot \left(1 - \frac{\varepsilon}{m}\right) \leq \frac{1}{n} \cdot \sum_{k=1}^{n} v_{ref,k} < v_n \tag{44}$$

Then, Eq.44 may be considered as a voltage deviation indicator. The voltages plan is well regulated as soon as the ratio ε/m is small. This is the case with the parameters considered set, which, by the way, is anything but particular.

$$\lim_{t \to \infty} \left(\frac{1}{n} \cdot \sum_{k=1}^{n} v_{o,k}(t) \right) \cong v_n \tag{45}$$

where $v_{o,k}$ is the ith DG's output voltage and v_n is the DC microgrid rated voltage.

Appendix B:

Assuming the output voltage regulation of each DGU is effective, i.e.$v_{o,k} = v_{ref\ ,k}$ in steady state, and considering the system at its equilibrium point, i.e. $\frac{i_{o,k}}{I_{r,k}} = \frac{v_n}{\alpha \cdot \bar{\rho}}$ then basic current and voltage Kirchhoff's laws lead to the following inequalities:

$$v_n \cdot \left(1 - \frac{\varepsilon}{m}\right) \leq \lim_{t \to \infty} \left(\frac{1}{n} \cdot \sum_{k=1}^{n} v_{o,k}(t)\right) < v_n \tag{46}$$

Where the parameters ε is defined as:

$$\varepsilon = 1 + \sum_{k=1}^{n} \left(\frac{R_{ld,pcc}}{R_{ld,k}}\right) - \frac{R_{ld,pcc}}{\alpha \cdot \bar{\rho}} \cdot \sum_{k=1}^{n} I_{r,k} \ll 1 \tag{47}$$

The approximative value of the consensus value $\bar{\rho}$ may be literally determined thanks to a power balance. The approximation implies neglecting the resistive lines losses and results in $\bar{\rho}_{app} = 2.5$.

However, the exact value of $\bar{\rho}$ may only be numerically determined.

x standing for the state variables vector, it follows the dynamics $\dot{x} = f(x)$ where f is a nonlinear functions vector. Numerically solving $f(x) = 0$ will provide the exact value, namely $\bar{\rho} = 2.505$. As a result $\varepsilon = 0.7665$.

Author’s publications

[1] H. Elouadoud, S. Pierfederici, M. Bakhouya, R. Ouladsine, M. Urbain, "Stratégie répartition de Puissance Améliorée Basée sur la Séparation Fréquentielle dans un Micro-Réseau DC," in *Symposium de Génie Électrique*, Lille, France, 2023.

[2] Elouadoud, H., Ouladsine, R., Elmouatamid, A., Pierfederici, S., Bakhouya, M.: Towards a Holistic Control Approach for Energy Management in Distributed Microgrid Systems. To appear in the book *Advances in Mechanics, Materials, and Energy' in the LNME series*, 2025.

[3] H. El Ouadoud, M. Urbain, S. Pierfederici, Y. Alidrissi, R. Ouladsine, and M. Bakhouya, “An Advanced Generic Control Strategy for Power Allocation and Energy Management in DC Microgrids with Hybrid Energy Storage Systems,” *submitted to Mathematics and Computers in Simulation (MATCOM)*, 2025.

[4] Alidrissi, Y., El Ouadoud, H., Pierfederici, S., Urbain, M., Ouladsine, R., Bakhouya, M.: A cooperative distributed droop gains adjustment in DC microgrids. *Math. Comput. Simul.* 229, 830–841 (2025).

[5] Alidrissi, Y., El Ouadoud, H., Pierfederici, S., Urbain, M., Ouladsine, R., Bakhouya, M.: Consensus-Based Droop-Free Control for Current Sharing and Voltage Regulation in Meshed DC Microgrid. *Submitted to Mathematics and Computers in Simulation (MATCOM)*, (2025).

References

[1] IRENA, *Global Energy Transformation: A Roadmap to 2050*, 2019 ed., Abu Dhabi: International Renewable Energy Agency, 2019.

[2] P. Lilienthal, *The Story of Microgrids: A Historical Perspective*, UL LLC / HOMER Energy by UL, Apr. 2020.

[3] Guerrero J.M. et al., "Microgrids: architectures and control," *IEEE Trans. Ind. Electron.*, 2011.

[4] Parhizi M. et al., "State of the art in microgrid research," *IEEE Access*, 2015.

[5] M. Liu et al., "Dynamic power allocation of battery-supercapacitor hybrid energy storage system in standalone PV microgrid," *International Journal of Electrical Power & Energy Systems*, 2016

[6] W. E. P. S. Ediweera and N. W. A. Lidula, "Design and protection of microgrid clusters: A comprehensive review," *AIMS Energy*, vol. 10, no. 3, pp. 375–411, May 2022.

[7] Office National de l'Électricité et de l'Eau Potable (ONEE), *Le PERG : une approche globale*.

[8] Atalayar, "Rural electrification in Morocco reaches 99.89%," *Atalayar*, Nov. 17, 2024.

[9] Ministère de l'Économie et des Finances, *Rapport sur les établissements et entreprises publics – PLF 2024*, Royaume du Maroc, Nov. 2023.

[10] Ministère de la Transition Énergétique et du Développement Durable, *Secteur de l'électricité au Maroc*, Royaume du Maroc.

[11] Institut Royal des Études Stratégiques (IRES), *Développement des énergies solaire et éolienne au Maroc*, 2020.

[12] Agence Nationale de Régulation de l'Électricité (ANRE), *Rapport Annuel 2022*, Royaume du Maroc, déc. 2023.

[13] A. Rochd, M. Bakhouya, D. Yousfi, S. Pierfederici, C. V. Hirschhausen, L. Baghli, N. Kebir, H. Belmili, and A. Mecherene, "Smart Microgrids for Agriculture: MG-FARM's Innovative Approach to Electrifying Farms in North Africa – Case Studies of Morocco and Algeria," *Proceedings of the 2023 IEEE PowerAfrica Conference*, 2023.

[14] Agence Marocaine pour l'Efficacité Énergétique (AMEE), « Pompage solaire : 30 000 exploitations agricoles sont équipées de panneaux photovoltaïques (étude) », *Industries.ma*, 2019.

[15] M. Boussetta, R. Elbachtiri, K. Elhammoumi, and M. Khanfara, “Optimal sizing of grid-connected PV-Wind system: Case study: Agricultural farm in Morocco,” *Journal of Theoretical and Applied Information Technology*, vol. 86, no. 2, pp. –, Apr. 2016.

[16] A. Elamrani, R. Ouladsine, A. Elmouatamid, H. El Ouadoud, S. Pierfederici, M. Bakhouya, “Community Networked Microgrids for a Resilient and Sustainable Energy Future in Smart Farming,” in *Proc. of the Int. Conf. on Smart Technologies for Sustainable Energy (STSE 2025)*, Errachidia, Morocco, Apr. 25–26, 2025.

[17] S. Chahi, A. Aqachtoul, A. ElAmrani, Y. Alidrissi, R. Naji El Idrissi, R. Ouladsine, N. Yousfi Steiner, A. Rochd, and M. Bakhouya, “Techno-economic Analysis of Energy Micro-Grids with Hydrogen Storage and Fuel Cell in Moroccan Farming Systems,” *Preprint submitted to Elsevier*, 2025.

[18] International Energy Agency (IEA), *Africa Energy Outlook 2019*, World Energy Outlook Special Report, Paris, France, 2019.

[19] H. Binqadhi, W. M. Hamanah, M. Shafiullah, M. S. Alam, M. M. AlMuhaini, and M. A. Abido, "A Comprehensive Survey on Advancement and Challenges of DC Microgrid Protection," *Sustainability*, vol. 16, no. 14, p. 6008, Jul. 2024.

[20] H. B. Ahmed, M. A. Abido, and S. M. Muyeen, "Fault Detection and Localization in a Ring Bus DC Microgrid Using Current Derivatives," *IEEE Transactions on Smart Grid*, vol. 11, no. 5, pp. 3988–3997, Sep. 2020.

[21] M. P. Nthontho, S. P. Chowdhury, S. Winberg, and S. Chowdhury, "Protection of Domestic Solar Photovoltaic Based Microgrid," *Conference Paper*, January 2012.

[22] M. Z. Nazeri and N. H. Abd Rahman, "Maximum Power Point Tracking Using Perturb and Observe Technique," *Journal of Engineering Technology*, vol. 10, no. 1, pp. 204-210, 2022.

[23] L. Shang, H. Guo, and W. Zhu, "An improved MPPT control strategy based on incremental conductance algorithm," *Protection and Control of Modern Power Systems*, vol. 5, Art. no. 14, 2020.

[24] R. K. Rai and O. P. Rahi, "Fuzzy Logic based Control Technique using MPPT for Solar PV System," in *Proc. IEEE International Conference on Electrical Engineering, Communications and Information Technology (ICEEICT)*, Feb. 2022.

[25] A. Houari, *Contribution à l’étude de micro-réseaux autonomes alimentés par des sources photovoltaïques*, Thèse de doctorat, Université de Lorraine, Vandœuvre-lès-Nancy, 2012.

[26] Gunawardane, Kosala & Padmawansa, Nisitha & Jayasinghe, Hasith, “A review: compatibility of fuel cells as promising technology for DC-microgrids,” *Renewable Energy and Environmental Sustainability*. 9. 7. 10.1051.2024.

[27] P. Thounthong, S. Raël, and B. Davat, “Analysis of a fuel starvation phenomenon of a PEM fuel cell,” *IEEE Transactions on Industrial Applications*, vol. 15, no. 4, pp. 833–843, Jul.–Aug. 2009.

[28] X. Luo, J. Wang, M. Dooner, and J. Clarke, "Overview of current development in electrical energy storage technologies and the application potential in power system operation," *Applied Energy*, vol. 137, pp. 511–536, 2015.

[29] J. Cheng and M. Zhou, "Lithium-ion battery smoothing power fluctuation strategy for DC microgrid," *International Journal of Low-Carbon Technologies*, vol. 18, pp. 802–808, Jul. 2023.

[30] J. Zhang, M. Gu, and X. Chen, "Supercapacitors for renewable energy applications: A review," *Micro and Nano Engineering*, vol. 21, p. 100229, Dec. 2023.

[31] F. Mariasiu and E. A. Kelemen, “Analysis of the energy efficiency of a hybrid energy storage system for an electric vehicle,” *Batteries*, vol. 9, no. 8, p. 419, 2023.

[32] Z. Song, H. Hofmann, J. Li, X. Han, X. Zhang, and M. Ouyang, “A comparison study of different semi-active hybrid energy storage system topologies for electric vehicles,” *Journal of Power Sources*, vol. 274, pp. 400–411, 2015.

[33] A. Khaligh and Z. Li, “Battery, ultracapacitor, fuel cell, and hybrid energy storage systems for electric, hybrid electric, fuel cell, and plug-in hybrid electric vehicles: State of the art,” *IEEE Transactions on Vehicular Technology*, vol. 59, no. 6, pp. 2806–2814, 2010.

[34] E. Espina, J. Llanos, C. Burgos-Mellado, R. Cárdenas-Dobson, M. Martínez-Gómez and D. Sáez, "Distributed Control Strategies for Microgrids: An Overview," *in IEEE Access*, vol. 8, pp. 193412-193448, 2020.

[35] L. Gil-Antonio, B. Saldivar, O. Portillo-Rodríguez, G. Vázquez-Guzmán and S. M. De Oca-Armeaga, "Trajectory Tracking Control for a Boost Converter Based on the Differential Flatness Property," in IEEE Access, vol. 7, pp. 63437-63446, 2019.

[36] B. Wang, U. Manandhar, X. Zhang, H. B. Gooi and A. Ukil, "Deadbeat Control for Hybrid Energy Storage Systems in DC Microgrids," in IEEE Transactions on Sustainable Energy, vol. 10, no. 4, pp. 1867-1877, Oct. 2019.

[37] P. Thounthong, P. Sethakul, S. Rael and B. Davat, "Control of fuel cell/battery/supercapacitor hybrid source for vehicle applications," *2009 IEEE*

International Conference on Industrial Technology, Churchill, VIC, Australia, 2009, pp. 1-6.

[38] K. Kollimalla, M. K. Mishra and N. L. Narasamma, "Design and Analysis of Novel Control Strategy for Battery and Supercapacitor Storage System," in *IEEE Transactions on Sustainable Energy*, vol. 5, no. 4, pp. 1137-1144, Oct. 2014.

[39] C. Xiang, Q. Cheng, Y. Zhu, and H. Zhao, "Sliding mode control of ship DC microgrid based on an improved reaching law," *Energies*, vol. 16, no. 3, p. 1051, Feb. 2023.

[40] N. Ghanbari and S. Bhattacharya, "Adaptive droop control method for suppressing circulating currents in DC microgrids," *IEEE Open Access Journal of Power and Energy*, vol. 7, pp. 100–110, 2020.

[41] S. E. Mhankale and A. R. Thorat, "Droop Control Strategies of DC Microgrid: A Review," 2018 *International Conference on Current Trends towards Converging Technologies (ICCTCT), Coimbatore, India*, pp. 372-376, 2018.

[42] S. Shekhar and A. Alam, "Adaptive droop control for enhanced stability and robustness in DC microgrids," *Computers and Electrical Engineering*, vol. 120, Part A, p. 109649, 2024.

[43] E. Youssef, A. Sharaf, A. Amin, and A. El Samhey, "Wind energy FACTS applications and stabilization schemes," in *Advances in Renewable Energies and Power Technologies*, I. Yahyaoui, Ed. Elsevier, 2018, pp. 431-460.

[44] J. M. Guerrero, J. C. Vasquez, J. Matas, L. G. de Vicuña, and M. Castilla, "Hierarchical Control of Droop-Controlled AC and DC Microgrids—A General Approach Toward Standardization," *IEEE Transactions on Industrial Electronics*, vol. 58, no. 1, pp. 158–172, Jan. 2011.

[45] A. M. Jasim, B. H. Jasim, V. Bureš, and P. Mikulecký, "A new decentralized robust secondary control for smart islanded microgrids," *Sensors (Basel)*, vol. 22, no. 22, p. 8709, Nov. 2022.

[46] E. Unamuno and J. A. Barrena, "Hybrid AC/DC microgrids—Part II: Review and classification of control strategies," *Renewable and Sustainable Energy Reviews*, vol. 52, pp. 1123-1134, 2015.

[47] O. Palizban and K. Kauhaniemi, "Secondary control in AC microgrids—Challenges and solutions," *Proceedings of the 4th International Conference on Smart Cities and Green ICT Systems (SMARTGREENS)*, pp. 294-299, 2015.

[48] F. S. Al-Ismail, "DC Microgrid Planning, Operation, and Control: A Comprehensive Review," *IEEE Access*, vol. 9, pp. 36154–36172, Mar. 2021.

[49] J. Duarte, M. Savaghebi, D. M. Vilathgamuwa, J. C. Vasquez, and J. M. Guerrero, "On Secondary Control Approaches for Voltage Regulation in DC Microgrids," *IEEE Transactions on Power Electronics*, vol. 37, no. 10, pp. 12135–12152, Oct. 2022,

[50] M. Yazdanian and A. Mehrizi-Sani, "Distributed Control Techniques in Microgrids," IEEE Trans. Smart Grid, vol. 5, no. 6, pp. 2901–2909, Nov. 2014.

[51] J. Rocabert, A. Luna, F. Blaabjerg and P. Rodríguez, "Control of Power Converters in AC Microgrids," *in IEEE Transactions on Power Electronics,* vol. 27, no. 11, pp. 4734-4749, Nov. 2012.

[52] A. Bidram and A. Davoudi, "Hierarchical Structure of Microgrids Control System," *in IEEE Transactions on Smart Grid*, vol. 3, no. 4, pp. 1963-1976, Dec. 2012.

[53] M. A. Hassan et al., "DC Shipboard Microgrids With Constant Power Loads: A Review of Advanced Nonlinear Control Strategies and Stabilization Techniques," in IEEE Transactions on Smart Grid, vol. 13, no. 5, pp. 3422-3438, Sept. 2022.

[54] Z. Zhao et al., "Modeling, Oscillation Analysis and Distributed Stabilization Control of Autonomous PV-based Microgrids," in CSEE Journal of Power and Energy Systems, vol. 9, no. 3, pp. 921-936, May 2023.

[55] T. Dragičević, X. Lu, J. C. Vasquez and J. M. Guerrero, "DC Microgrids—Part I: A Review of Control Strategies and Stabilization Techniques," in IEEE Transactions on Power Electronics, vol. 31, no. 7, pp. 4876-4891, July 2016.

[56] X. Chen et al., "Consensus-Based Distributed Control for Photovoltaic-Battery Units in a DC Microgrid," in IEEE Transactions on Industrial Electronics, vol. 66, no. 10, pp. 7778-7787, Oct. 2019.

[57] N. Zohrabi, J. Shi, and S. Abdelwahed, "An overview of design specifications and requirements for the MVDC shipboard power system," *International Journal of Electrical Power & Energy Systems*, vol. 104, pp. 680-693, 2019.

[58] D. B. W. Abeywardana, B. Hredzak, V. G. Agelidis, G. D. Demetriades, "Supercapacitor sizing method for energy-controlled filter-based hybrid energy storage systems, " *IEEE Transactions on Power Electronics* 32 (2) (2016) 1626–1637.

[59] K. A. Khan, M. Khalid, "Improving the transient response of hybrid energy storage system for voltage stability in dc microgrids using an autonomous control strategy, " *IEEE Access* 9 (2021) 10460–10472.

[60] H. Liao, J. Peng, Y. Wu, H. Li, Y. Zhou, X. Zhang, Z. Huang, "Adaptive split-frequency quantitative power allocation for hybrid energy storage systems, " *IEEE Transactions on Transportation Electrification* 7 (4) (2021) 2306–2317.

[61] Y. Wu, Z. Huang, H. Liao, B. Chen, X. Zhang, Y. Zhou, Y. Liu, H. Li, J. Peng, "Adaptive power allocation using artificial potential field with compensator for hybrid energy storage systems in electric vehicles, " *Applied Energy* 257 (2020) 113983.

[62] Y. Zhang, G. Du, Y. Lei, " Deadbeat control with power sharing for supercapacitor/battery-based hybrid energy storage systems in dc microgrids, " in: *IECON 2020 The 46th Annual Conference of the IEEE Industrial Electronics Society*, *IEEE*, 2020, pp. 1785–1790.

[63] Y. Wu, Z. Huang, H. Liao, B. Chen, X. Zhang, Y. Zhou, Y. Liu, H. Li, J. Peng, "Adaptive power allocation using artificial potential field with compensator for hybrid energy storage systems in electric vehicles, " *Applied Energy* 257 (2020) 113983.

[64] Q. Li, W. Chen, Z. Liu, M. Li, L. Ma, "Development of energy management system based on a power sharing strategy for a fuel cell–battery supercapacitor hybrid tramway, " *Journal of Power Sources* 279 (2015) 267–280.

[65] O. Erdinc, B. Vural, M. Uzunoglu, "A wavelet-fuzzy logic-based energy management strategy for a fuel cell/battery/ultra-capacitor hybrid vehicular power system, " *Journal of Power sources* 194 (1) (2009) 369–380.

[66] S. Njoya Motapon, "Design and simulation of a fuel cell hybrid emergency power system for a more electric aircraft: evaluation of energy management schemes, " *Ph.D. thesis, Ecole de technologie supérieure* (2013).

[67] M. Zandi, A. Payman, J.-P. Martin, S. Pierfederici, B. Davat, F. Meibody-Tabar, "Energy management of a fuel cell/supercapacitor/battery power source for electric vehicular applications, " *IEEE transactions on vehicular technology* 60 (2) (2010) 433–443.

[68] L. Mamouri, T. Mesbahi, P. Bartholomeus, P. Theophile, "Design of a dc/dc power converter for li-ion battery/supercapacitor hybrid energy storage system in electric vehicles, " in *2020 IEEE Vehicle Power and Propulsion Conference (VPPC), IEEE*, (2020).

[69] R. D. Middlebrook and S. Cuk, “A general unified approach to modelling switching-converter power stages,” in 1976 IEEE Power Electronics Specialists Conference, pp. 18–34, 1976.

[70] S. Piller, M. Perrin, and A. Jossen, “Methods for state-of-charge determination and their applications,” *Journal of Power Sources*, vol. 96, no. 1, pp. 113–120, 2001.

[71] J. M. Guerrero, J. C. Vasquez, and J. Matas, “158 IEEE TRANSACTIONS ON INDUSTRIAL ELECTRONICS, VOL. 58, NO. 1, JANUARY 2011 Hierarchical Control of Droop-Controlled AC and DC Microgrids—A General Approach Toward Standardization,” New Zealand Journal of Educational Studies, vol. 58, no. 1, pp. 35–51, 2011.

[72] A. Maknouninejad, Z. Qu, F. L. Lewis, and A. Davoudi, “Optimal, nonlinear, and distributed designs of droop controls for DC microgrids,” IEEE Transactions on Smart Grid, vol. 5, no. 5, pp. 2508–2516, Sep. 2014.

[73] A. Khorsandi, M. Ashourloo, H. Mokhtari, and R. Iravani, "Automatic droop control for a low voltage DC microgrid," *IET Gener. Transm. Distrib.*, vol. 10, no. 1, pp. 41–47, Jan. 2016.

[74] Y. Zhang, X. Qu, M. Tang, R. Yao, and W. Chen, “Design of Nonlinear Droop Control in DC Microgrid for Desired Voltage Regulation and Current Sharing Accuracy,” IEEE Journal on Emerging and Selected Topics in Circuits and Systems, vol. 11, no. 1, pp. 168–175, Mar. 2021.

[75] B. A. Taye and N. B. D. Choudhury, “A dynamic droop control for a DC microgrid to enhance voltage profile and proportional current sharing,” Electric Power Systems Research, vol. 221, p. 109438, Aug. 2023.

[76] P. Wang, X. Lu, X. Yang, W. Wang, and D. Xu, “An Improved Distributed Secondary Control Method for DC Microgrids with Enhanced Dynamic Current Sharing Performance,” IEEE Transactions on Power Electronics, vol. 31, no. 9, pp. 6658–6673, Sep. 2016.

[77] M. Moradi, M. Heydari, and S. F. Zarei, “An overview on consensus-based distributed secondary control schemes in DC microgrids,” Electric Power Systems Research, vol. 225, p. 109870, Dec. 2023.

[78] P. Nahata, M. S. Turan, and G. Ferrari-Trecate, “Consensus-based current sharing and voltage balancing in DC microgrids with exponential loads,” IEEE Trans. Control Syst. Technol., vol. 30, no. 4, pp. 1668–1680, Jul. 2022.

[79] Q. Wan and S. Zheng, “Distributed cooperative secondary control based on discrete consensus for DC microgrid,” Energy Reports, vol. 8, pp. 8523–8533, Nov. 2022.

[80] Q. Li, C. Yan, Y. Han, et al., “Optimizing power sharing and voltage control in DC microgrids using a novel adaptive droop control strategy based on current consensus algorithm,” Sustainable Energy, Grids and Networks, vol. 38, p. 101386, Jun. 2024.

[81] V. Nasirian, S. Moayedi, A. Davoudi, and F. L. Lewis, “Distributed Cooperative Control of DC Microgrids,” IEEE Transactions on Power Electronics, vol. 30, no. 4, pp. 2288–2303, Apr. 2015.

[82] Y.Li, Z. Zhang, T. Dragicevic, and J. Rodriguez, “A Unified Distributed Cooperative Control of DC Microgrids Using Consensus Protocol,” IEEE Transac tions on Smart Grid, vol. 12, no. 3, pp. 1880–1892, May 2021.

[83] Ciornei, I., Albu, M., Sănduleac, M., Rodriguez-Diaz, E., Teodorescu, R., Guerrero, J.: Adaptive distributed EMS for small clusters of resilient LVDC microgrids. In: 2018 IEEE Int. Conf. on Environment and Electrical Engineering (EEEIC), pp. 1–6. IEEE (2018).

[84] Lu, X., Lai, J., Yu, X., Wang, Y., Guerrero, J.M.: Distributed coordination of islanded microgrid clusters using a two-layer intermittent communication network. IEEE Trans. Ind. Inform. 14(9), 3956–3969 (2017).

[85] Han, Y., Zhang, K., Li, H., Coelho, E.A.A., Guerrero, J.M.: MAS-based distributed coordinated control and optimization in microgrid and microgrid clusters: A comprehensive overview. IEEE Trans. Power Electron. 33(8), 6488–6508 (2017).

[86] Palizban, O., Kauhaniemi, K.: Hierarchical control structure in microgrids with distributed generation: Island and grid-connected mode. Renew. Sustain. Energy Rev. 44, 797–813 (2015).

[87] Novickij, I., Joós, G.: Model predictive control-based approach for microgrid energy management. In: 2019 IEEE Canadian Conf. Electr. Comput. Eng. (CCECE), pp. 1–4. IEEE (2019).

[88] Espí, J.M., Castello, J., García-Gil, R., Garcera, G., Figueres, E.: An adaptive robust predictive current control for three-phase grid-connected inverters. IEEE Trans. Ind. Electron. 58(8), 3537–3546 (2010).

[89] Hu, J., Zhu, Z.Q.: Improved voltage-vector sequences on dead-beat predictive direct power control of reversible three-phase grid-connected voltage-source converters. IEEE Trans. Power Electron. 28(1), 254–267 (2012).

[90] Timbus, A.V.: Grid monitoring and advanced control of distributed power generation systems. (2007).

[91] Mohamed, Y.A.R.I., El-Saadany, E.F.: An improved deadbeat current control scheme with a novel adaptive self-tuning load model for a three-phase PWM voltage-source inverter. IEEE Trans. Ind. Electron. 54(2), 747–759 (2007).

[92] Malesani, L., Mattavelli, P., Buso, S.: Robust dead-beat current control for PWM rectifiers and active filters. In: 1998 IEEE Industry Applications Conf., vol. 2, pp. 1377–1384. IEEE (1998).

[93] Ehsani, M., Saeidi, M., Radmanesh, H., Abrishamifar, A.: Comparisons between Generalized Predictive Control and Linear Controllers in Multi-Input DC-DC Boost Converter. Int. J. Ind. Electron. Control Optim. 3(1), 27–34 (2020).

[94] Richalet, J., Rault, A., Testud, J.L., Papon, J.: Model predictive heuristic control: Applications to industrial processes. Autom. 14, 413–428 (1978).

[95] Richalet, J., O'Donovan, D.: Predictive Functional Control: Principles and Industrial Applications. (2009).

[96] Haber, R., Bars, R., Schmitz, U.: Predictive Control in Process Engineering: From the Basics to the Applications. (2011).

[97] Moayedi, S., Davoudi, A.: Distributed tertiary control of DC microgrid clusters. IEEE Trans. Power Electron. 31(2), 1717–1733 (2015).

[98] Eddy, Y.F., Gooi, H.B., Chen, S.X.: Multi-agent system for distributed management of microgrids. IEEE Trans. Power Syst. 30(1), 24–34 (2014).

[99] Hadri, S., Najib, M., Bakhouya, M., Fakhri, Y., El Arroussi, M.: Performance Evaluation of Forecasting Strategies for Electricity Consumption in Buildings. Energies (2021).

[100] Maaroufi, N., Najib, M., Bakhouya, M.: Predicting the Future is Like Completing a Painting: Towards a Novel Method for Time-Series Forecasting. IEEE Access 9, 119918–119938 (2021).

[101] Bullich-Massague, E., Díaz-González, F., Aragüés-Peñalba, M., Girbau-Llistuella, F., Olivella-Rosell, P., Sumper, A.: Microgrid clustering architectures. Appl. Energy 212, 340–361 (2018).